UNIVERSIDAD PONTIFICIA COMILLAS

ESCUELA TÉCNICA SUPERIOR DE INGENIERÍA (ICAI)

INGENIERO INDUSTRIAL

MASTER THESIS

STUDY OF THERMODYNAMIC AND CHEMICAL PROPERTIES IN NON-EQUILIBRIUM FLOW IN A SHOCK TUBE

AUTHOR: Alejandro Blanco Hurtado

DIRECTOR: Nick Parziale

MADRID, June 2016

AUTORIZACIÓN PARA LA DIGITALIZACIÓN, DEPÓSITO Y DIVULGACIÓN EN RED DE PROYECTOS FIN DE GRADO, FIN DE MÁSTER, TESINAS O MEMORIAS DE BACHILLERATO

1º. Declaración de la autoría y acreditación de la misma.

El autor D Alejandro Blanco Hurtado

DECLARA ser el titular de los derechos de propiedad intelectual de la obra: Master Thesis, 'Study of Thermodynamic and Chemical Properties in Non-Equilibrium Flow in a Shock Tube', que ésta es una obra original, y que ostenta la condición de autor en el sentido que otorga la Ley de Propiedad Intelectual.

2º. Objeto y fines de la cesión.

Con el fin de dar la máxima difusión a la obra citada a través del Repositorio institucional de la Universidad, el autor **CEDE** a la Universidad Pontificia Comillas, de forma gratuita y no exclusiva, por el máximo plazo legal y con ámbito universal, los derechos de digitalización, de archivo, de reproducción, de distribución y de comunicación pública, incluido el derecho de puesta a disposición electrónica, tal y como se describen en la Ley de Propiedad Intelectual. El derecho de transformación se cede a los únicos efectos de lo dispuesto en la letra a) del apartado siguiente.

3º. Condiciones de la cesión y acceso

Sin perjuicio de la titularidad de la obra, que sigue correspondiendo a su autor, la cesión de derechos contemplada en esta licencia habilita para:

a) Transformarla con el fin de adaptarla a cualquier tecnología que permita incorporarla a internet y hacerla accesible; incorporar metadatos para realizar el registro de la obra e incorporar "marcas de agua" o cualquier otro sistema de seguridad o de protección.

b) Reproducirla en un soporte digital para su incorporación a una base de datos electrónica, incluyendo el derecho de reproducir y almacenar la obra en servidores, a los efectos de garantizar su seguridad, conservación y preservar el formato.

c) Comunicarla, por defecto, a través de un archivo institucional abierto, accesible de modo libre y gratuito a través de internet.

d) Cualquier otra forma de acceso (restringido, embargado, cerrado) deberá solicitarse expresamente y obedecer a causas justificadas.

e) Asignar por defecto a estos trabajos una licencia Creative Commons.

f) Asignar por defecto a estos trabajos un HANDLE (URL *persistente*).

4º. Derechos del autor.

El autor, en tanto que titular de una obra tiene derecho a:

a) Que la Universidad identifique claramente su nombre como autor de la misma

b) Comunicar y dar publicidad a la obra en la versión que ceda y en otras posteriores a través de cualquier medio.

c) Solicitar la retirada de la obra del repositorio por causa justificada.

d) Recibir notificación fehaciente de cualquier reclamación que puedan formular terceras personas en relación con la obra y, en particular, de reclamaciones relativas a los derechos de propiedad intelectual sobre ella.

5º. Deberes del autor.

El autor se compromete a:

a) Garantizar que el compromiso que adquiere mediante el presente escrito no infringe ningún derecho de terceros, ya sean de propiedad industrial, intelectual o cualquier otro.

b) Garantizar que el contenido de las obras no atenta contra los derechos al honor, a la intimidad y a la imagen de terceros.

c) Asumir toda reclamación o responsabilidad, incluyendo las indemnizaciones por daños, que pudieran ejercitarse contra la Universidad por terceros que vieran infringidos sus derechos e

interests a causa de la cesión.

d) Asumir la responsabilidad en el caso de que las instituciones fueran condenadas por infracción de derechos derivada de las obras objeto de la cesión.

6°. *Fines y funcionamiento del Repositorio Institucional.*

La obra se pondrá a disposición de los usuarios para que hagan de ella un uso justo y respetuoso con los derechos del autor, según lo permitido por la legislación aplicable, y con fines de estudio, investigación, o cualquier otro fin lícito. Con dicha finalidad, la Universidad asume los siguientes deberes y se reserva las siguientes facultades:

➤ La Universidad informará a los usuarios del archivo sobre los usos permitidos, y no garantiza ni asume responsabilidad alguna por otras formas en que los usuarios hagan un uso posterior de las obras no conforme con la legislación vigente. El uso posterior, más allá de la copia privada, requerirá que se cite la fuente y se reconozca la autoría, que no se obtenga beneficio comercial, y que no se realicen obras derivadas.

➤ La Universidad no revisará el contenido de las obras, que en todo caso permanecerá bajo la responsabilidad exclusive del autor y no estará obligada a ejercitar acciones legales en nombre del autor en el supuesto de infracciones a derechos de propiedad intelectual derivados del depósito y archivo de las obras. El autor renuncia a cualquier reclamación frente a la Universidad por las formas no ajustadas a la legislación vigente en que los usuarios hagan uso de las obras.

➤ La Universidad adoptará las medidas necesarias para la preservación de la obra en un futuro.

➤ La Universidad se reserva la facultad de retirar la obra, previa notificación al autor, en supuestos suficientemente justificados, o en caso de reclamaciones de terceros.

Madrid, a 20 de Junio de 2016

ACEPTA

Fdo..

Motivos para solicitar el acceso restringido, cerrado o embargado del trabajo en el Repositorio Institucional:

Declaro, bajo mi responsabilidad, que el Proyecto presentado con el título STUDY OF THERMODYNAMIC AND CHEMICAL PROPERTIES IN NON-EQUILIBRIUM FLOW IN A SHOCK TUBE en la ETS de Ingeniería - ICAI de la Universidad Pontificia Comillas en el curso académico 2015-2016 es de mi autoría, original e inédito y no ha sido presentado con anterioridad a otros efectos. El Proyecto no es plagio de otro, ni total ni parcialmente y la información que ha sido tomada de otros documentos está debidamente referenciada.

Fdo.: .... Fecha: .20 / ..06 / ...16..

Autorizada la entrega del proyecto
EL DIRECTOR DEL PROYECTO

Nick Parziale
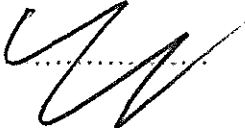
Fdo.: .... Fecha: 25 / 07 / 16...

Vº Bº DEL COORDINADOR DE PROYECTOS

José Ignacio Linares Hurtado

Fdo.: .... Fecha: ...... / ...... / ....

UNIVERSIDAD PONTIFICIA COMILLAS

ESCUELA TÉCNICA SUPERIOR DE INGENIERÍA (ICAI)

INGENIERO INDUSTRIAL

MASTER THESIS

STUDY OF THERMODYNAMIC AND CHEMICAL PROPERTIES IN NON-EQUILIBRIUM FLOW IN A SHOCK TUBE

AUTHOR: Alejandro Blanco Hurtado

DIRECTOR: Nick Parziale

MADRID, June 2016

ESTUDIO DE LAS PROPIEDADES TERMODINÁMICAS Y QUÍMICAS DE
FLUJOS EN NO-EQUILIBRIO EN UN TUBO DE ONDAS DE CHOQUE

Autor: Blanco Hurtado, Alejandro.

Director: Parziale, Nicholaus.

Entidad Colaboradora: Stevens Institute of Technology.

RESUMEN DEL PROYECTO

1. Introducción

El desarrollo de la aeronáutica y vuelos espaciales ha sido desarrollado por un impulso científico necesario: el deseo de volar más rápido y más alto. El propósito de este proyecto es la construcción de un tubo de ondas de choque para evaluar los efectos termodinámicos y químicos en el flujo no-equilibrio de un modo experimental, tratando de dar un mejor enfoque en el flujo hipersónico para futuras investigaciones sobre este tema. Aparte del interés en la aeronáutica, este trabajo también tiene aplicaciones en campos tales como la combustión, aplicándose a su vez a la reacción de los flujos y las detonaciones.

2. Estado del arte

Un tubo de ondas de choque es un dispositivo para la generación de alta temperatura y alta presión de una manera controlada, con el fin de desarrollar un estudio de las propiedades químicas y termodinámicas de los gases atravesado por una onda de choque. El principio de funcionamiento es el siguiente: una onda de choque se propaga a través de la sección de baja presión como consecuencia de la ruptura del diafragma. El gas se calienta y comprime por la acción de la onda de choque. Una

vez que la onda de choque alcanza el extremo del tubo se refleja, por lo que el fluido eleva su temperatura y presión incluso más, haciéndose estacionario. Esta parte del tubo se utiliza para la visualización de efectos termodinámicos y monitorización de los parámetros deseados. Por otro lado, después de la ruptura del diafragma, los gases de separan por una superficie de contacto que viaja en la dirección de la onda de choque, pero a una velocidad más baja. Su velocidad y la presión vienen dadas por las condiciones iniciales de los gases. También un conjunto de ondas de expansión se propagan a través de la sección de alta presión. La Figura 1 muestra la distribución de las diferentes ondas y su velocidad.

3. Diseño de la facilidad

La siguiente figura muestra una representación gráfica de la instalación, donde se pueden identificar los diferentes subsistemas:estructura, tubo, instrumentación y el diafragma:
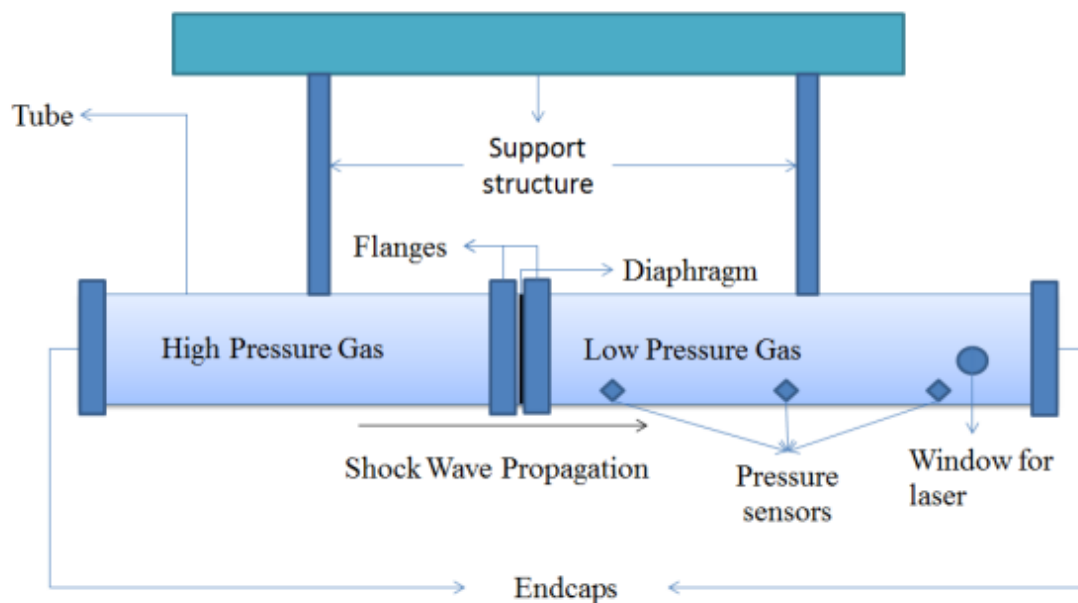

Figure 1: Representación esquemática del sistema

4. Modelo - Flujo en no-equilibrio tras la onda de choque

El primer paso para entender el comportamiento de los gases en el tubo es estudiar y predecir la presión y la velocidad de la superficie de contacto. Con el fin de obtener las relaciones que rigen tanto la presión como la velocidad, lo primero es suponer que las velocidades y la presión en cada lado de la superficie de contacto son iguales. El siguiente paso es expresar la velocidad en función de la presión (2-3). Es decir, la representación los estados posibles de 1-2 y de 4-3. La solución es la intersección entre las dos curvas.

La segunda parte del estudio es el desarrollo de las propiedades termodinámicas en el flujo congelado y en equilibrio. Los resultados para la capacidad calorífica a volumen constante C_V, capacidad calorífica a presión constante C_p, fracción molar, entalpía y la energía interna serán comparados con los resultados proporcionados por Cantera. Cantera es un software de cinética química que resuelve flujos químicos, además de evaluar las propiedades químicas y termodinámicas.

Finalmente se llevará a cabo un análisis sobre las propiedades del gas en no-equilibrio después de la onda de choque.

5. Resultados y discusión

Los gráficos representados son la presión-velocidad de la superficie de contacto y las comparaciones entre los resultados de mecánica cuántica y Cantera para flujo congelado y en equilibrio.

El aspecto más importante del proyecto es la variación de la temperatura de traslación, de rotación y de vibración. La temperatura de traslación y rotación se considera instantánea al equilibrio. Por lo tanto, su valor inicial es el de la relación de temperatura después del choque. La temperatura de vibración necesita más tiempo, ya que las

colisiones necesitan tiempo para ocurrir. Cuando se alcanza el equilibrio, las tres temperaturas convergen al mismo valor. También se monitoriza la velocidad, presión, densidad y entalpía del gas.
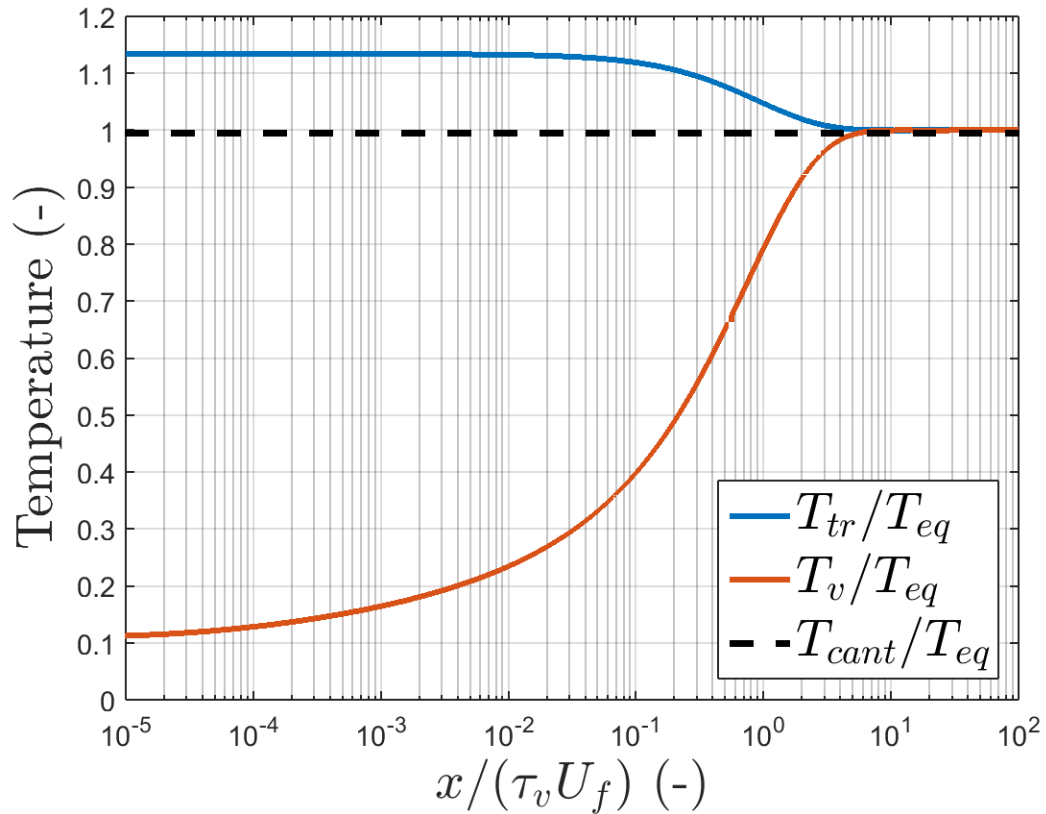

Figure 2: Variación de las temperaturas de translación/rotación y de vibración después de la onda de choque

6. Conclusiones

El diagrama de presión-velocidad ha mostrado todos los estados de los gases para las condiciones dadas. La velocidad y la presión de la superficie de contacto (región que separa ambos gases) se han estimado, mostrando que sus valores estuvieron en el rango esperado, entre las presiones de ambos gases y por debajo de la velocidad de la onda de choque.

El estudio ha probado y comparado diferentes formas de calcular las propiedades termodinámicas. Se ha demostrado cómo el software Cantera y las ecuaciones de la mecánica cuántica (utilizado para el cálculo del proyecto) concuerdan con gran precisión (aproximadamente 95 %). El efecto de la disociación y la presencia de la energía de vibración se ha medido y controlado. Para las condiciones iniciales dadas en la sección de baja presión (10 torr y temperatura ambiente), la disociación tuvo lugar para número de Mach 8, que se corresponde con una temperatura de post-on de choque de 4000 K. Este efecto también se pudo apreciar en el gráfico C_V , donde las comparaciones entre ecuaciones y Cantera ya no eran tan precisas para $T > 4500K$.

La última sección del proyecto, en el que convergieron todos los temas presentados antes, explicó el comportamiento transitorio en no equilibrio después de la onda de choque. Mediante el control de la temperatura de traslación / rotación y vibración, se ha podido apreciar cómo la temperatura de vibración comenzó a aumentar y alcanzar el valor de equilibrio. La distancia de equilibrio puede visualizarse fácilmente ejecutando el *script* correspondiente. Aparte de eso, la energía interna de traslación y de rotación se ve que es más del 80% de la energía interna total, en el que el resto corresponde a la energía vibracional.

Teniendo en cuenta que el proceso de no equilibrio es isobárico, se ha visto cómo la densidad y la velocidad del gas aumentado debido a los cambios en la temperatura y la energía interna. La energía interna también se controló y se comparó con la entalpía total, argumentando que representa más de 75% de su cantidad total.

Al final del apartado de resultados se ha mostrado la variación de la distancia de relajación y el número de Mach en función de la relación de presión. Si bien se encontró que la variación de la distancia de relajación no seguía un patrón especifico (ya que la distancia de relajación depende también en otros parámetros, como la

temperatura de los diferentes gases), el número de Mach mostró un comportamiento claramente exponencial. Es decir, cuanto más grande era la diferencia de presiones, más grande era el número de Mach. Como se explica en el informe, el número de Mach dentro de un tubo de choque representa la fuerza del choque.

Aunque este proyecto pretende dar una explicación teórica el efecto de la dinámica de gases en no-equilibrio, nuevos estudios e investigaciones experimentales deben llevarse a cabo.

Una vez finalizado el tubo de ondas de choque, la comparación entre los resultados teóricos y experimentales se realizarán. La exactitud de las predicciones podría evaluarse y se podrían conseguir mejores resultados.

También se debe investigar más sobre la constante de relajación de vibración tau. Es uno de los componentes cruciales en la predicción de la distancia de relajación vibracional, por lo que hay una gran necesidad de estudiarla profundamente. También los resultados experimentales ayudarán a evaluar la exactitud del modelo de Millikan-White.

STUDY OF THERMODYNAMIC AND CHEMICAL PROPERTIES

IN NON-EQUILIBRIUM FLOW IN A SHOCK TUBE

Author: Blanco Hurtado, Alejandro.

Director: Parziale, Nicholaus.

Collaborating Entity: Stevens Institute of Technology.

PROJECT SUMMARY

1. Introduction

The development of aeronautics and spaceflight has been driven by one primary urge: the desire of flying faster and higher. The purpose of this project is the construction of a shock tube to evaluate the thermodynamic and chemical effects in non-equilibrium flow in an experimental way, trying to give a better approach on hypersonic flow for future research on this topic. Apart from the aeronautics interest, this work also has applications in fields such as combustion where it can be applied to reacting flows and detonations.

2. Literature review

A shock tube is an ideal device for producing high temperature, high pressure conditions in a controlled and repeatable way for the study of the chemical and thermodynamic properties of gases when being traversed by a shock wave. The working principle is that a shock wave propagates though the driven (low pressure) section as a consequence of the rupture of a diaphragm. The test gas (driven gas) is heated and compressed by the action of the shock wave. Once the shock wave reaches the end of the shock tube it is reflected, making the fluid even raise its temperature and pressure

but making it stationary. This part of the tube (near the end wall) is the one used for visualizing the thermodynamic effects and monitoring desirable parameters with transducers or other tools . On the other hand, after rupturing of the diaphragm, the driver and driven section is separated by a contact surface traveling on the direction of the shock wave but at lower speed. Its speed and pressure are given by the initial conditions of the different gases. Also a set of expansion waves are propagated through the driver section. Figure 1 shows the distribution of the different waves and their velocity (as a function of x-t diagram) within the shock tube.

3. Experimental Setup

Next figure shows a graphical display of the facility, where the different subsystems can be identified. They are support structure, tube, instrumentation and diaphragm section:
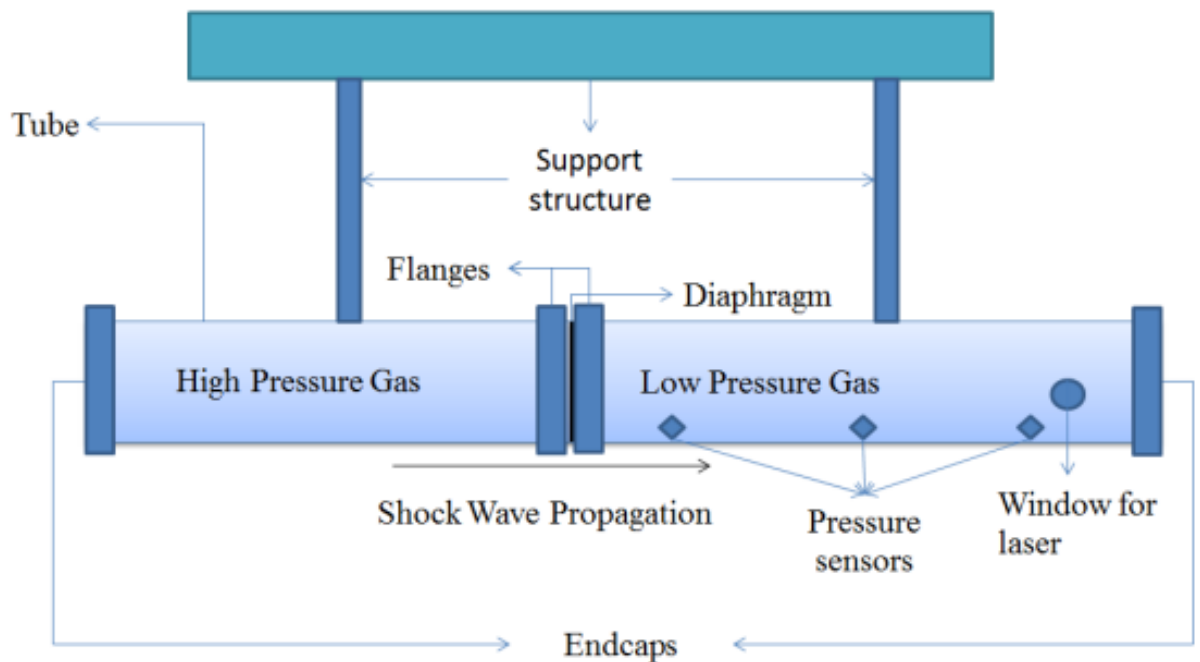
Figure 3: Graphical layout of the system

4. Model - Flow behind shock in vibrational non-equilibrium

First step to understand the behavior of the gas-dynamics in the shock tube is studying and predicting the pressure and velocity of the contact surface. In order to obtain the relations that govern both pressure and velocity, the first step is assuming that velocities and pressure in each side of the contact surface are equal. Next step is arranging the equation velocity-pressure for each of the regions (2-3). That is, plotting all possible states from 1-2 and for 4-3. The solution is the intersection between the two curves.

The second part of the study is the development of the thermodynamic properties in frozen and equilibrium flow. The results for the heat capacity at constant volume C_v, heat capacity at constant pressure C_p, mole fraction, enthalpy and internal energy will be compared with the results provided by Cantera. Cantera is a chemical kinetics software that solves chemically reacting flows, evaluating the properties and chemical source terms of the flows.

Finally a deep analysis on the non-equilibrium gas properties after the shock wave will be conducted.

5. Results and discussion

Graphs is for representing the pressure-velocity of contact surface and comparisons between quantum-mechanics and Cantera results for frozen and equilibrium flow are included.

The most important aspect of study is the variation of the translational, rotational and vibrational temperature. The translational and rotational temperature are considered to be instant to equilibrium. Thus, their initial value is the one for the temperature relation after the shock. The vibrational temperature needs more time,

as the collisions need time to occur. When equilibrium is reached, the three temperatures converge to the same value. Besides, the variation of velocity, pressure, density and enthalpy are also monitored.
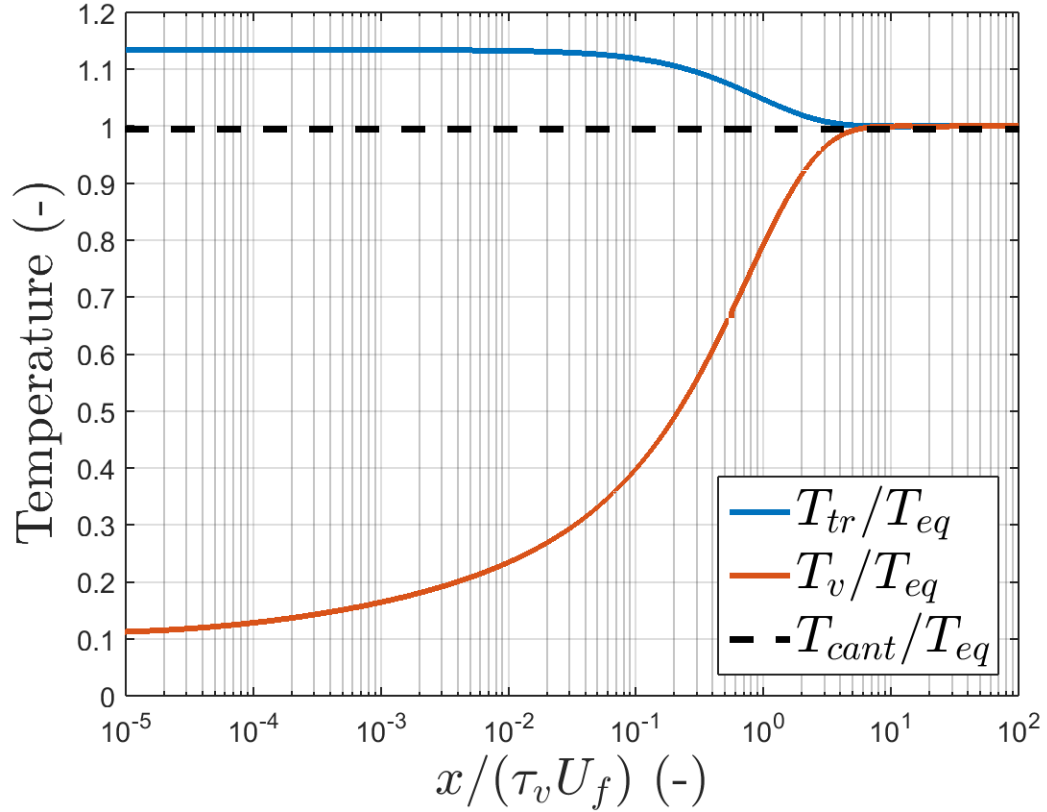

Figure 4: Variation of translational/rotational and vibrational temperature after the shock front

6. Conclusions

The pressure-velocity diagram showed all different states withing the gases for specified given conditions. The velocity and pressure of the contact surface (region that separates both gases) were estimated, showing that their values fell in the expected range, between the driven-driver pressure and below the shock wave velocity.

The study continued testing and comparing different forms of computing the thermo-

dynamic properties. It was shown how software Cantera and the quantum-mechanics equations (used for the computation of the project) matched with great accuracy (approximately 95%). The effect of disassociation and the presence of the vibrational energy was measured and monitored. For given initial conditions in the driven section (10 torr and room temperature), disassociation happened for Mach number of 8, which corresponds with a post-shock temperature of 4000K. This effect could also be appreciated in the C_v graph, where the comparisons between equations and Cantera was no longer accurate for $T > 4500K$.

Last section of the project, in which converged all topics presented before, explained the non-equilibrium transient behavior after the shock wave. By monitoring translational/rotational and vibrational temperature, it could be appreciated how vibrational temperature started increasing and reaching the equilibrium value. The equilibrium distance can be easily displayed by running the corresponding script. Apart from that, the translational and rotational internal energy was seen to be more than 80% of total internal energy, where the rest corresponds to the vibrational energy.

Considering the process in non-equilibrium to be isobaric, it was seen how density and velocity of the gas increased due to the changes in temperature and internal energy. Internal energy was also monitored and compared to the total enthalpy, computing that it represents over 75% of its total quantity.

Last aspect of results showed the variation of relaxation distance and Mach number as a function of pressure ratio. While the variation of relaxation distance was found not to follow a specified patter (as relaxation distance also depends in other parameters, such as temperature of the different gases), Mach number showed a clear exponential behavior. That is, for larger differences in driven and driver pressure (smaller ratio), the Mach number was bigger. As it was explained in the body of the report, the

Mach number within a shock tube represents the strength of the shock.

Although this project aimed to give a theoretical predictions on the effect of non-equilibrium gas dynamics, further studies and experimental research must be conducted.

Once the shock tube is finished, comparison between theoretical and experimental results must be done. The accuracy of the predictions could be evaluated and better results could be achieved.

More research must also be completed when dealing with the vibrational relaxation constant τ. It is one of the crucial components when predicting the vibrational relaxation distance, so there is a huge necessity on deeply studying it. Also the experimental results will give an approach on how good this Millikan and White expression is.

STUDY OF THERMODYNAMIC AND CHEMICAL PROPERTIES IN

NON-EQUILIBRIUM FLOW IN A SHOCK TUBE

by

Alejandro Blanco Hurtado

A THESIS

Submitted to the Faculty of the Stevens Institute of Technology
in partial fulfillment of the requirements for the degree of

MASTER OF ENGINEERING - MECHANICAL

Alejandro Blanco Hurtado, Candidate

ADVISORY COMMITTEE

Nicholas J. Parziale, Advisor   Date

Alexander de Rosa, Reader   Date

STEVENS INSTITUTE OF TECHNOLOGY
Castle Point on Hudson
Hoboken, NJ 07030
2016

STUDY OF THERMODYNAMIC AND CHEMICAL PROPERTIES IN NON-EQUILIBRIUM FLOW IN A SHOCK TUBE

ABSTRACT

The development of aeronautics and spaceflight demand a deeper study on hypersoic flow, where the effect of non-equilibrium flow after the shock-wave front plays a crucial role. This project gives an approach on how the parameters of interest in themodynamic and chemical gas-dynamics vary within the relaxation distance. After an introduction compiling latest research and operating principle of shock tubes, the report presents the results obtained by the combination of different softwares (Cantera, Matlab), showing the evolution and rate of change of the parameters during non-equilibrium flow. Results for disassociation and vibrational energy guide the results for high Mach numbers and post-shock temperature. Besides, while the translational/rotational temperature (instantaneous to equilibrium) decrease until equilibrium is reached, vibrational temperarure and energy increase due to the collisions of molecules. Density and velocity of the gas increase over 15% in the isobaric process of non-equilibrium. Mach number, indicator of the strength of the shock wave, follows an exponential curve for different pressure ratio between the driver and diven pressure. In order to test these predictions and compare with experimental data, the shock tube was constructed at the same time this study was conducted, so future experiments will be very useful for the better undestanding of these phenomena.

Author: Alejandro Blanco Hurtado

Advisor: Nicholas J. Parziale

Date: May 30, 2016

Department: Mechanical

Degree: Master of Engineering - Mechanical

Acknowledgments

I would like to thank Professor Nick Parziale for his guidance and passion during the whole project. His mentoring and patient impulsed me to understand the advanced topics of the project, as well as transmitting the novelty and interest on the different aspects of the work. I would also like to thank my advisor Frank Fisher for helping me find this fantastic group and introducing me to Stevens Institute of Technology.

Professor Alexander de Rosa, Nick Parziale and the group of senior students; Ryan Chu, Jonathan Escobar, Luke Hillers, Muhammad Mustafa and Eric Oswin, did a fantastic job buliding the shock tube, which will serve for future experiments in the University.

Lastly, I would like to thank my family and friends for their support. From Spain or United States, I felt their confidence and love during this year as an exchange student.

Table of Contents

List of Tables

List of Figures

List of Symbols

A Slope for relaxation time computation, (-)

γ Ratio of specific heats, (-)

ρ Density, (kg/m^3)

P Pressure, (Pa)

t Time, (s)

τ Relaxation time, (s)

C_p Heat capacity and constant pressure, (J/(kgK))

C_v Heat capacity and constant volume, (J/(kgK))

R Universal Gas Constant $((Pa\ m^3)/(kg\ mol\ K))$

T Temperature, (K)

M Mach Number, (-)

U Velocity, (m/s)

x Distance, (m)

e Internal energy, (J/kg)

h Enthalpy, (J/kg)

Θ Characteristic temperature of vibration, (K)

h Planck constant, (m^2kg/s)

ν Frequency of vibration, (s^{-1})

k Boltzmann constant, (m^2kg/s^2K^{-1})

μ Weighted molecular weight, (kg/kmol)

Chapter 1

Introduction

1.1 Background

The development of aeronautics and spaceflight has been driven by one primary urge: the desire of flying faster and higher. During the 20th century there has been an exponential growth in both speed and altitude, starting from the first elementary aircrafts to the latest more advanced rockets and hypersonic airplanes.

Therefore, the study of hypersonic flow has nowadays turned crucial in order to predict the behavior of fluids traveling at supersonic speed. In fact, as experts explain, hypersonic flow will dictate many of the new exciting vehicle designs for the 21st century.

Recent studies during the last decades have been conducted based on high-temperature gas dynamics, where sudden changes in temperature and pressure, as well as chemical reactions in the testing gases have taken place. These studies were focused mainly on the equilibrium value that these magnitudes take after the chemical reactions.

The purpose of this project is the construction of a shock tube to evaluate the thermodynamic and chemical effects in non-equilibrium flow in an experimental way, trying to give a better approach on hypersonic flow for future research on this topic. Apart from the aeronautics interest, this work also has applications in fields such as combustion where it can be applied to reacting flows and detonations.

1.1.1 Background of the problem

Existing studies concerning non-equilibrium flow are not as deep and accurate as aeronautic engineering demands. In fact, most of these studies relate with the equilibrium value of the thermodynamic and chemical properties, excluding the non-equilibrium regime before reaching the steady state conditions; but, what happens in the small region after the shock wave front?

There is a small distance, characterized by the time constant and the initial properties, where the density, velocity and temperature (among other fluid's properties) suffer sudden changes. That is one of the topics of study in the project, where these magnitudes will be theoretically monitored for future experimental data to be taken.

These tests will be conducted from the first problems of interest and expanding it to monitor the whole behavior of the test gas inside the shock tube. Comparisons between the values obtained and the ones given by software Cantera, which predicts the equilibrium values of certain gas properties, will be given.

1.2 Goal of the work

The purpose of this project is modeling and studying the thermodynamic and chemical properties in non-equilibrium flow in an experimental way, trying to give a better approach on hypersonic flow for future research on this topic. At the same time, the construction of a shock tube will be performed in order to evaluate these properties in an experimental way afterwards.

First, the theoretical study will be held in order to predict the behavior of the driven gas in the shock tube when being zapped by the shock wave. After carrying all the

desirable research, the theoretical data will be compared with the experimental results obtained by the facility. These results could serve as a basis for future research on hypersonic flow.

1.3 Scope of the work

The work will be focused on the study of different parameters that characterize hypersonic flow, starting with the pressure-velocity diagram of the contact surface. After this, the post-state gas properties will be studied and compared with the values given by Cantera, the Matlab tool used in this project to predict the parameters of interest. The vibrational rate and non-equilibrium properties after the shock will conduct the main part of the project.

In order to investigate and measure these characteristics values, the governing equations will be analyzed and tested by varying the initial conditions of the problem.

1.4 Report structure

The report is divided into different chapters which are focused on various aspects of the non-equilibrium flow characteristics. After the introduction on this first chapter, Chapter 2 explains the different aspects concerning the shock tube: its history, development, principle of operation and parameters of interest when carrying experiments. Results on recent studies on shock waves within shock tubes will be displayed in order to state the current situation of the investigations. Chapter 3 presents the instrumentation and elements of the facility in which the experiments are carried out (shock tube), giving a brief explanation on the subsystems and components that form the device. Different pictures of the shock tube will be provided. Chapter 4 presents s the

software and instrumentation. It also explains the resources and methodology used to obtained the desirable theoretical results. After that, Chapter 5 will display the results of the experiments presented on Chapter 3, comparing the results and setting a milestone for future research. Conclusions and recommendations for further work will be finally exposed on Chapter 6. At the end of the project, MatLab files used to perform the different graphs for each set of results will be exposed in the appendix.

Chapter 2

Literature review

2.1 History and development of the shock tube

Interest in high-temperature gasdynamics has been present in science news for more than a hundred years. Different devices have served scientists to study the variation in temperature and pressure caused by sudden supersonic acceleration of fluids. One of the most accurate and useful is the shock tube. Vieille's was first constructed by Paul Vieille in 1899, who conducted studies on combustion and detonation in tubes.[4] This discovery was brought about earlier experiments and studies made by Sir George Stokes[5] in 1848 and the French physicists Mallard, Le Chatelier and Berthelot and Vieille himself in 1881. Stokes studied the intensity and instability of a sound wave of finite amplitude produced by an explosion.[5] On the other hand, the French physicist detected the deflagration-detonation transition in the flame propagation when filling a tube with combustible mixture.[4]

Roughly, a shock tube is an apparatus that consists on a simple duct which may be either closed or opened at one end and closed at the other. It is divided into two different chambers (driver and driven) separated by a diaphragm. Each chamber contains a gas at different pressure; the driver gas at high pressure and driven gas at low pressure. When the diaphragm is ruptured, a shock wave is propagated through the driven (low pressure) chamber due to the pressure difference between the two compartments. Following the rupture of the diaphragm, a set of expansion waves are propagated through the driver section (high pressure). A contact surface serve as the separation of the two different gases in each chamber, which keeps moving in the

direction of the shock wave at a lower velocity.[6]

The first prototype of shock tube achieved by Vieille, it had a diameter of 22 mm and a length of 6 meters. He recorded Mach number of 2 with a pressure difference of 2 MPa (20 atm). in the driver section and air at atmospheric pressure in the driven section. Afterward, the Austrian scientist Kobes developed the theory of origination of a shock wave, and with the help of Hubert constructed a shock tube of 10 meters of length in 1932.[6]

The first pure shock tube was not achieved until the British scientist Payman and Shepherd designed it. They were motivated by the necessity of studying the explosion and combustion problem in UK mines.[7] In fact, it was the first shock tube consisting on a diaphragm that broke as a result of the pressure difference of the two chambers. Investigations on the thickness and length of the diaphragm and sections were carried. Besides, this invention led the U.S. and Canadian scientists to build a system of shock tubes to begin research on hypersonic gasdynamics in 1940.

During and after the Second World War, the most prestigious universities, laboratories and government institutions developed deeper studies on shock tubes for aeronautical research.[5] At the same time, different countries in Europe joined this innovative technique and starting contributing to the development of it. Particularly, B.D. Henshall defended his doctoral thesis on shock tubes at Bristol University (Great Britain) in 1952.[7] Afterward, the German scientist Hubert Schardin continued performing work in 1958, as well as other countries around the world. He is considered one of the pioneers of shock tubes as he did many breakthroughs on measuring devices.[7]

In 1957, the U.S. Air Force and Navy held the First Symposium on Shock Tubes,[4] which in 1967 became international and has been held every two years for fifty years

now. Also in the 50s, the USSR showed interest in hypersonic flow and shock tubes, operating successfully at Moscow State University and different institutes in the USSR. Soloukhin, a member of the USSR Academy of Science, dedicated himself to study the optical diagnostics of shock-wave processes. Voevodskii and he[4] recorded the period of induction in ignition using high sensitive interferometer. In general, all these studies were motivated by the necessity of creating quicker and more powerful aircraft.

Studies in the 70s and 80s were conducted based on gasdynamics lasers. They are basically high-power converters of thermal energy into the energy of light emission, behaving as thermal methods of excitation. They simulated the effect of a shock wave exciting the test gas and suddenly increasing its temperature and pressure, producing a rapid adiabatic expansion.[8]

In the recent years there have been advancements in the field of shock tubes, working on software to simulate the behavior of shock waves. Also increasing test times has been achieved and it has turned very important for studying the temperature and pressure variations.[4]

At present, only optical methods are applicable to shock tubes in order to carry the flow analysis. To elevate shock tubes above supersonic tunnels as the premier tool for studying hypersonic flow and aerodynamic research, developments to measure the transient forces must be achieved. However, shock tubes actually offer an economic and accurate way of demonstrating and investigating the steady and non-equilibrium thermodynamic phenomena.[9] They can only keep gaining adaptability by continuing researching on them and performing experiments.

2.2 Recent studies on shock tubes

Apart from explaining the history of shock tubes from its beginning to what it is known nowadays, it is also important to do research on the latest experiments and investigations with shock tubes.

Hanson et Al.[10] studied combustion chemistry applying recent advances in laser absorption and shock tube methods. By reducing the test times (<50ms), high-bandwidth measurements of time-histories can be taken and new kinetics target data can be achieved. Their work concluded that CO_2 laser absorption had the ability of capturing reaction modes and measuring heat release. Measurements on the change of temperature at constant pressure can be related with the bond energy (chemical contribution to enthalpy change). They also suggested continuing with the investigation of new laser systems to provide wider wavelength coverage and measure more species in the laboratory.

Apart from this work, Hanson et Al.[11] also researched combustion kinetics with shock tube techniques. They concluded that improvements in these devices can lead to reduce uncertainty in ignition time delay. Apart from that, they suggested that improvements in shock tubes allow new studies on real fuels to investigate how jet and diesel fuels behave when compressing and changing their temperature.

Moving to a different field, Chen et Al.[12] studied the shock/boundary later interaction in a reacting flow in a shock tube. They observed that the shock front bends near the surface of shock tube due to viscous effects, causing a successively contact and reflection of the shock front at different position of the end-wall. This process generates a vertical pressure gradient near the end-wall, which contributes to the formation of the lambda-shape structure during the shock wave/boundary-layer interaction.

Finally, Andreotti et Al.[13] studied the impact response of structures in a shock tube. They used a shock tube composed of two diaphragms. Accounting for tube walls vibration, boundary layers and other minor sources of dissipation, and using a finite element model, they estimated the different contributuions to the overall efficiency of shock tubes. The two parameters of interest where the incident and reflected peak pressures. They concluded that the highest source of dissipation comes from the opening of the diaphgram.

As it can be appreciated, last research on shock tube concerned chemical reactions, structural issues and boundary layer importance in shock tubes. Then, the study of chemical and thermodynamic rate of change after the shock front turns crucial in order to predict sudden changes in gas properties.

2.3 Operating principle of a shock tube

Once reviewed the research time-line of the shock tube and last research on this device, this section gives an explanation of its operating principle: how it works and the different equations that govern its performance.

As described, a shock tube is an ideal device for producing high temperature, high pressure conditions in a controlled and repeatable way for the study of the chemical and thermodynamic properties of gases when being traversed by a shock wave. The working principle is that a shock wave propagates though the driven (low pressure) section as a consequence of the rupture of a diaphragm. The test gas (driven gas) is heated and compressed by the action of the shock wave[14] .

Once the shock wave reaches the end of the shock tube it is reflected, making the fluid even raise its temperature and pressure but making it stationary. This part of

the tube (near the end wall) is the one used for visualizing the thermodynamic effects and monitoring desirable parameters with transducers or other tools.[15]

On the other hand, after rupturing of the diaphragm, the driver and driven section is separated by a contact surface traveling on the direction of the shock wave but at lower speed. Its speed and pressure are given by the initial conditions of the different gases. Also a set of expansion waves are propagated through the driver section. Figure 2.1 shows the distribution of the different waves and their velocity (as a function of x-t diagram) within the shock tube.[1]
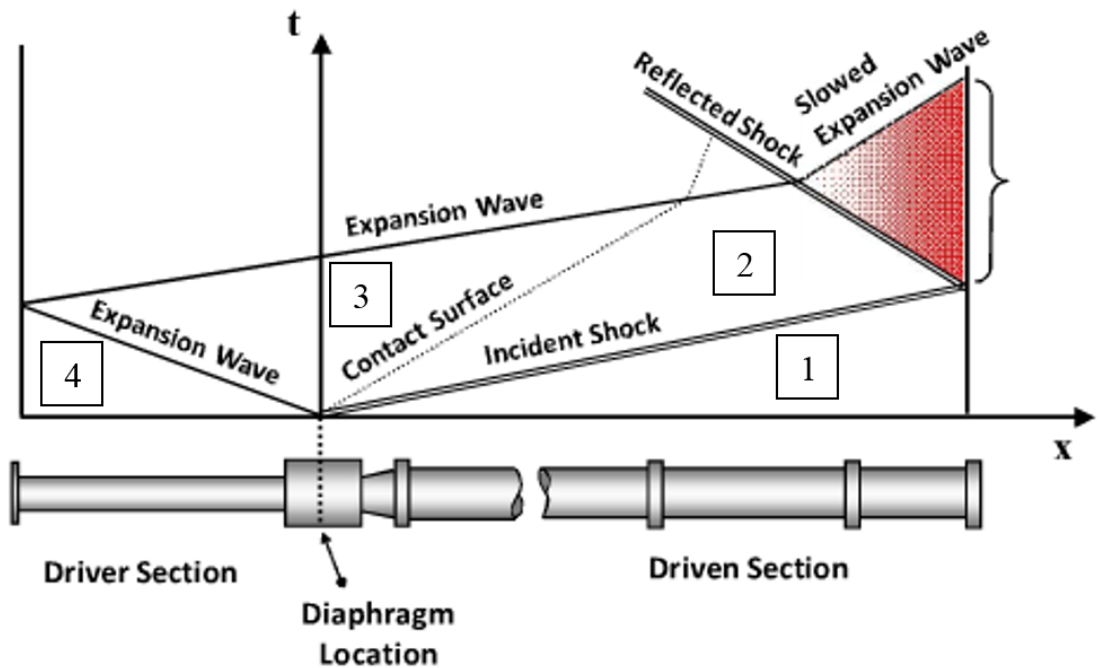
Figure 2.1: Shock tube layout and x-t diagram[1]

As seen in figure 2.1 the incident shock (shock wave) travels much faster than the contact surface (region between 2-3). When the reflected shock is produced, the gas becomes static at high temperature and pressure. The red section in the graph refers to the region in which the velocity is zero.

Next step is to explain the set of governing equations in each section of the shock tube that rule how temperature, pressure and other parameters of interest change. The analysis of the ideal behavior of a shock tube assumes:

- Initial constituents of the gas do not change.

- Flow processes are adiabatic.

- Opening of the diaphragm is instantaneous and complete.

- No reflected waves from the expansion fan overtake the contact surface.

The equations expressing the conservation of mass, momentum, and energy across a normal shock front are, respectively:

$$\rho_1 v_1 = \rho_2 v_2 \tag{2.1}$$

$$\rho_1 (v_1)^2 + p_1 = \rho_2 (v_2)^2 + p_2 \tag{2.2}$$

$$\frac{v_1^2}{2} + h_1 = \frac{v_2^2}{2} + h_2 \tag{2.3}$$

Where the coordinate system is referred to the moving shock wave, being p, ρ, h and v the pressure, density, enthalpy and velocity of the gas. Subscripts refer to the conditions expressed in figure 2.1 being 1 the initial driven section, 2 the gas behind the shock wave, 3 the gas behind the contact surface and 4 the initial driver section. Transforming these equation to the shock tube coordinates (fixed to the laboratory),

it can be defined:

$$v_1 = u_s \tag{2.4}$$

$$v_2 = u_s - u_2 \tag{2.5}$$

2.3.1 Shock-wave relations

When a shock wave takes place, viscosity and thermal conduction drive the changes that occur to the fluid being traversed. However, as the shock wave is extremely thin, a macroscopic observer appreciate the changes as being discontinuous. As the Mach number increases, the same shock relations are obtained for both supersonic aerodynamics and hypersonic speed.[2]

The jump between regions 1 and 2 is described by the Rankine Hugoniot relations. This jump is caused by the compressibility effect of the gas. For compressible flows with small turning, the flow is reversible and isentropic (no change in entropy). However, when shock waves are generated the process is irreversible and the entropy increases, and as the shock wave does not add work, there is no addition of heat and the total enthalpy is constant. From the equation of mass, momentum, energy and the state for a perfect gas, the following reactions across the shock are obtained:[14]

$$\frac{p_2}{p_1} = \frac{2\gamma_1}{\gamma_1 + 1} M_s^2 - \frac{\gamma_1 - 1}{\gamma_1 + 1} \tag{2.6}$$

$$\frac{\rho_2}{\rho_1} = \frac{2\gamma_1}{\gamma_1 + 1}\frac{1}{M_s^2} + \frac{\gamma_1 - 1}{\gamma_1 + 1} \tag{2.7}$$

$$\frac{T_2}{T_1} = \frac{[2\gamma_1 M_s^2 - (\gamma_1 - 1)][2 + M_s^2(\gamma_1 - 1)]}{(\gamma_1 + 1)^2 M_s^2} \tag{2.8}$$

$$M_2^2 = \frac{(\gamma_1 - 1)M_s^2 + 2}{(2\gamma_1 M_s^2) - (\gamma_1 - 1)} \tag{2.9}$$

Where p, ρ and T are the pressure, density and temperature, respectively, for each of the sections, M_s is the Mach number of the shock, defined in physical units as $M_s = U/\alpha$ (where U is the velocity and α is the velocity of sound at the specified gas). Finally, γ is the ratio of specific heat.

2.3.2 Expansion waves

Subsequently, after the diaphragm breaks and the shock wave is generated, a series of expansion waves are generated in the opposite direction of the shock wave. The relations between the driven (number 4 in figure 2.1) and section 3 is given by the isentropic relations were:

$$\frac{T_3}{T_4} = \frac{p_3}{p_4}^{\frac{\gamma_4 - 1}{\gamma_4}} \tag{2.10}$$

$$\frac{p_3}{p_4} = \frac{\dfrac{p_2}{p_4}}{\dfrac{p_4}{p_1}} \tag{2.11}$$

2.3.3   Contact surface

The contact surface is the name given to the interface between 2-3 in Figure 2.1 In the contact surface, there is a discontinuity in temperature and density, but the pressure and velocity are continuous (the same) between each face. Therefore, in order to calculate the pressure and velocity of the contact surface it is necessary to define the equations that govern each of the sections of the shock tube (2-3 in Figure 2.1):

$$u_3 = u_2 \tag{2.12}$$

$$p_3 = p_2 \tag{2.13}$$

Once set the conditions in the contact surface, next step is deriving the equation from last section in order to define the relations of pressure and velocities of each section of the shock tube. Hence:

Deriving equation 2.6, the velocity of region 2 is:

$$u_2 = \gamma_1 - (\frac{p_2}{p_1} - 1)(\frac{2}{\gamma_1(\gamma_1 - 1 + \frac{p_2(\gamma_1 + 1)}{p_1})})^{\frac{1}{2}} \tag{2.14}$$

And from the expansion wave relations:

$$u_3 = \frac{2\gamma_4}{\gamma_4 - 1}[1 - (\frac{p_3}{p_4})^{\frac{\gamma_4 - 1}{2\gamma_4}}] \tag{2.15}$$

As it can be appreciated from last equations, both velocities in regions 2 and 3 depend

on pressure 2 and 3. Hence, as $u_2 = u_3$ and $p_2 = p_3$, a graph can be obtained for each curve p-u, and the pressure and velocity of the contact surface can be known. This is going to be the first part of Chapter 5, results.

2.4   Difference between frozen and equilibrium flow

This section gives an approach on what frozen and equilibrium flow stand for. These terms are widely used through the body of the report, so it is important to set the differences between them.

First of all, it is important to cite that both flows, frozen and equilibrium, share an important property. They are both isentropic (ignoring friction and heat losses). Whereas in frozen flow there are no chemical changes, equilibrium flow is assumed to be reversible.[16]

Equilibrium flow implies infinite chemical and vibrational rates. Moreover, talking about local thermodynamic equilibrium implies that a local Bolzmann distribution exists at each point in the flow. That is, the energy of each species of the flow is given by a set of equations as follow. These equations will be explained in next section (Translational, rotational and vibrational energy explanation). For atoms:[2]

$$e = \frac{3}{2}RT + e_{electronic} \tag{2.16}$$

And for molecules:

$$e = \frac{5}{2}RT + e_{electronic} + e_{vibrational} \tag{2.17}$$

Apart from that, flow in local chemical equilibrium refers to the state in which the composition of the flow differs depending on the local temperature and pressure.[2]

However, such flows (chemical and thermodynamic equilibrium) never occur in nature, as all chemical reactions and vibrational energy exchange need certain number of collisions of molecules to occur.[16] Unlike last statement, where equilibrium refers to the state with infinite chemical and thermodynamic rates, such reactions require a finite period. It will be explained later, when defining the different modes of internal energy and heat capacity of fluids.[2]

The opposite of this situation is called frozen flow. In this case, reactions rates are zero, and as a result, the chemical composition of frozen flow remains constant throughout space and time.[16]

The qualitative difference between the flows can be best understood by Figure 2.2. It sketches the case in which oxygen dissociated completely. Oxygen atoms starts at a concentration of 1 ($C_O = 1$ and $C_{O_2} = 0$). When considering the equilibrium flow, as temperature decreases, atoms of oxygen will recombine forming O_2. It can be appreciated in the increasing concentration of O_2.[2]

If the expansion through the nozzle is large enough that the temperature at the exit of the nozzle is equal to the room temperature, all the initial oxygen will recombine and transformed to C_{O_2}. It can be appreciated by the solid curves in figure 2.2 c).

Apart from that, because the temperature is proportional to the translational energy, frozen flow temperature distribution is lower than for the case of equilibrium flow, as the vibrational energy for frozen flow remains constant through the process. That gives less energy to the translational and rotational energy, and thus the temperature is lower.
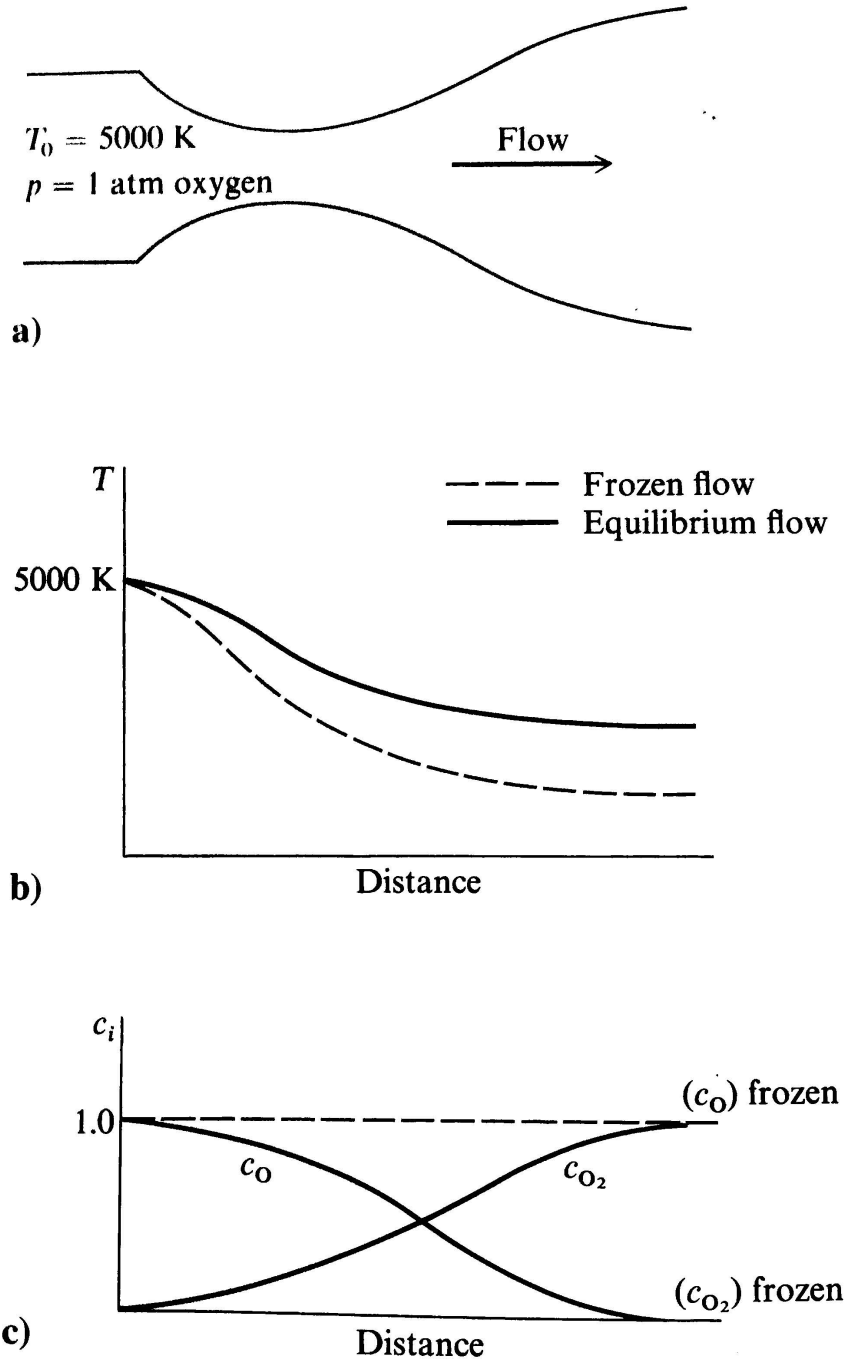
Figure 2.2: Comparison equilibrium and frozen flows through a nozzle[2]

For frozen flow, the vibrational energy remains constant through the nozzle.

2.5   Energy modes

Once reviewed the basics of shock tube, shock waves and the difference between frozen and equilibrium flow, next step is conducting a literature review on the different parameters that compose the internal energy and specific heat. This section is crucial for the better understanding of future results and research concerning the properties in the test section of the shock tube.

In the development of statistical thermodynamics, it is assumed that the gas consists of a large number of molecules, where a molecule consists on a number of atoms.[17]

Hence, the total internal energy of a molecule is composed by different energies depending on the mode of excitation. These parameters are translational, rotational, vibrational and electronic energy:[2]

$$e_{molecule} = e_{translational} + e_{rotational} + e_{vibrational} + e_{electronic} \qquad (2.18)$$

A simple concept illustrating this can be appreciated in figure 2.3:

Giving an explanation for each kind of energy:[2]

- Translational energy is sketched on Figure 2.3 b). The source of energy is the translational energy of the center of mass of the molecule. The molecule is said to have three degrees of freedom as it can move along the different dimensions of space.

- Rotating energy is sketched on Figure 2.3 c). Its source of energy comes from

a) Diatomic molecule

b) Translational energy ε'_{trans}

V_y

V_x

V_z

Source

Translational kinetic energy of
the center of mass (thermal
degrees of freedom—3)

c) Rotational energy ε'_{rot}

y

x

z

Rotational kinetic energy; (thermal
degrees of freedom—2 for diatomic;
2 for linear polyatomic; and 3 for
nonlinear polyatomic)

Rotational energy about the
internuclear axis for a diatomic
molecule is negligibly small

d)

O   C   O

CO_2; linear polyatomic molecule

O

H   H

H_2O; nonlinear polyatomic molecule

e) Vibrational energy ε'_{vib}

1. Kinetic energy
2. Potential energy

(Thermal degrees of freedom—2)

f) Electronic energy ε'_{el}

Electrons

1. Kinetic energy of electrons
   in orbit
2. Potential energy of electrons
   in orbit

Nucleus

Figure 2.3: Modes of molecular energy[2]

the moment of inertia. The diatomic molecule is said to have only two thermal

degrees of freedom as the rotation through the z axis is negligible. However, for

Alejandro Blanco Hurtado

non-linear molecules, it can be said that there are three degrees of freedom.

- Vibrational energy is given by the vibration of the atoms with respect to the equilibrium location. For a diatomic molecule, it is modeled as a spring. The sources for the vibrational energy are the kinetic energy of the linear motion and the potential energy of the intermolecular force. It has one geometric degree of freedom and two thermal degrees of freedom. Polyatomic molecules are more complex and have more degrees of freedom.

- Finally, the electronic energy has its source from the electron energy. It comes from the kinetic energy of movement of electrons and its potential energy depending on its position. However, this mode of energy is much lower than the previous, so it will be considered negligible in the tests and results of the project.[2]

For a single atom, only translational and electronic energy exists. Then:

$$e_{atom} = e_{translational} + e_{electronic} \tag{2.19}$$

2.6 Evaluation of thermodynamic properties for single chemical species

Now it is the time to assemble all previous content and evaluate the high-temperature thermodynamic properties in a single species gas. Different formulas for the translational, rotational and vibrational are given, as well as the specific heat at constant volume. Besides, this section will provide the basis for the future tests and results, where the non-equilibrium rules will be displayed.

Equations for the different modes of energy are give:

$$e_{translational} = \frac{3}{2}RT \tag{2.20}$$

Where R is the universal constant of ideal gases and T the temperature of the gas.

$$e_{rotational} = RT \tag{2.21}$$

$$e_{vibrational} = \frac{h\nu/kT}{e^{h\nu/kT} - 1}RT \tag{2.22}$$

Where h is the Planck's constant, ν the frequency and represents the rate at which the bond is pushed together and pulled apart again and k the Boltzmann constant.

Besides, recalling the specific heat at constant volume:

$$C_v = (\frac{\delta e}{\delta T})_v \tag{2.23}$$

Thus, for an atom:

$$C_v = \frac{3}{2}R + \frac{\delta e_{el}}{\delta T} \tag{2.24}$$

And for molecules:

$$C_v = \frac{3}{2}R + R + \frac{(h\nu/kT)^2 e^{h\nu/kT\,2}}{e^{h\nu/kT} - 1}R + \frac{\delta e_{el}}{\delta T} \tag{2.25}$$

Based on previous equations, the following statements can be extracted[18] [192021] [22]

- From previous equations, it is noted that both e and c_v are a function of temperature. This is true assuming the case in which the molecules are independent form each other, that is, the intermolecular forces are negligible and not considered in the equations[18] [192021] [22]

- For a gas with only translational and rotational energy, the following equations are stated[18] [192021] [22] For atoms:

$$C_v = \frac{3}{2}R \tag{2.26}$$

For molecules:

$$C_v = \frac{5}{2}R \tag{2.27}$$

That is, C_v is constant. This is the case of caloric ally perfect gases, where vibrational and electronic energy are not considered (suitable for air at room temperature, for example). However, when the gas is heated at high temperature, vibrational energy is no longer negligible and C_V becomes a function of temperature[18] [192021] [22]

- In the case in which $T \rightarrow \infty$, $C_v = \frac{7}{2}$, and again it is assumed to be constant.

- Besides, note that the internal energy also has a ground value (or zero point). However, a calculation of this zero value cannot be provided, and the results provided by equations 2.20 2.21 2.22 are the statistical thermodynamic sensible energy[18] [192021] [22]

- The theoretical l variation of C_v is sketched in figure 2.4.
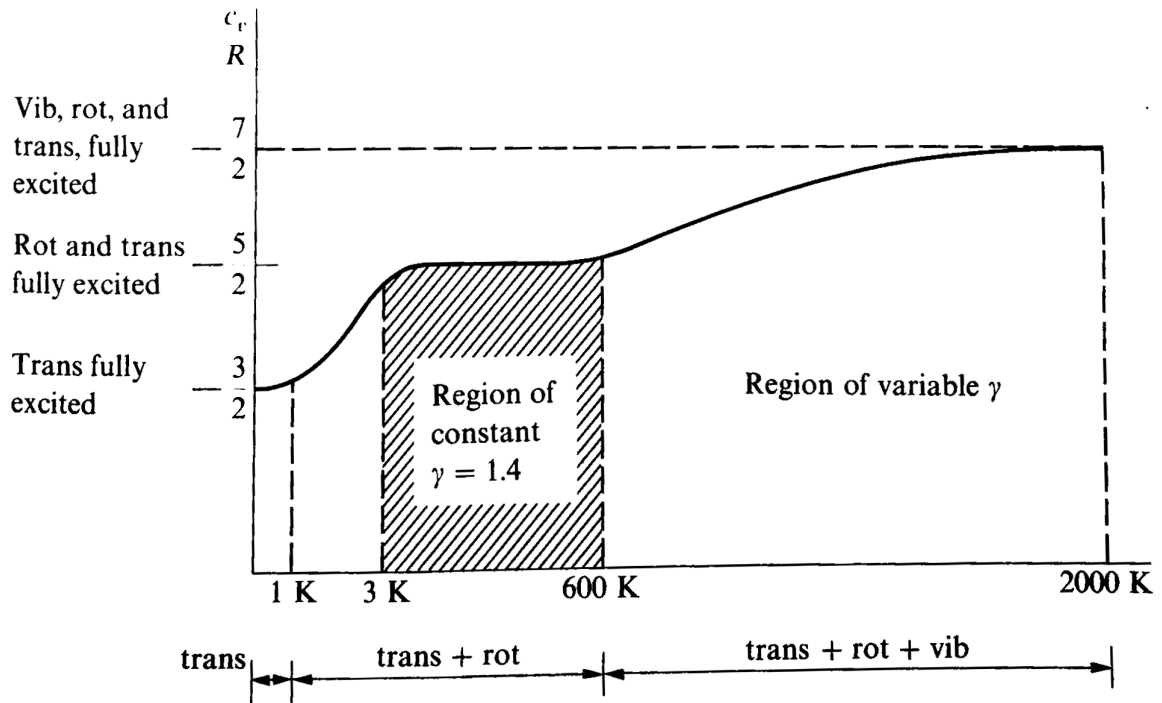
Figure 2.4: Schematic of temperature variation of the specific heat for a diatomic gas[?]

It can be appreciated that between 1-3 K rotation is the dominant energy. Translational appears from 3-600 K, where it is considered a constant region (vibrational is still negligible). However, from 600 K, vibrational energy is no longer negligible and C_V depends on the temperature of the gas. From 2000 K, chemical reactions start to occur and C_v suffer variations. These variations will be a topic of study in this project, displaying the results in future chapters of the report.

2.7 Chemical and vibrational non-equilibrium

Last section of the literature review serves to study the equilibrium values for the thermodynamic and chemical properties of reacting mixtures. However, before reaching that equilibrium value, reacting gases go through a process of non-equilibrium in which these parameters suffer several changes. This sections provides a summary of the literature review on non-equilibrium flow, which will be the based for the last set of tests in the project.

In order to situate the context of this section, let's consider a chunk of air. And let's consider that chunk of air being suddenly excited and having its temperature incremented up to 1500 K. The vibrational energy will need time to increase, and it will not be instantaneous as the collisions between molecules need time to occur. How much time need these collisions to occur and reach the equilibrium state? That is the key part of the project and the point of this section.

There are many problems in high-speed gas dynamics where the gas does not have the ability to reach equilibrium in a period of time to be considered instantaneous. And that is the typical case of the gas behind a shock front (topic of interest in this project). Its temperature and pressure are suddenly increased and the fluid (gas) starts seeking its equilibrium value.[2]

However, as reviewed before, there are different modes of internal energy, and each of them has a different time to reach equilibrium. Considering the electronic energy negligible, three modes energies are left: translational, rotational and vibrational.

Translational and rotational energy are considered to reach equilibrium instantaneously.[2]

On the other hand, vibrational energy take some time to reach equilibrium. The vibrational rate equation is defined by the next differential equation:

$$\frac{de_{vib}}{dt} = \frac{1}{\tau}(e_{vib}^{eq} - e_{vib}) \qquad (2.28)$$

Where e_{vib} is the vibrational energy in each step of integration, e_{vib}^{eq} is the equilibrium vibrational energy at the translational/rotational temperature and τ is the relaxation time, which will be explained later in this section.[2]

The physical implications of equation 2.28 can be seen as follows:

Consider a unit mass of gas in equilibrium at a given temperature. Thus, the internal energy is given by equation (considering the electronic energy negligible):

$$e_{gas} = e_{translational} + e_{rotational} + e_{vibrational} \qquad (2.29)$$

Where $e_{translational}$, $e_{rotational}$ and $e_{vibrational}$ are given by equations 2.20, 2.21 and 2.22, respectively.

Now, the unit of mass is suddenly traversed by a shock wave, increasing its temperature and pressure. As explained before, the translational and rotational energy reach the equilibrium temperature instantaneously, while the vibrational energy need more time. But, where does the energy for the collisions come from?

When this happens, the vibrational temperature increases by exchanging energy with the 'excess' of rotational and translational energy. That is, at the time the vibrational energy increases, the translational and rotational energies decrease until the three of them reach the equilibrium temperature.

This is illustrated in Figure 2.5:
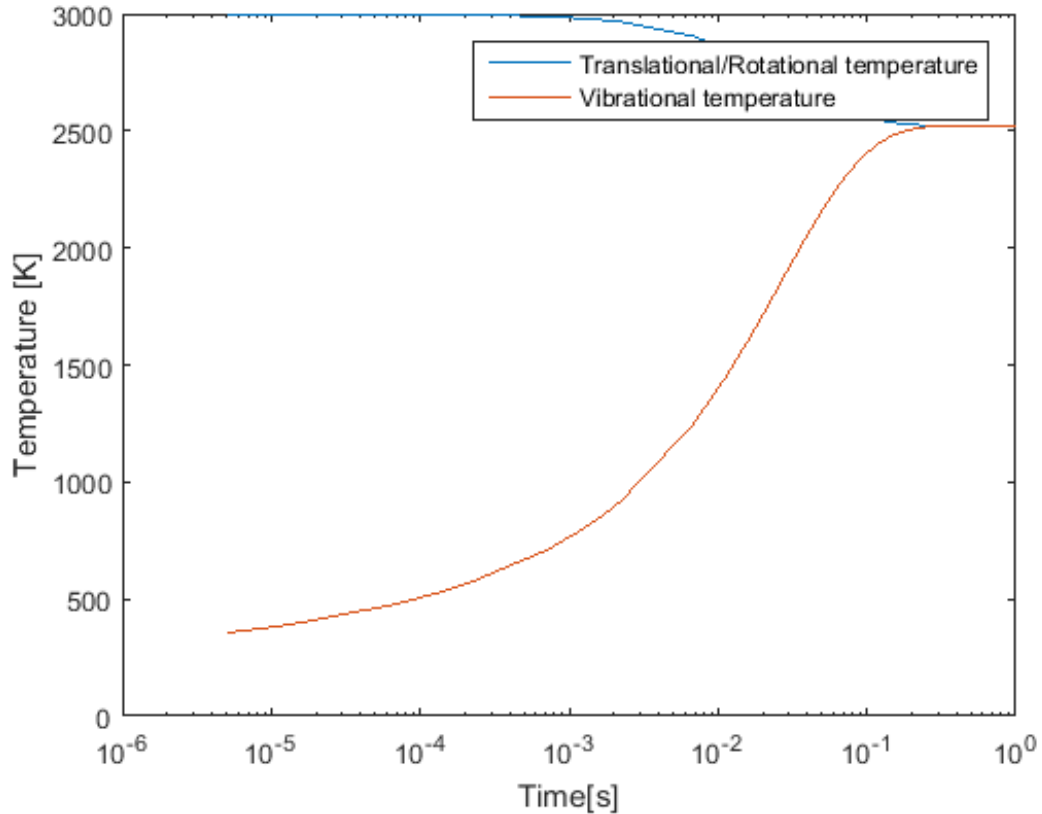
Figure 2.5: Vibrational equilibrium towards equilibrium

As it can be appreciated, the equilibrium temperature is obtained after 0.5 seconds approximately. This is the point in time in which the translational, rotational and vibrational temperatures converge to the same point. Conditions were chosen arbitrarily, as the objective was the qualitative understanding of the concept. Deeper analysis on this topic will be held in Results (Chapter 5).

Apart from that, figure 2.6, shows how the vibrational energy varies until reaching equilibrium. One may expect the vibrational energy to start being almost negligible (low temperature and no collisions) and start increasing to an equilibrium value, where all collisions have taken place and the flow is stationary in thermodynamic

sense.
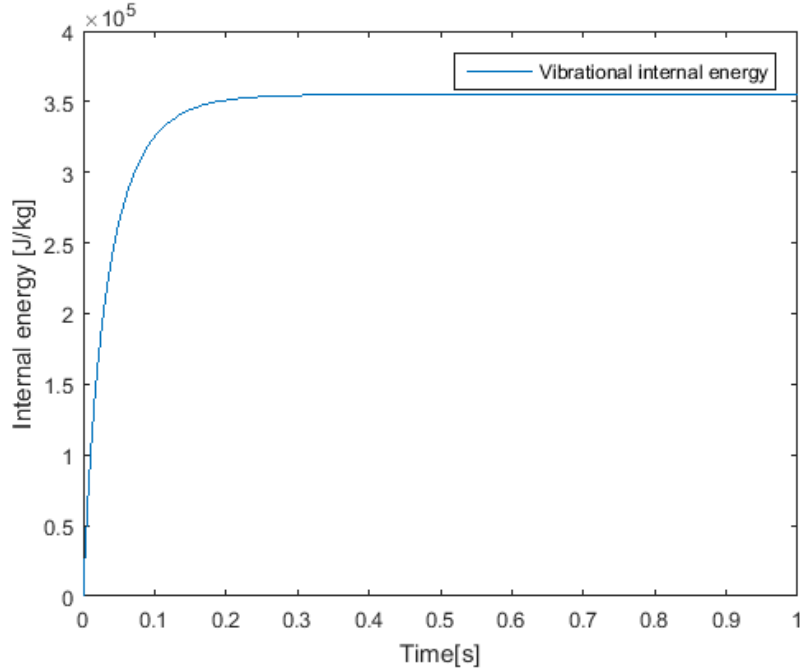
Figure 2.6: Vibrational energy variation

Once shown how translational, rotational and vibrational temperatures change, and how vibrational energy vary towards equilibrium (2.28), final step is referring to each parameters in non-equilibrium flow. These parameters are the temperature (T), vibrational relaxation time (τ) and pressure p. While the temperature and pressure of gas varies locally following the equation of continuity, momentum and energy 2.1 2.2 2.3, the relaxation time depends upon the expression used.

2.7.1 Relaxation time τ

The relaxation time expressed in equation 2.28 is a function of both local pressure and temperature, as it is a combination of the probability of collision frequency and kinetic energy of the gas.[2]

Lately, accurate data on vibrational relaxation time as a function of these parameters is becoming available, where they predict accurately the behavior of non-equilibrium flow[23] [24][25][26] .[27]

Anderson et Al.[2] states that for most diatomic gases, the variation of τ is given by the form:

$$\tau p = C_1 e^{C_2/T1/3} \tag{2.30}$$

Where C_1 and C_2 are values obtained experimentally depending on the test gas. Values for different species is given in table

Species	$C_1 atm - \mu\tau$	$C_2 K$
O_2	5.42 * 10^{-5}	2.95 * 10^6
N_2	7.12 * 10^{-3}	1.91 * 10^6
NO	4.86 * 10^{-3}	1.37 * 10^5

Table 2.1: Vibrational rate parameters

More research has been done in order to give more accurate correlations for its definition. Millikan and White[23][24][25][26][27] plotted the product of the total pressure p in atm and the vibrational relaxation time τ in a logarithmic scale against $(TK)^{-1/3}$ for different systems. The conclusion obtained by[23] was that the systems followed linear relationships . It can be appreciated in the oxygen line of figure 2.7 from 500-8000 K. Besides, for all systems the lines can converge in a common point, so it can be easy from an easy point to connect with that common point and draft the behavior at each temperature.

However, figure 2.7 was constructed by finding intersection points from the graphs O_2 and N_2. Thus, it is not completely accurate.

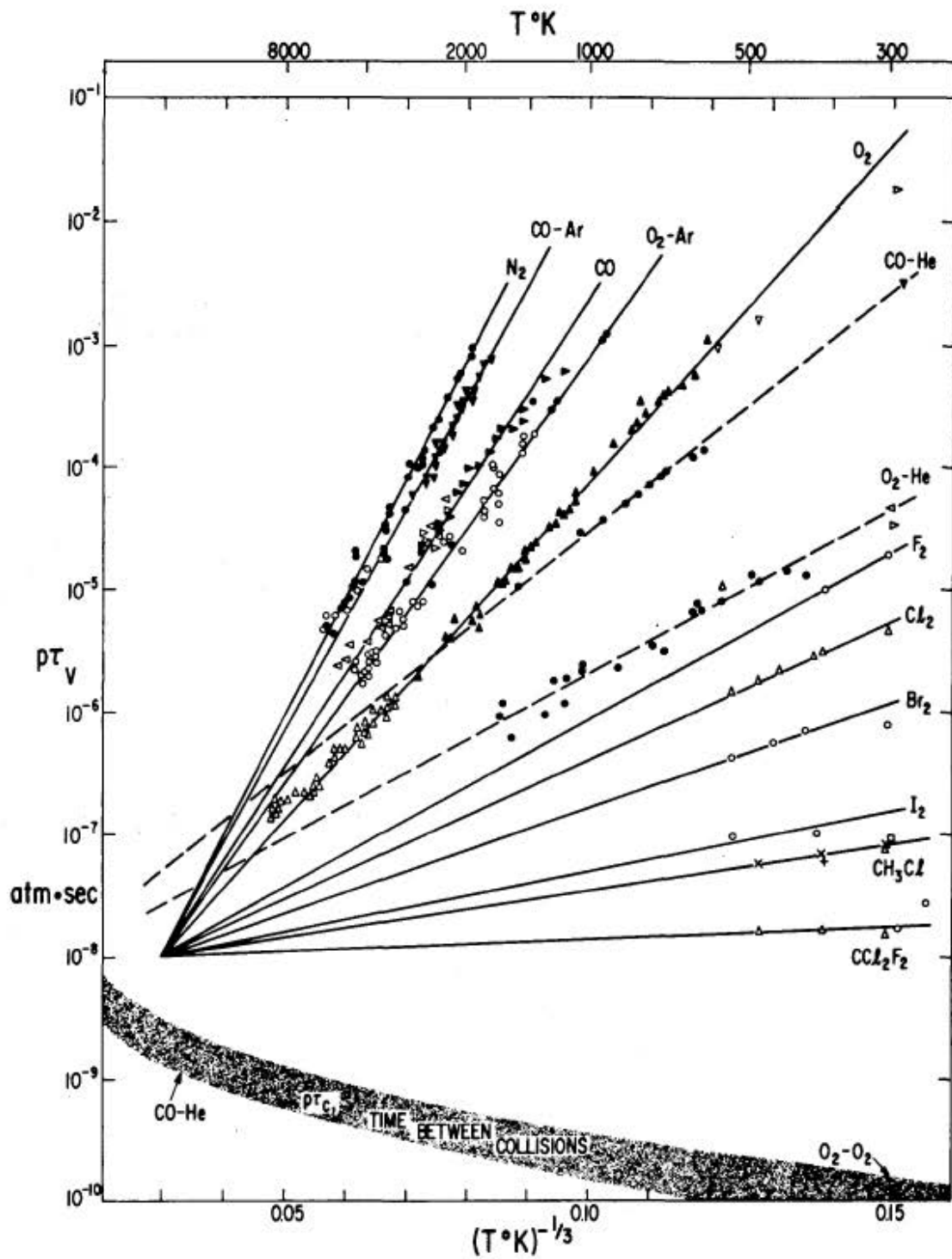Figure 2.7: Origin plot of vibrational relaxation times 2.7

A refinement of this correlations has been made in Figure 2.8. The common point has been replaced by a set of initial points:
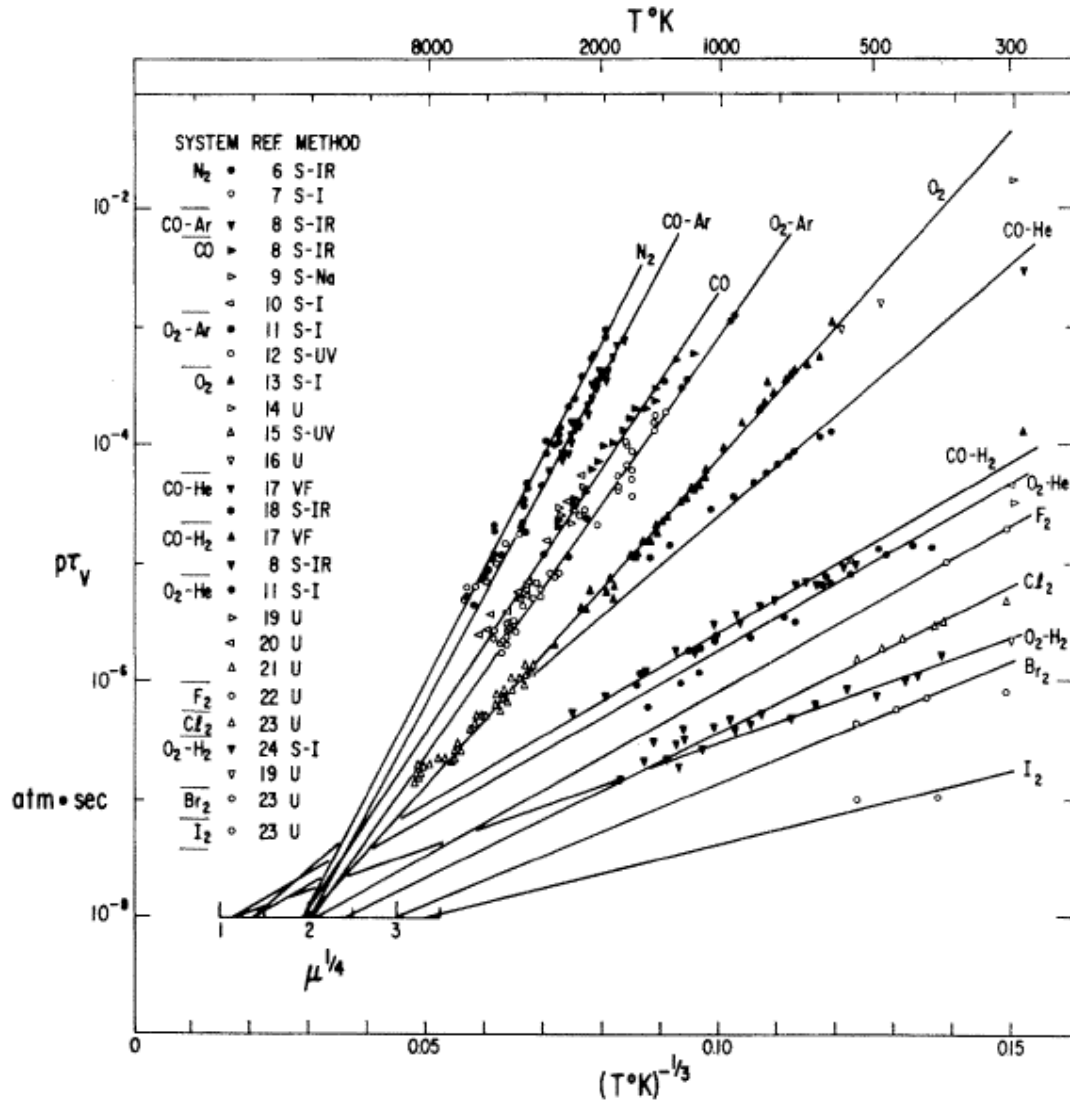
Figure 2.8: Refinement correlations for different test gases 2.7

The data lines of figure 2.8 are given by the equation[23][24][25][26][27] :

$$\tau p = exp[A(T^{-1/3} - 0.015\mu^{1/4}) - 18.42] \tag{2.31}$$

Where A the slope defined in table 2.2, T the local temperature of the gas and μ the reduced mass of the colliding pair. The slope A is presented in the following table, giving also the values for the reduced mass and characteristic temperature $h\nu/k$:

System	ν	$\theta(K)$	A (slope)
N_2	14	3395	220
CO-Ar	16.5	3080	213
CO	14	3080	175
Co-He	3.5	3080	99
CO-H_2	1.75	3080	68
$O_2 - Ar$	17.8	2239	165
O_2	16	2239	129
$O_2 - He$	3.58	2239	67
$O_2 - H_2$	1.88	2239	42
F_2	19	1284	65
Cl_2	35.5	812	58
Br_2	79.9	465	48
I_2	127	310	29

Table 2.2: Molecular data for vibrational relaxation

More recent studies have been conducted on the topic of vibrational relaxation, although they are not fully achieved[28].[29] A new correlation by Park model,[24] considering the effect due to high temperature is defined by:

$$\tau_{park} = \frac{1}{n\sigma C} \tag{2.32}$$

And he makes an addition to Millikan expression:

$$\tau_{FinalPark} = \tau_{Millikan} + \tau_p \tag{2.33}$$

As this last expression is not scientifically proven, the one that is going to be used through this project is the one in 2.8, the Millikan and White expression.

Chapter 3

Experimental Setup

This section provides an overview of the needs of the project, as well as the design considerations and pictures of the shock tube. The different sections that compose the shock tube will be briefly explained, ending with updated pictures of the facility.

3.1   Needs of the shock tube

The shock tube will serve for carrying on experiments and research by the professors of the mechanical department of Stevens Institute of Technology and graduate research staff. There were several requirements to ensure the viability of the project and accuracy of the results. These requirements involved aspects related with the materials, support structure and mounting for instrumentation:[30]

- In order to ensure that the shock speed is constant, the shock tube dimensions must not permit a laminar flow to become fully developed.

- The shock tube is constructed with PVC, with a full length of approximately 6 meters including driver section, diaphragm and driven section.

- Shock tube driver section must withstand a pressure of $1 * 10^6$ Pa, while the driven section must be able to evacuate up to 133 Pa.

- Driver and driven sections must be hermetic in order to achieve the desirable pressures and avoid leakage and loose of pressure and temperature due to the contact with the ambient. They must also be detachable to allow access to the diaphragm section.

3.2 Design overview

As explained in the literature review, the shock tube consists of the driver and driven section, separated by the diaphragm section. Apart from these subsystems, the construction of the shock tube needed from a support structure to hold the facility and the instrumentation to carry on the experiments. Next lines support a brief explanation on each of the subsystems.[30] Figure 3.1 shows a graphical display of the facility, were the different subsystems can be identified. They are support structure, tube, instrumentation and diaphragm section, which will be analyzed in the following lines:
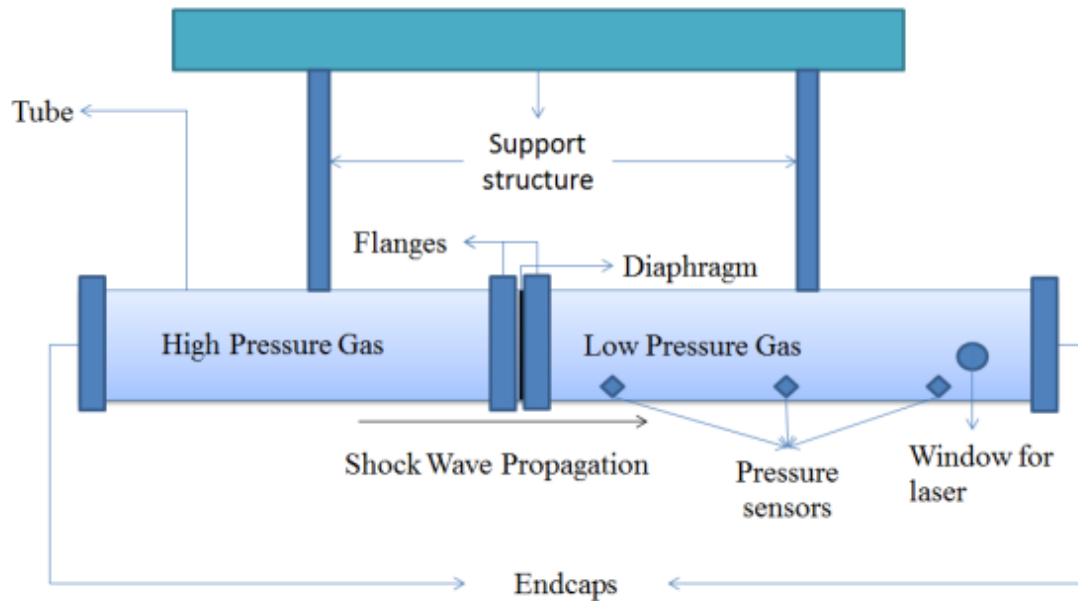

Figure 3.1: Graphical layout of the system

- Shock Tube: circular tube containing both driver and driven gases. The nominal diameter of the shock tube is 152.4 mm and the thickness 22.86 mm, made with PVC. The length of the driver section is 1 meter and the driven section 4.32 meters. The remaining part is the test section, with a length of 0.76 meters,

making a total length of the shock tube of 6.08 meters. Besides, the different parts of the shock tube were sealed to avoid leakage. Eight flanges made with PVC and two end caps made from steel were chosen.[30]

- Support structure: it allowed the system to be supported at a comfortable height for its users, supporting stability and safety. A v-style support was chosen to support stability to the structure.[30]

- Diaphragm section: it consisted on flanges to connect the different parts of the shock tube, allowing the shock wave to propagate once ruptured. The diaphragm was made of aluminum with a thickness of 1 mm and radius of 73.15 mm. Blades were picked to allow the diaphragm to break in petals.[30]

- Instrumentation: in order to allow the users to carry on experiments on the facility, transducers, windows and allowance for the gases to be placed and evacuated were installed. Dealing with the windows, 4 circular fused silica were chosen with a diameter of 20.8 mm and a thickness of 12 mm. Parallelism between the windows turned crucial in order to allow the laser (215 nm range) to pass through them without loosing accuracy in the results. Besides, 3 pressure transducers were installed to measure the pressure in the shock tubes. Finally, 3 valves were assembled in order to allow the air flow into the tube for the driver section.[30]

An animation of the shock tube was modeled before the shock tube was constructed. Figure 3.2 shows its layout in 3 dimensions. The different lengths of the driven, driver and test section can be appreciated.[30]
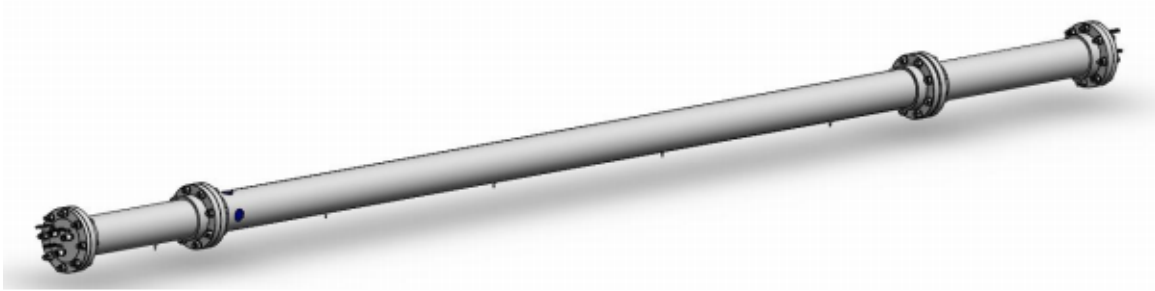
Figure 3.2: Graphical animation of the shock tube

3.3 Summary of budget

The total budget of the project can be appreciated in table 3.1. It includes fittings, test section, transducers, windows, support structure, blades and other additional stuff. Each of the components and materials were chosen by the group of students,[30] as a result of their Engineering Design Course (ME423, Stevens Institute of Technology).

Section	Components	Vendor	Total ($)
Senior ID Budget	PVC pipe, bolt, flanges and nuts	Memaster-Carr	654.6
Fittings	Vacuum fitting and brass fitting	Memaster-Carr	722.8
Test section	Gasket and PVC	Memaster-Carr	228.29
Transducers	Pressure transducers	PCB Piezoelectronics	2094
Windows$_2$	Windows and adaptors	Memaster-Carr	599.09
Support structure	Tripod and V support	Memaster-Carr	803.20
Blades	Steel bar	Memaster-Carr	16.08
Miscellaneous-He	Tape, plate and RTV	Memaster-Carr	82.20
		Total	**5200.26**

Table 3.1: Total budget of the shock tube

3.4 Layout graphical view

The following pictures show the shock tube and its different components. The pictures above in figure 3.3 show the driven and test section, while the picture below shows

---

the whole assembly of the shock tube, including driver section (right part), driven section and test section.

Different components to support the structure can be appreciated, as well as the connecting parts for each of the sections.

The driver section will be pressurized with the valves shown in the picture on the left.

(a) Driver section

(b) Driver and test section

(c) Shock tube

Figure 3.3: Shock tube construction

Chapter 4

Model - Flow behind shock in vibrational non-equilibrium

This chapter provides the approach and mathematical model of each of the studies of interest in the project. For each section, the governing equations and the logical development to achieve the desired results will be given.

4.1   Pressure-velocity diagram for the contact surface

First step to understand the behavior of the gas-dynamics in the shock tube is studying and predicting the pressure and velocity of the contact surface. As explained in the literature review [2], the contact surface separates the driver and driven gas. It travels at a lower speed than the shock tube and at a pressure between the ones for the driver and driven section.

For the better understanding of the explanations, different numbers are given to each section of the shock tube once ruptured the diaphragm. These numbers are the same as stated in Figure 2.1 in Chapter 2, Literature review. That is:

- Region 1: Driven gas at the initial conditions.

- Region 2: Driven gas traversed by the incident shock wave.

- Region 3: Driver gas traversed by the expansion wave.

- Region 4: Driver gas at the initial conditions.

In order to obtain the relations that govern both pressure and velocity, the first step is assuming that velocities and pressure in each side of the contact surface are equal,

as stated in equations 2.12 and 2.13.

Once stated these conditions, next step is arranging the equation velocity-pressure for each of the regions (2-3). That is, plotting all possible states from 1-2 and for 4-3. These equations are the ones arranged in literature review, equations 2.14 and 2.15. Once plotted both curves using MatLab, the solution that gives the pressure and velocity of the contact surface is the intersection bewtween the two curves.

4.2 Study of thermodynamic properties and comparison with Cantera Software

The second part of the study is the development of the thermodynamic properties in frozen and equilibrium flow. The results for the heat capacity at constant volume C_v, heat capacity at constant pressure C_p, mole fraction, enthalpy and internal energy will be compared with the results provided by Cantera.

Although a deeper explanation on how Cantera works is explained in the next chapter, here is a brief overview on its functions. It is a chemical kinetics software that solves chemically reacting flows, such as the one in the driven section of the shock tube. It evaluates the properties and chemical source terms of the flows, being used in applications related with combustion, detonations, batteries and supersonic effects.

The next procedure is followed in order to achieve the goals set. As the test gas is *Nitrogen*, formulas applied to molecules will be used:

- First topic of interest is the study of the heat capacity at constant volume C_v. Results obtained with the quantum-mechanics equations and the results obtained with Cantera will be displayed. For the quantum-mechanics analysis, the equation to be used are 2.23 and its developed equation 2.25. Thus, the

different factors that compose the equation are:

$$Cv_{translational} = \frac{3}{2}R \tag{4.1}$$

$$Cv_{rotational} = RT \tag{4.2}$$

$$Cv_{vibrational} = \frac{(h\nu/kT)^2 e^{h\nu/kT\,2}}{e^{h\nu/kT} - 1} R \tag{4.3}$$

$$Cv_{total} = \frac{3}{2}R + R + \frac{(h\nu/kT)^2 e^{h\nu/kT\,2}}{e^{h\nu/kT} - 1} R \tag{4.4}$$

A plot showing the variation of C_v as a function of the temperature T will be displayed. After that, it will be compared with the results given by Cantera and an analysis of the results will be provided.

- Analogously to previous point, the internal energy and enthalpy from quantum-equations 2.20, 2.21 and 2.22 will be plotted as a function of the temperature. As shown, the total internal energy is given by equation:

$$e_{total} = \frac{3}{2}RT + RT + \frac{h\nu/kT}{e^{h\nu/kT} - 1}RT \tag{4.5}$$

And total enthalpy is given by:

$$h_{total} = e_{total} + \frac{P}{\rho} \tag{4.6}$$

Where P is the local pressure of the gas and ρ is the local density of the gas.

Results for internal energy and enthalpy will be displayed and analized comparing with the exact solution from Cantera.

- Finally, it is also interesting to analyze the different solutions that Cantera gives for the study of the heat capacity at constant pressure C_p, gamma Cp/Cv and mole fraction of the test gas (in this case N_2 and enthalpy for both frozen and equilibrium flow). It will provide figures and information to support the differences explained in the literature review about frozen and equilibrium flow, where the thermodynamic and chemical parameters show a different behavior in steady state.

4.3 Non-equilibrium gas dynamics after the shock wave

Finally a deep analysis on the non-equilibrium gas properties after the shock wave will be conducted. This is the key part of the project, and all previous studies converge to this point.

As explained before, when a shock wave traverses a fluid, there is a discontinuity in pressure and temperature in the fluid, as they are suddenly increased. Translational and rotational energy are considered to reach equilibrium instantaneously, whereas the vibrational energy needs more time at the rate of equation 2.28.

In this last part of the project, all the different properties that characterize the gas will be studied. Velocity, pressure, density, enthalpy and the different temperatures and energies (translational, rotational and vibrational) will be plotted as a function of distance behind the shock for different initial conditions. Thus, the distance of the gas to reach the equilibrium state will be found and several conclusions will be stated.

In order to achieve this, a system of differential equations will be obtained and evaluated with the solvers provided by MatLab. The variables in the system of equations are: Velocity, pressure, density, translational/rotational energy and vibrational energy.

By the equations of continuity and momentum, definitions of the derivative of velocity and pressure are obtained. The flow is considered one-dimensional and steady:

$$du = -\frac{u}{\rho}d\rho \tag{4.7}$$

$$dp = -\rho u du \tag{4.8}$$

From energy equation 2.3, the following expression is obtained:

$$h_0 = h + \frac{v^2}{2} \tag{4.9}$$

Due to one-dimensional and steady flow $dh_0 = 0$, so:

$$dh + u du = 0 \tag{4.10}$$

As stated before, the expression for the total enthalpy is given in equation 4.6. Deriving the equation:

$$dh = de + \frac{dp}{\rho} - \frac{p}{\rho^2}d\rho \tag{4.11}$$

Adding this term to equation 2.3, the third different equation is obtained:

$$0 = de + \frac{dp}{\rho} - \frac{p}{\rho^2}d\rho - udu \qquad (4.12)$$

Finally, the equations for the translational/rotational energy and the vibrational energy must be obtained in order to complete the system equation as $de = de_{tr} + de_{vib}$

As explained before, the energy from translational and rotational energy are given by equations **??** and 2.21. Therefore:

$$e_{t/r} = \frac{3}{2}RT + RT = \frac{5}{2}RT \qquad (4.13)$$

And deriving last equation 4.23:

$$de_{t/r} = \frac{5}{2}RdT \qquad (4.14)$$

And since the ideal gas equation states:

$$T = \frac{p}{\rho R} \qquad (4.15)$$

Hence:

$$\frac{dT}{dx} = \frac{1}{R}\left(\frac{dp}{dx}\frac{1}{\rho} - \frac{p}{\rho^2}\frac{dp}{dx}\right) \qquad (4.16)$$

Including equation 4.16 in 4.14, the fourth equation of the system is obtained:

$$\frac{de_{t/r}}{dx} = \frac{5}{2}\left(\frac{dp}{dx}\frac{1}{\rho} - \frac{p}{\rho^2}\frac{dp}{dx}\right) \qquad (4.17)$$

Finally, the equation for the vibrational energy must be derived. As stated in the literature review, the expression is given by the vibrational rate equation 2.28. In order to transform $1/dt$ to $1/dx$:

$$\frac{1}{dt} = u\frac{1}{dx} \qquad (4.18)$$

So equation 2.28 is rearranged as follows, which gives the fifth and last equation of the system:

$$\frac{de_{vib}}{dx} = u\frac{1}{\tau}\left(e_{vib}^{eq} - e_{vib}\right) \qquad (4.19)$$

Where τ is given by equation 2.31.

Therefore, the system of differential equations that will be integrated and studied is as follows:

$$du = -\frac{u}{\rho}d\rho \qquad (4.20)$$

$$dp = -\rho u du \qquad (4.21)$$

$$dp = \frac{\rho^2}{p}d(e_{t/r} + e_{vib}) \tag{4.22}$$

$$de_{t/r} = \frac{5}{2}\left(\frac{dp}{dx}\frac{1}{\rho} - \frac{p}{\rho^2}\frac{dp}{dx}\right) \tag{4.23}$$

$$de_{vib} = u\frac{1}{\tau}(e_{vib}^{eq} - e_{vib}) \tag{4.24}$$

Which gives a total of 5 equations and 5 unknowns $(u, p, \rho, e_{t/r}, e_{vib})$. The derivatives are derived over distance (dx).

Apart from the unknowns variables, which will be plotted after solving the system of equations, it is also key part of the project to see the variation of translational/rotational and vibrational temperature through distance after the shock wave.

The translational/rotational temperature is evaluated at the local vibrational/rotational energy:

$$T_{t/r} = \frac{2e_{t/r}}{5R} \tag{4.25}$$

And for the vibrational temperature, equation 2.22 is rearranged, where $\theta_v = h\nu/k$:

$$T_{vib} = \frac{\theta_V}{log(1 + \dfrac{\theta_v R}{e_{vib}})} \tag{4.26}$$

Finally, note that the initial conditions for the gas (pressure, temperature, density, velocity and internal energy) are calculated from the equations 2.6 2.8 2.9 and 2.7

(shock-wave relations). Besides, as the test gas is *Nitrogen*, parameters such as the specific heat (C_p/C_v), speed of sound, weighted average and θ_v have specific values.

4.4 Numerical methods

Last part of this chapter is related with the numerical methods used to solve the previous expressions and system of differential equations. It is important to set the differences between implicit and explicit methods and which algorithms MatLab uses to solve the systems.

Overall, numerical methods are approaches used in numerical analysis to obtain approximations on time-dependent differential equations[31][32].[33]

4.4.1 Explicit methods

Explicit methods calculate the state of a system at a later time from the state of the system at than current time without solving algebraic equations. The Euler's method (forward method) is the common for these kind of systems[31] [32] .[33]

Forward method begins choosing a step size of δt, which determines the accuracy of the solution as well as the number of computation. It produces a series of line segments graphically, which approximate the solution curve. The formula for the slope at a line is[31] [32] .[33]

$$Y_{k+1} = Y_k + f(t_k, Y_k)\delta t \tag{4.27}$$

Where Y_k and Y_{k+1} are the approximate solution at the current state and the state after. As the step size (δt) is reduced, the error between the actual and approximated

solution is reduced.

Most solvers in MatLab for Ordinary Differential Equations (ODE) solve differential systems by implicit methods. Ode45, ode23 and ode113 are non-stiff solvers, while ode15s, ode23s, ode23t and ode23tb are stiff solvers (stiffness is the ability of a system of having time constants in a model that vary by several orders of magnitude). Although there are not many differences in the final solutions using stiff or non-stiff methods, the a wrong use of the solver can led to longer time of computations and loose of accuracy[31] [32] .[33]

4.4.2 Implicit methods

Implicit methods find the solution of the system by solving the equation in the current state and in the later state. Analogously to explicit methods, Euler's background method is chosen to solve these kind of systems. It is presented as:

$$Y_{k+1} = Y_k + f(t_k, Y_{k+1})\delta t \tag{4.28}$$

These systems present a larger computational charge (as it includes inversion of matrix) but they are more numerically stable. The system presented in last section demands an implicit solver to integrate, since the differential parameters are encountered implicitly[31] [32] .[33]

MatLab includes a solver for implicit systems, ode15i, which is the one used for the evaluation of the system in this project. It is important to understand the numerical method behind it. It uses the variable order BDF method[34] :[35]

BDF (Backward differentiation formulas) methods are useful for stiff differential equa-

tions and differential-algebraic equations. BDFs are formulas that give an approximation to a derivative of a variable at a time t_n in terms of its function values $y(t)$ at t_n and earlier times. They aproximate the function $y(t)$ using $y(t_n)$, $y(t_{n-1})$, etc. For example, the linear interpolating polynomial through $y(t_n$ and $y(t_{n-1})$is:

$$y_t = yt_n + (t - t_n)\frac{y_n - y_{n-1}}{t_n - t_{n-1}} \tag{4.29}$$

So the derivative is:

$$y'_n = \frac{y_n - y_{n-1}}{t_n - t_{n-1}} = f(y, t) \tag{4.30}$$

And replacing the derivative, one obataines the Backward Euler method:

$$y_t = yt_n + (t_n - t_{n-1})f(y_n, t_n) \tag{4.31}$$

If y_{n-1} is known, the equation is implicit in y_n.

When higher order-order methods are discussed, it is easier to discuss constant step size methods (gap between adjacent time h_n):

$$h_n = t_n - t_{n-1} \tag{4.32}$$

The equation for the BDF in higher order methods is:[35]

$$hy'_n = \sum_{j=0}^{k} a_{kj} y_{n-j} \tag{4.33}$$

Where the coefficients a_{kj} are

Order k	a_{k0}	a_{k1}	a_{k2}	a_{k3}	a_{k4}	a_{k5}	a_{k6}
1	1	-1					
2	3/2	-2	1/2				
3	11/6	-3	3/2	-1/3			
4	25/12	-4	3	-4/3	1/4		
5	137/60	-5	5	-10/3	5/4	-1/5	
6	49/20	-6	15/2	-20/3	15/4	-6/5	1/6

Table 4.1: BDF Coefficients

Finally, once explained the computational background behind the solver ode15i, last step is defining each of its components in the syntax. It has the form:[36]

$$[t, y] = ode15i(@function, tspan, y0, yp0, options) \tag{4.34}$$

$$[y0, yp0] = decic(@function, t0, y0, fixedy0, yp0, fixedyp0) \tag{4.35}$$

Where *tspan* sets the initial and final time for integration, y0 and yp0 are the initial conditions for the equations and its derivatives and 'options' is set by the user.[36]

The function *decic* uses the inputs y0 and yp0 as initial guesses for an iteration to find output values that satisfy the requirement $f(t0, y0, tp0) = 0$. If $fixedy0(i) = 1$, no change is permitted in the guess. For $y0(i) = 0$, the initial conditions can be flexible and the program can change them in order to satisfy the system. The system does not allow to fix more than length(y0) components.[36]

Chapter 5

Results and discussion

This chapter provides the results and discussions of the topic of interest in the project. The procedures, governing equations and development of the mathematical model were exposed on chapter 4.

For the better understanding and clarity of the results, this chapter will be break down in different sections, where an analysis and comparisons with available data and theoretical results will be discussed.

Results for the first two sections (pressure-velocity diagram and study of thermodynamic properties with Cantera) will be based in specific initial conditions conditions. For future simulations with the Shock Tube, initial conditions can be changed as desirable.For the last part of results (non-equilibrium flow) graphs and plots will be dimensionless in order to appreciate the impact of each of the variables in the output.

5.1 Pressure-velocity diagram for the contact surface

First of all, the pressure-velocity diagram of the contact surface is to be studied. As seen in the literature review, the contact surface travels at a lower speed than the shock wave. Pressure and velocity depend on the initial conditions on the driver and driven section. Thus, the following conditions are assumed as a base point for the start of the simulation.

- Driver section: Fill with $Helium$.

    − $p4 = 102040.82 Pa$;

– $\gamma 4 = 5/3$;

– $T4 = 273.15 + 22K$;

– $R4 = 2.0773e + 03\,J/kgK$;

– $a4 = \sqrt{g4 * R4 * T4} = 1.0109 * 10^3 m/s$;

- Driven section: Fill with *Nitrogen*.

  – $p1 = 666.61 Pa$;

  – $\gamma 1 = 7/5$;

  – $T1 = 273.15 + 22K$;

  – $R1 = 296.95\,J/kgK$;

  – $a1 = \sqrt{g1 * R1 * T1} = 350.29 m/s$;

By plotting the equations 2.14 and 2.15 with Matlab, the following graph (figure 5.1) is obtained, which include all possible states from 1-2 and 4-3 and the intersection between both curves, which is the desirable result.

Therefore, the velocity and pressure of the contact surface is obtained from the intersection of the curves. For the whole chapter, subscripts indicate the region of the flow, as stated in chapter 4. As a reminder of the meaning of each subscript, they are specified as follows:

- Region 1: Driven gas at the initial conditions.

- Region 2: Driven gas traversed by the incident shock wave.

- Region 3: Driver gas traversed by the expansion wave.

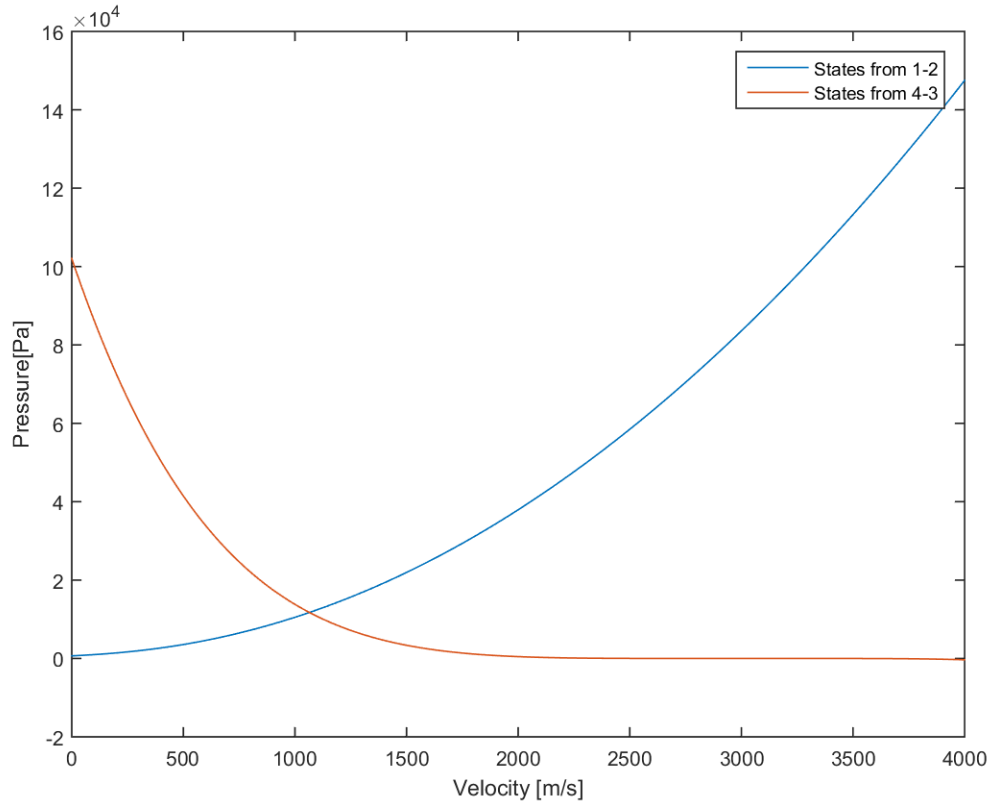- Region 4: Driver gas at the initial conditions.

Figure 5.1: Possible states from 1-2 and 4-3

Table 5.1 summarizes the results obatained:

Parameter	Value
Initial Mach number	3.8980
Initial shock speed (m/s)	1365.4
Pressure contact surface p2=p3 (Pa)	11706
Velocity contact surface u2=u3 (m/s)	1064
Temperature $T_2(K)$	1148.1
Temperature $T_3(K)$	124.14

Table 5.1: Data contact surface

As it can be appreciated, the pressure of the contact surface lies between the values for driver and driven section, while its velocity is lower than the initial shock wave velocity. There is also a huge difference between the temperature at each side of the

contact surface. On the one hand, the flow traversed by the shock wave (subscript 2) increases its temperature to high values, while the flow behind the expansion wave (subscript 3) is considered to be frozen ($T = 124.14K$). By varying the script in Appendix I (Pressure-velocity diagram), different conditions for the contact surface will be obtained.

5.2 Study of thermodynamic properties and comparison with Cantera Software

Next step is the study of the thermodynamic properties in frozen and equilibrium flow, where results for the heat capacity at constant volume C_v, heat capacity at constant pressure C_p, mole fraction, enthalpy and internal energy will be compared with the results provided by Cantera.[37]

First of all, let us give a brief explanation of how Cantera works. As said before, it is a powerful tool for representing values for steady one-dimensional reacting flows. It includes different demos, systems and mathematical models for the simulation of combustion detonation, electromechanical energy conversion... in both frozen and equilibrium flow.[37]

It can work with different species (specified at the beginning of the program) and computes the results by applying polynomials of different orders. For example, the NASA 7-coefficient polynomial parametrization is used to compute the species reference-state thermodynamic properties heat capacity at constant pressure (C_p), enthalpy and entropy.[37] Besides, there is another method of calculation; The NASA 9-coefficient polynomial parametrization is an extension of the NASA 7-coefficient polynomial parametrization which includes two additional terms in each temperature region, as

well as supporting an arbitrary number of temperature regions.[37]

As it can be appreciated, Cantera is a really useful and accurate tool for simulating different flow conditions. It transforms experimental data by fitting the values into high-order polynomials. In this project, Cantera will be used to compare the result obtained theoretically, and extract conclusions from the differences between them.[37]

The following initial conditions, which are in concordance with future experimental data, will be assumed for the driven section. Mach number, temperature behind the shock front or shock wave speed will be the variables for this section of results.

- Driven section: Fill with N_2.

    - $p1 = 1333.22 Pa (10 torr)$;

    - $g1 = 7/5$;

    - $T1 = 273.15 + 22K$;

    - $R1 = 296.95 J/kgK$;

This conditions will the same for this whole section of results (Study of thermodynamic properties and comparison with Cantera Software). The reason is that there is a need of homogenization in order to compare the results and extract interesting conclusions.[37]

5.2.1   Heat capacity at constant pressure C_p

First aspect of study is the heat capacity at constant pressure C_p. In this case, it will be plotted as a function of Mach number and temperature after the shock for both equilibrium and frozen flow. Different conclusions will be extracted from the plots by comparing the graphs and the variations within them.

- Equilibrium state

  For equilibrium flow (infinite reaction rate), the following graphs are obtained as a function of different parameters:
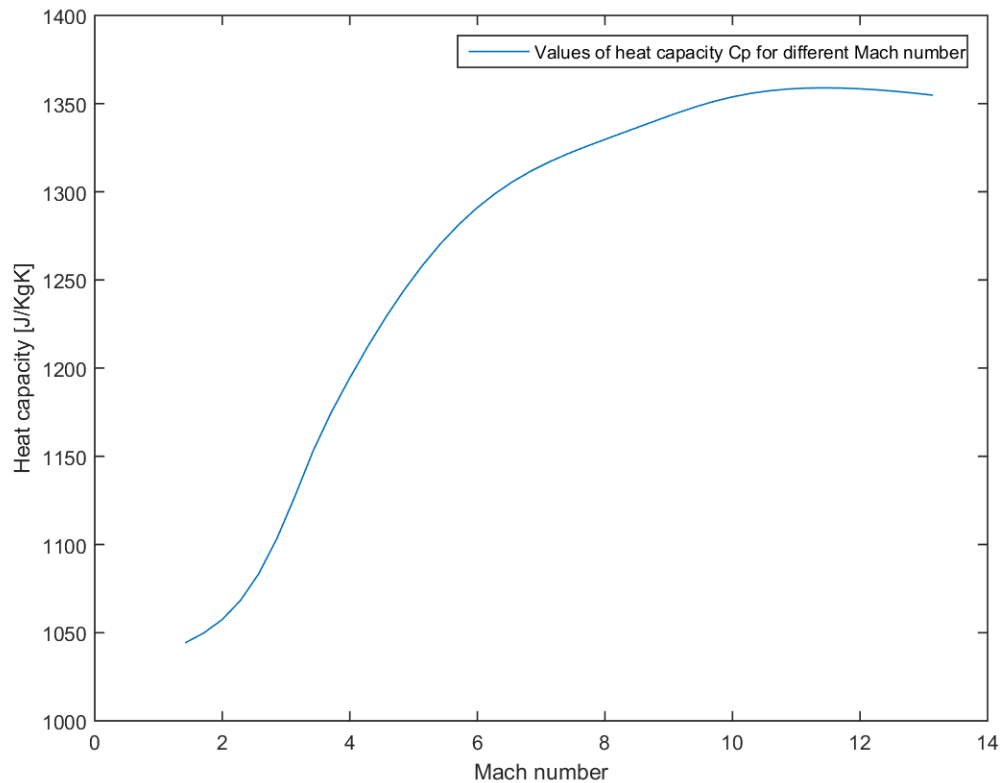
  As a function of Mach number:

Figure 5.2: Heat capacity C_p in equilibrium flow as a function of Mach number

  As it can be appreciated, heat capacity starts raising at the time the Mach number is increased. This is due to the fact that the temperature is also higher when increasing the Mach number. However, when Mach number is close to 7, that increase is reduced. This happens because the initial N_2 is being dissociated, counterbalancing the effect of temperature. When the dissociation dominates against the temperature effect (the heat capacity of N is lower than

N_2, so it has an important impact on total heat capacity), the heat capacity remains constant and is even reduced.

And as a function of post-shock equilibrium temperature (equilibrium temperature right after the shock front):
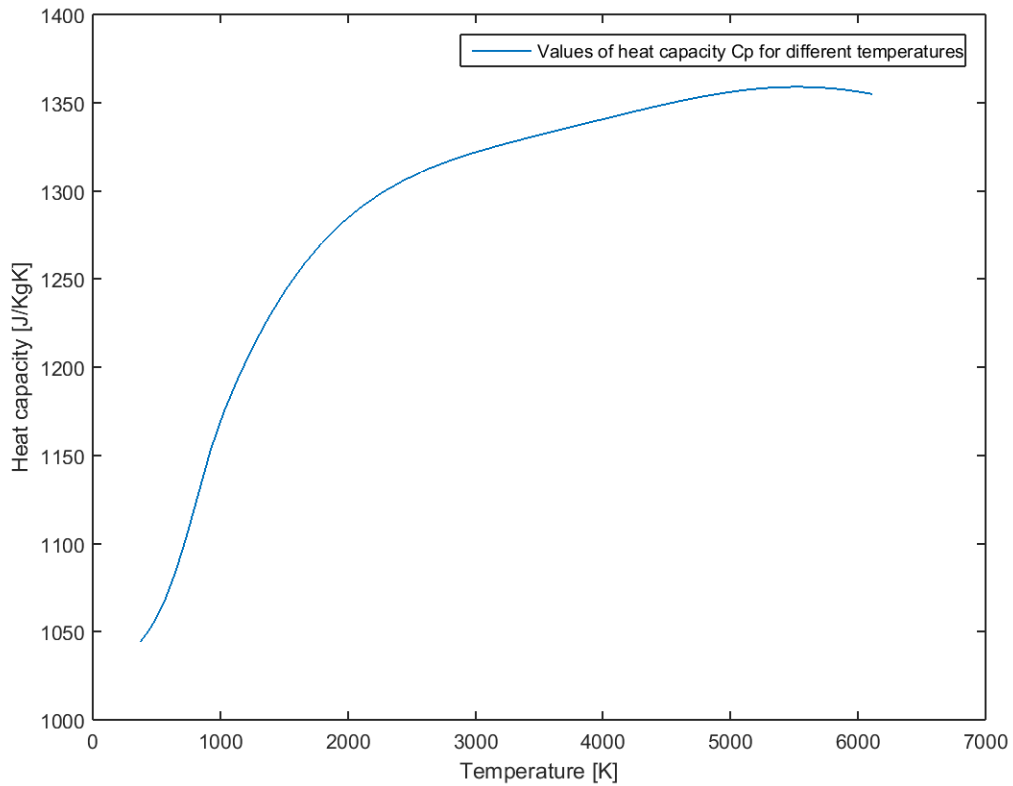

Figure 5.3: Heat capacity C_p in equilibrium flow as a function of post-shock temperature

The same effect as explained before can be appreciated in figure 5.3. Disassociation of N_2 starts for temperature close to 3500-4000, which is the value equivalent to a Mach number of 7-8.

- Frozen state

For frozen flow, there is no change in chemical reactions. Thus, the concentra-

tion of N_2 remains constant (100%) for all states of the simulation.
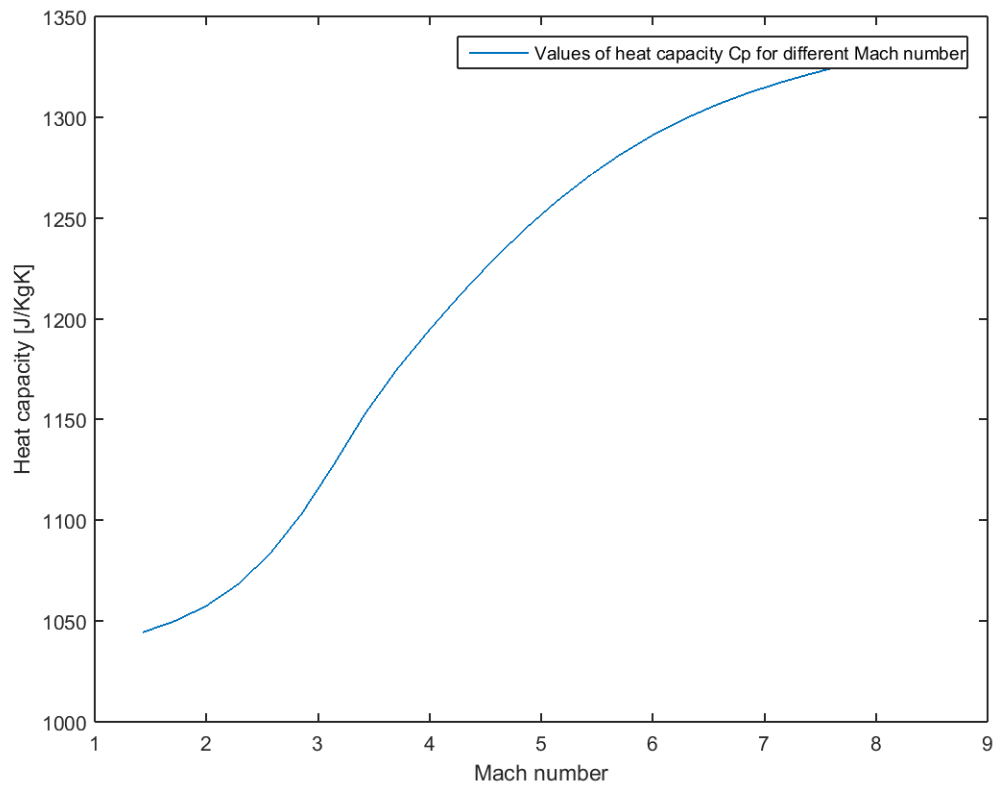
As a function of Mach number:

Figure 5.4: Heat capacity C_p in frozen flow as a function of Mach number

As it can be appreciated in figure 5.4 , the heat capacity increases as a higher rate for low numbers of Mach number. However, the greater the Mach number, the lower the rate of change of heat capacity as the temperature does not have a dominant effect. As there is no change in chemical composition, the existing diatomic nitrogen does not disassociate into mono atomic nitrogen.

The same effect can be appreciated in figure 5.5, where the effect of the temperature in the heat capacity (C_p) is plotted and quantified. The shape of the graphs are almost identical, where the effect of temperature has a lower impact

for $T > 2500K$.
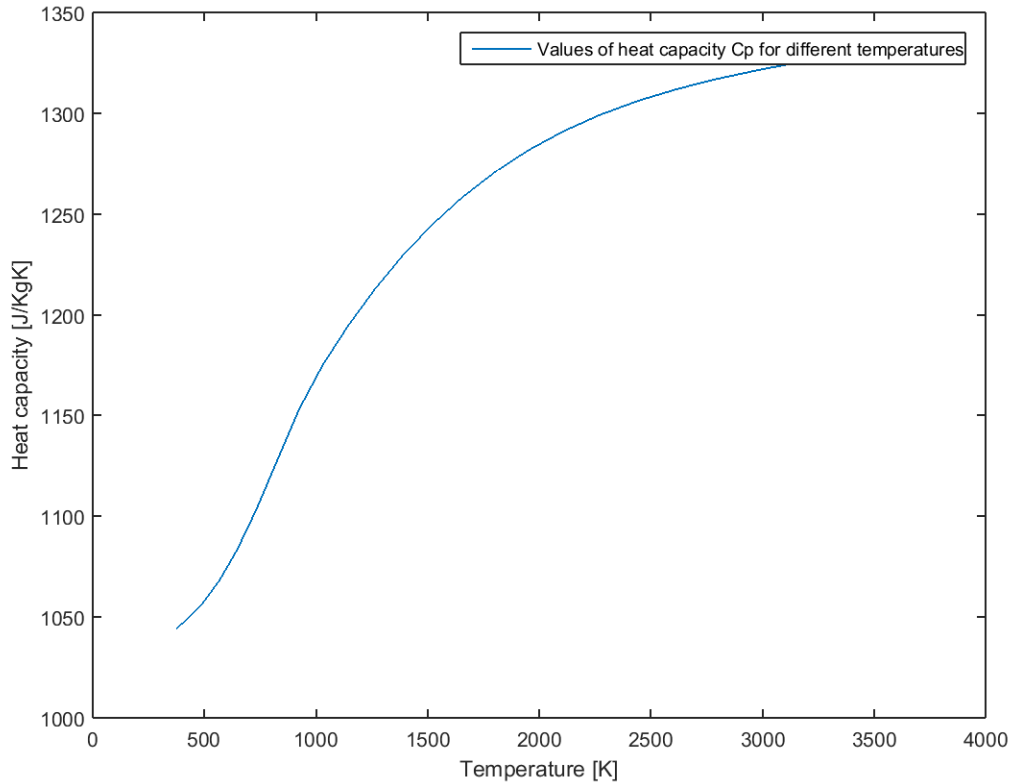
Figure 5.5: Heat capacity C_p in frozen flow as a function of post-shock temperature

5.2.2 Ratio of specific heats γ

Second aspect of interest is the study of the ratio of specific heat C_p/C_v. The variations of C_p and C_v can be appreciated in this subsection. As did before, it is being plotted as a function of Mach number and Temperature.

- Equilibrium state

    Starting with the equilibrium flow, one obtains the following graphs. As a function of the Mach number:
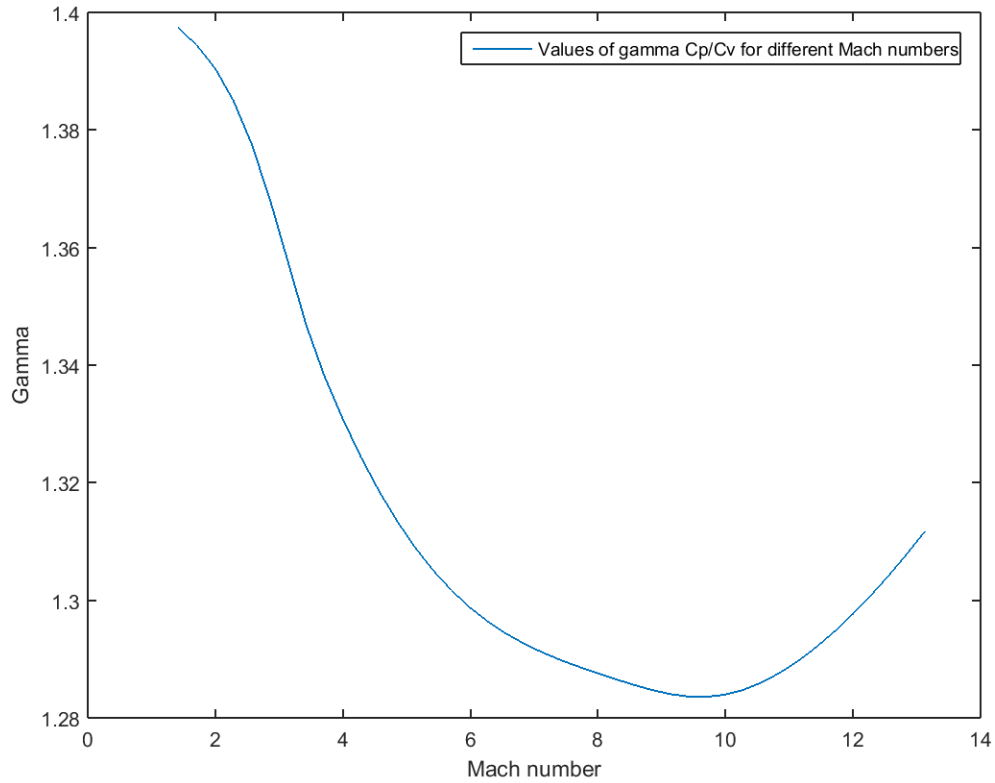
Figure 5.6: Gamma in equilibrium flow as a function of Mach number

Figure 5.6 is interesting to analyze since it suffers many changes along the distribution of Mach number. From Mach number 0-7, it can be appreciated that the specific ratio (γ) is clearly decreasing. That is because the vibrational excitation (explained in equation 2.25 in the literature review) starts acting with T>600 K (M=1.5), increasing the total C_v at a greater rate than the C_p. However, as seen before when disassociation starts to occur (M=7.5) the flow suffers a series of changes. In this point, the ratio between specific ratios stops decreasing and start to increase again as the effect of disassociation and temperature in C_v is greater than in C_p).

The same effect can be appreciated in figure 5.7, where it keeps the shape of

previous graph. From 600-2000 K, the vibrational excitation comes into play, and for T>3500 K the disassociation of nitrogen occurs.
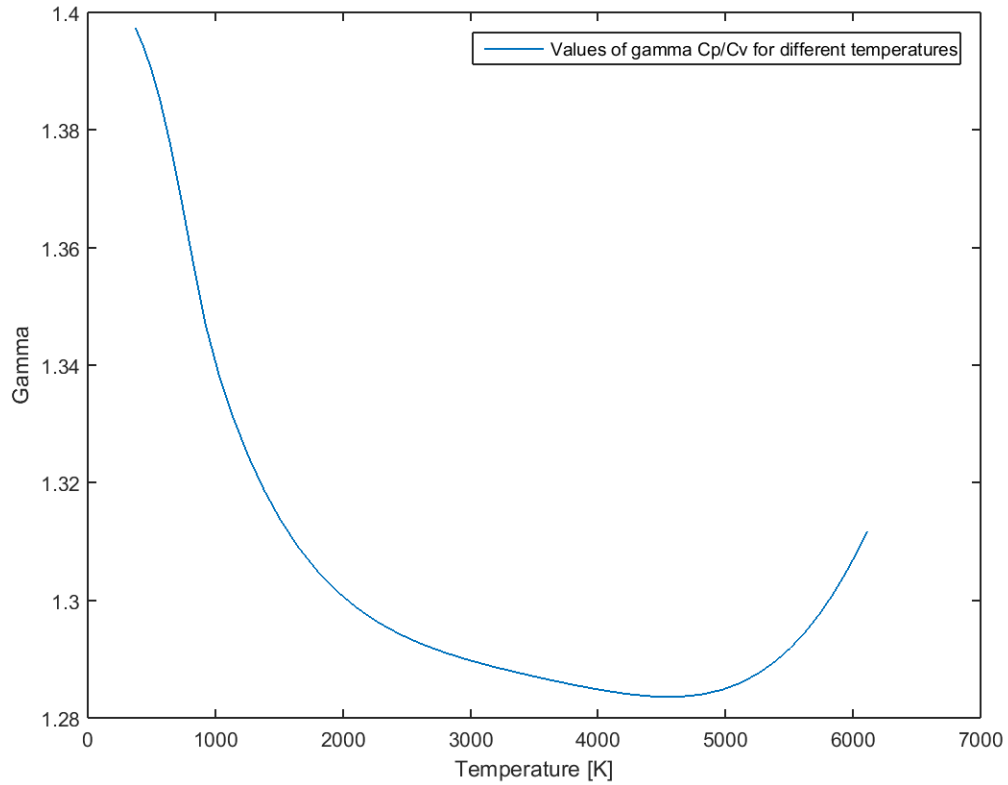
Figure 5.7: Gamma in equilibrium flow as a function of post-shock temperature

- Frozen state

Once reviewed the variation of the specific ratio (γ) in equilibrium flow, let us do it for frozen flow. Figures 5.8 and 5.9 show the variation as a function of Mach number and temperature, respectively. As there is no chemical reactions, the composition of the gas remains constant and the only variations are due to the effect of temperature. It can be appreciated that from 600<T<2000 K, the rate of change of C_v is greater than C_p due to the vibrational mode, as explained. However, when T>2000 K, the variation of C_p is larger than for C_v.
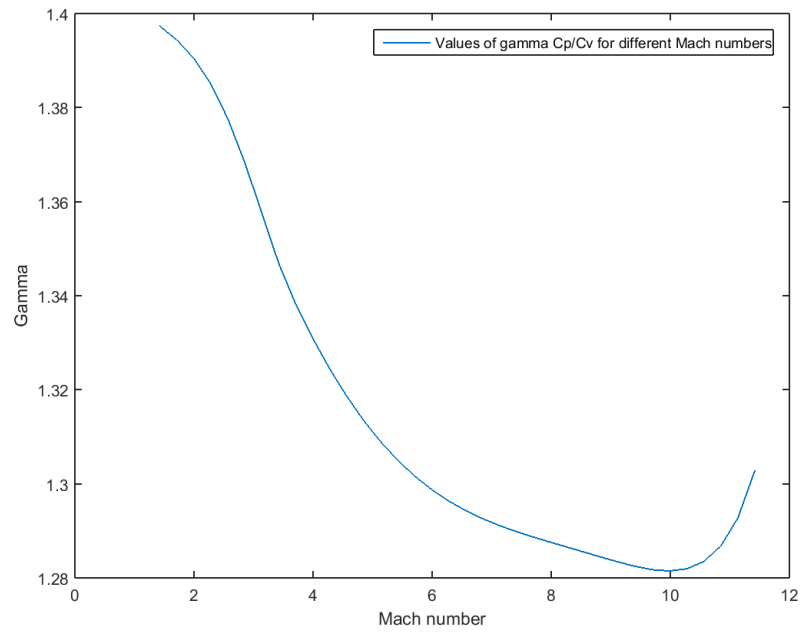
Figure 5.8: Gamma in frozen flow as a function of Mach number
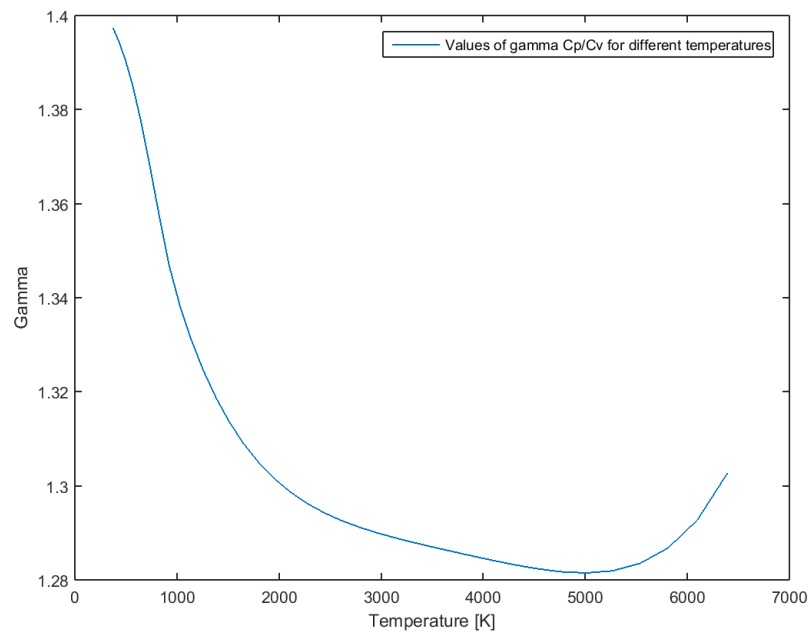
Figure 5.9: Gamma in frozen flow as a function of post-shock temperature

5.2.3 Mole fraction of N and N_2

After the heat capacity and specific ratio, a brief display of the mole fraction depending on the Mach number and temperature will be displayed for the region of study.

- Equilibrium state

  When computing the variation in concentration of N_2 and N as a function of Mach number and temperature, the following graphs are obtained:
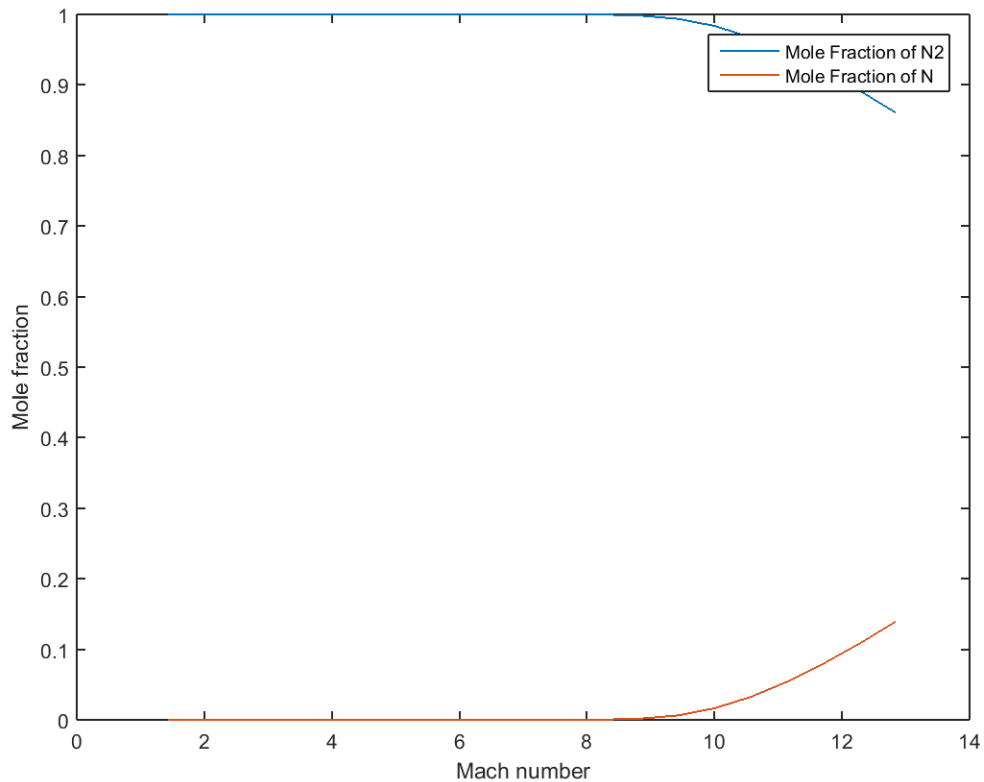
Figure 5.10: Mole fraction in equilibrium flow as a function of Mach number

As it can be appreciated, the disassociation of N_2 starts with $M = 8$ approximately. From that point, the concentration of N increases and the one for N_2

decreases. As the test in the shock tube will rarely consist on mach number greater than 10, the graph shows the distribution until $M = 13$.

Besides, the mole fraction as a function of post-shock temperature is shown in Figure 5.11
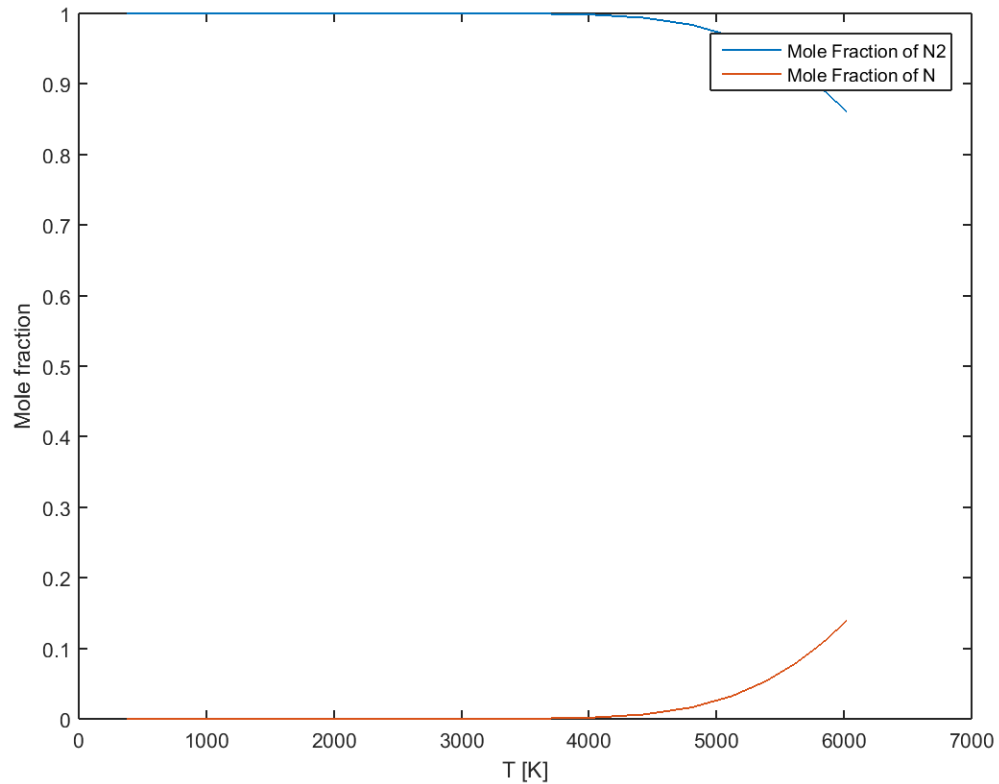
Figure 5.11: Mole fraction in equilibrium flow as a function of post-shock temperature

The figure is exactly the same as 5.10, but showing the range of temperature. As expected, the disassociation of N_2 starts at $T = 4000K$. From that point, the concentrations change at the same rate but opposite signs, where the decrease on N_2 turns in an increase of N, changing all thermodynamic properties (C_p, C_v...) seen before.

- Frozen state

The definition of frozen state states that there is no chemical reaction, so the composition remains constant. Thus, the concentration of N_2 will be 1. Figure 5.12 shows the evidence.
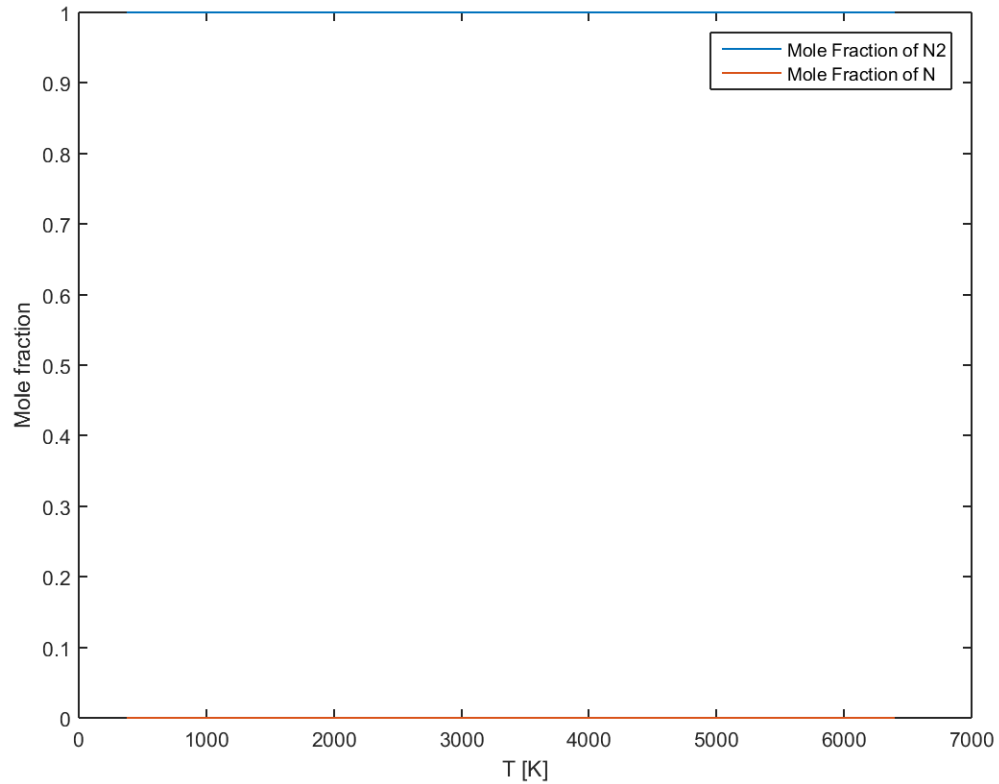
Figure 5.12: Mole fraction in frozen flow as a function of post-shock temperature

5.2.4 Heat capacity at constant volume C_v

As explained in chapter 2, literature review, the theoretical variation of heat capacity would be studied in the results 2.4. It is an interesting topic since the quantum-mechanics equations exposed in the literature review (with equation 2.25) do not take into account the effect of disassociation, while Cantera does. That effect will be easily quantified by inspecting the graphs.

- Comparison between quantum-mechanics and Cantera

  In order to accomplish this task, equation 2.25 will be plotted and compared with Cantera results. Figure 5.13 shows this approach:
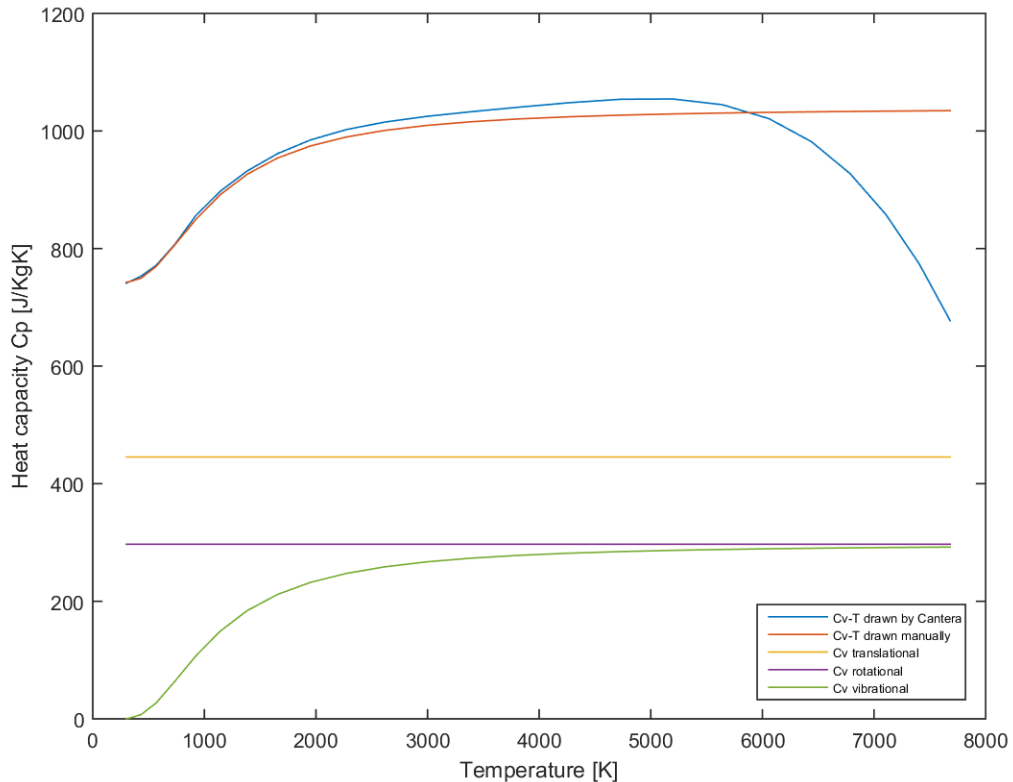
Figure 5.13: C_v comparison with quantum-mechanics equations and Cantera results

  As it can be appreciated in figure 5.13, the plots show agreement at the beginning of the graphs. Besides, the translational, rotational and vibrational contributions are plotted. As specified in the literature review, both translational and rotational modes (3/2 R and R, respectively) are constant as they do not depend on the temperature. However, the vibrational mode does, and it starts to be noticeable from T=600 K, becoming higher with the post-shock temperature. Graph can be compared with figure 5.13.

The main disagreement between the graphs come when T>3500 K. That is the point in which disassociation starts and changes the situation, as the thermodynamic properties are different from diatomic and mono-atomic nitrogen. From T>6000 K the heat capacity falls dramatically, presumably as a results of the complete disassociation of N_2.

5.2.5 Internal energy e

- Comparison between quantum-mechanics and Cantera

  Analogously to previous concept, internal energy is compared with Cantera:
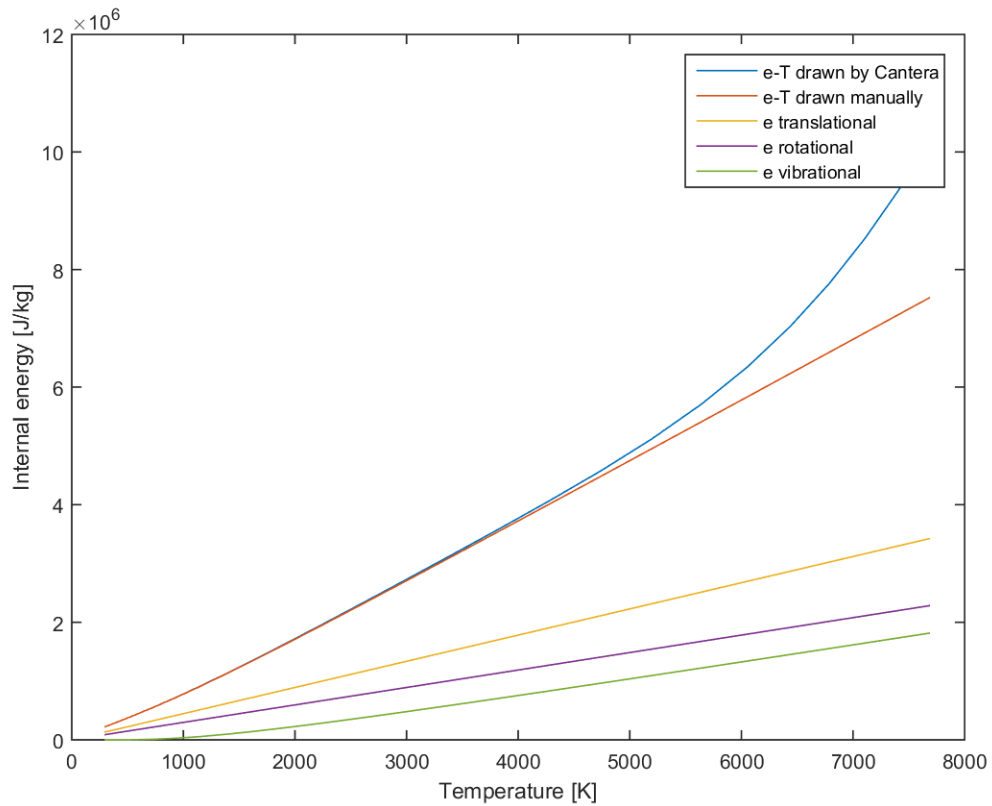
Figure 5.14: Internal energy comparison with quantum-mechanics equations and Cantera results

---

As done before, the translational, rotational and vibrational energies are plotted in the graph to see the evolution of each one. Equations used are 2.20, 2.21 and 2.22. The graph shows agreement again until the disassociation starts to take place, approximately T>4000 K. The mode of energy that most contributes is to internal energy is the translational , followed by the rotational, and with the vibrational energy being important from T>1000 K.

5.2.6   Enthalpy h

- Comparison between quantum-mechanics and Cantera

  Finally, in order to complete this section, a graph showing the enthalpy drawn by quantum-mechanics equations and Cantera is presented.

  The formula for the total enthalpy is equation 4.6. As a reminder:

$$h_{total} = e_{total} + \frac{P}{\rho} \tag{5.1}$$

  Therefore, the local pressure and density is computed in order to calculate the total enthalpy. Figure 5.15 represents it.

  The total energy is almost linear, and the graph show great agreement between both curves. Again, the disagreement comes with the disassociation of the diatomic nitrogen (N_2), where the enthalpy increases.

  As a summary of this subsection (C_v, internal energy and enthalpy), it can be said that the quantum-mechanics equations used in this project give a very accurate solution. However, as it was considered frozen flow (no chemical reaction), all differences in the comparison come when the nitrogen starts dissociating.

Once analyzed the thermodynamics properties in both frozen and equilibrium, next section analyzes the key part of this project: Non-equilibrium flow. What happens after the shock front and before reaching equilibrium? How do the properties of the gas change? How much distance does it take to reach equilibrium? These questions, complemented with extra information, will be solved in the next section.
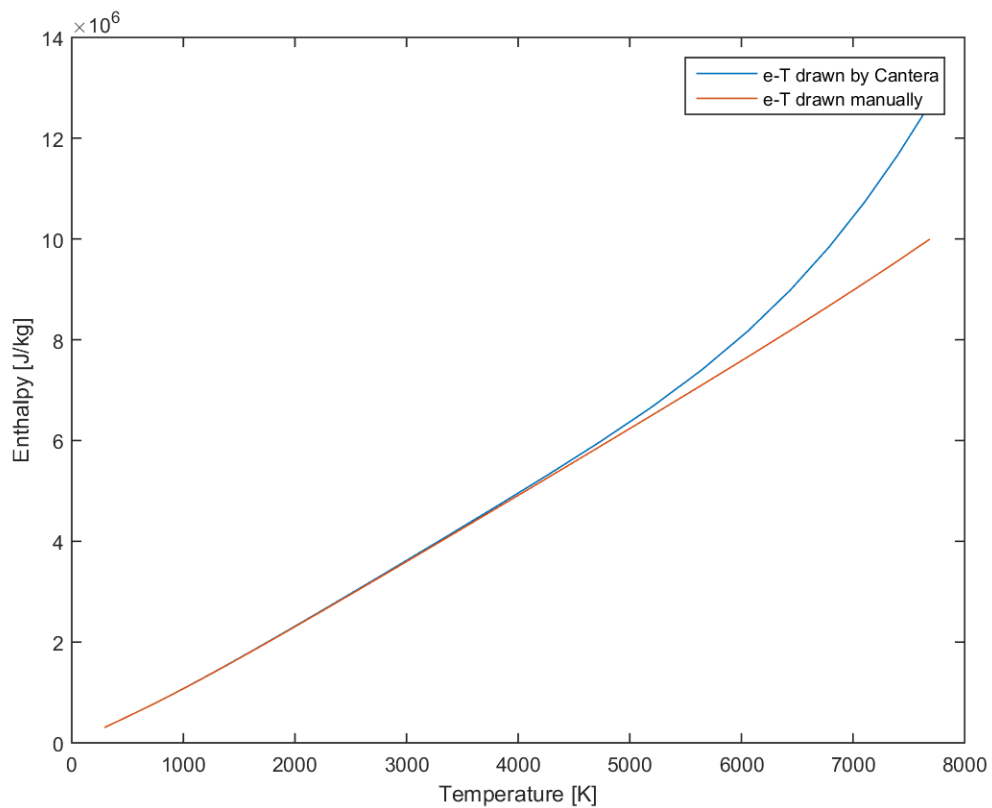
Figure 5.15: Enthalpy comparison with quantum-mechanics equations and Cantera results

5.3 Non-equilibrium gas dynamics after the shock wave

This last section of results give an approach on non-equilibrium gas dynamics after the shock front. In order to do a complete study, the following properties will be studied as a function of the relation distance: Pressure, density, velocity, translational/rotational and vibrational energies as well as their corresponding temperatures. Besides, the study of the relaxation distance and Mach number as a function of driven pressure will be conducted. The set of equations used for this section is the system of differential equations shown in chapter 4: 4.20 4.21 4.22 4.23 and 4.24. The vibrational relaxation (τ) used is the model of Millikan and White equation 2.31.

Results will be based in dimensionless magnitudes, where the parameters of study will be divided by the equilibrium value of that specific magnitude. By making results dimensionless, the qualitative study and variations can be interpreted in a better way. Once the shock tube is ready, different experimental tests will be conducted and compared with the theoretical solutions got with the system of differential equations. In order to have a better comprehension on how properties of the gas change when it is traversed by the shock wave, a first set of conditions will be taken. As the first tests will be conducted for driven pressure around 10 torr (1333 Pa), this is the value that is taken for running the simulation and exposing the results, with the following data:

- Conditions: driven section filled with N_2.

    - $p1 = 1333.22 (10 torr) Pa$;

    - $g1 = 7/5$;

    - $T1 = 273.15 + 22K$;

- $R1 = 296.95 \, J/kgK$;

- $Dens1 = p1./(T1. * R1) = 0.1521 kg/m_3$;

- $M = 7 (Machnumber)$;

In order to get the initial post-shock values for the parameters of interest (pressure, temperature, density, velocity, translational/rotational energy and vibrational energy), the shock wave relations exposed in chapter 2 are used : 2.6, 2.8, 2.7 and 2.9. For the translational/rotational energy the expression used is $2.20 + 2.21$ using the post-shock temperature as it is instant to equilibrium. For the vibrational energy, equation 2.22 will be used, using the initial temperature T_1, as the gas did not produce any collisions to make the vibrational energy to increase.

Table 5.2 summarizes the post-shock properties, which are the initial conditions for the system:

Velocity (m/s)	450.37
Pressure (Pa)	759937.5
Density (kg/m$_3$)	0.8282
Initial vibrational temperature (K)	295.15
Initial trans/rot temperature (K)	3090.03
Trans/Rot energy (J/kg)	229,393.30
Vibrational energy (J/kg)	10.34

Table 5.2: Initial conditions-Post-shock relations

However, as said before, following plots are based in dimensionless numbers, That is, instead of using the relaxation distance, the x-axis will show $(x/\tau U_s)$ being (x) the relaxation distance, τ the relaxation time and U_s the velocity at the first time of integration. The different parameters of study will be plotted in the y-axis, dividing them into their corresponding equilibrium value given by Cantera.

5.3.1 Variation of temperatures along relaxation distance

The first and most important aspect of study is the variation of the translational, rotational and vibrational temperature. The translational and rotational temperature are considered to be instant to equilibrium. Thus, their initial value is the one for the temperature relation after the shock. The vibrational temperature needs more time, as the collisions need time to occur. When equilibrium is reached, the three temperatures converge to the same value. As the driven gas is N_2, parameters associated with the vibrational relaxation time, such as the slope, reduced mass or characteristic temperatures are the ones exposed on table 2.2.
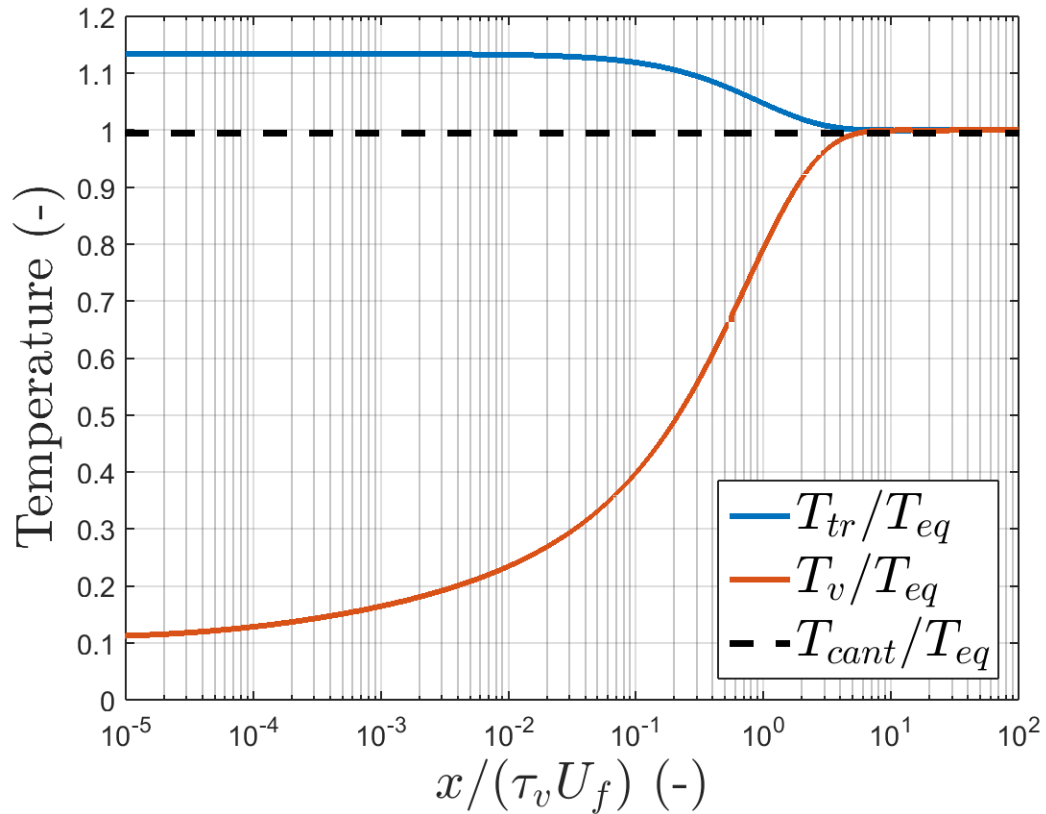

Figure 5.16: Variation of translational/rotational and vibrational temperature after the shock front

---

The dashed line represents the results obtained with Cantera, which uses equilibrium flow (collisions are infinitely quick equilibrium is reached for $T = 0$). It can serve as an approximation on how accurate are the results and extract potential conclusions, comparing the equilibrium value for this software and quantum-mechanics equations.

As is can appreciated in figure 5.16, vibrational temperature starts being proximately 10% of the equilibrium temperature, while translational/rotational temperature starts about 15% over that value (115%). Besides, the effect explained in chapter 2 about the exchange of energy of each mode is seen. When equilibrium is reached, the temperature converge to the same point (the temperature in equilibrium must be unique).

The results from Cantera (which does not work with non-equilibrium flow), give a very precise value for the equilibrium temperature. The effect of non-equilibrium flow also affects to the different parameters of study, such as internal energy, density or enthalpy.

5.3.2 Variation of internal energies along relaxation distance

Next interesting aspect of the study is monitoring the variation of the different modes of energy (translational, rotational and vibrational). Presumably, the vibrational energy will increase while the sum of translational and rotational (they are considered together as they operate with the same temperature) will decrease, due to the exchange of energy between the different modes of energy.

As explained, this happens as the translational and rotational energies reach equilibrium instantaneously, so they are excited right after the shock front.

It is represented in figure 5.17:
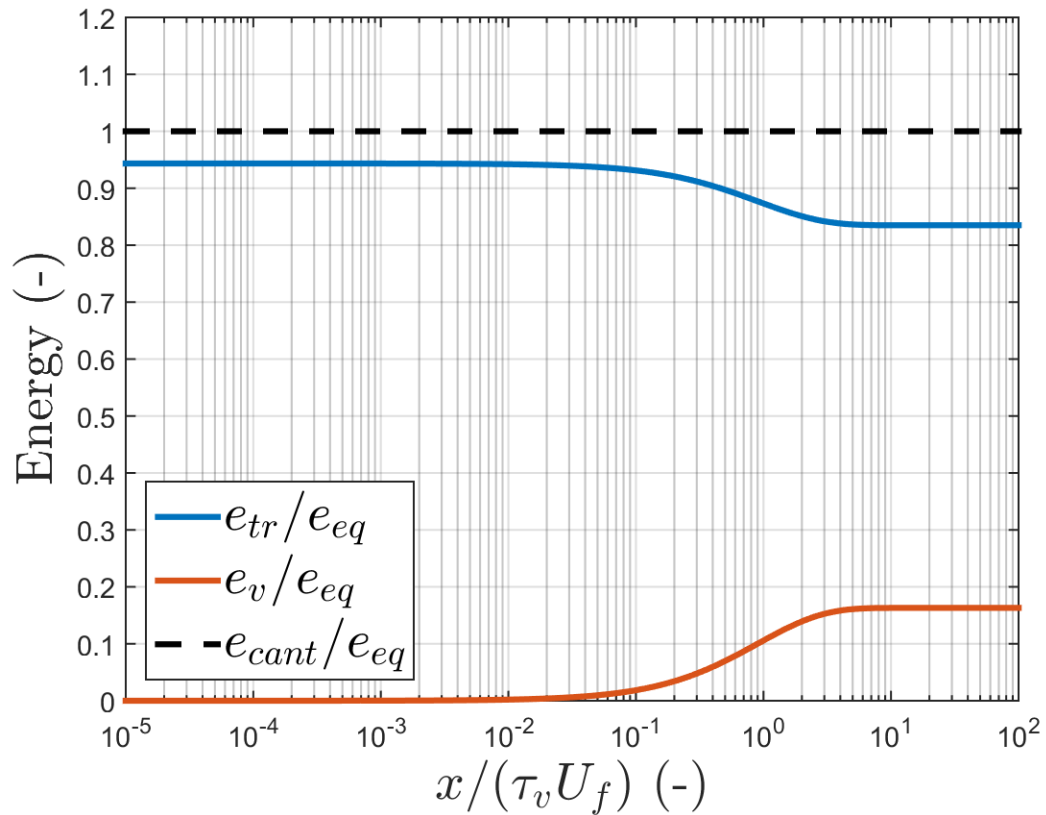
Figure 5.17: Variation of translational/rotational and vibrational energies after the shock front

As theoretically assumed before, vibrational energy starts to be important from $/x(\tau_v U_f) > 0.1$. From that point in distance, translational and rotational energy starts decreasing until they reach equilibrium. The graph also shows that the combination of translational and rotational energies are almost five times the amount of vibrational energy when equilibrium is reached, and that the combination of both gives the total energy given by Cantera. Translational+Rotational get more than 80% of total internal energy.

5.3.3 Variation of velocity along relaxation distance

When plotting the velocity as a function of the relaxation distance the following must be taken into account: The system of differential equations considers the velocity to be in the 'shock-frame'. This concept is called moving shock and it is represented in figure 5.18:
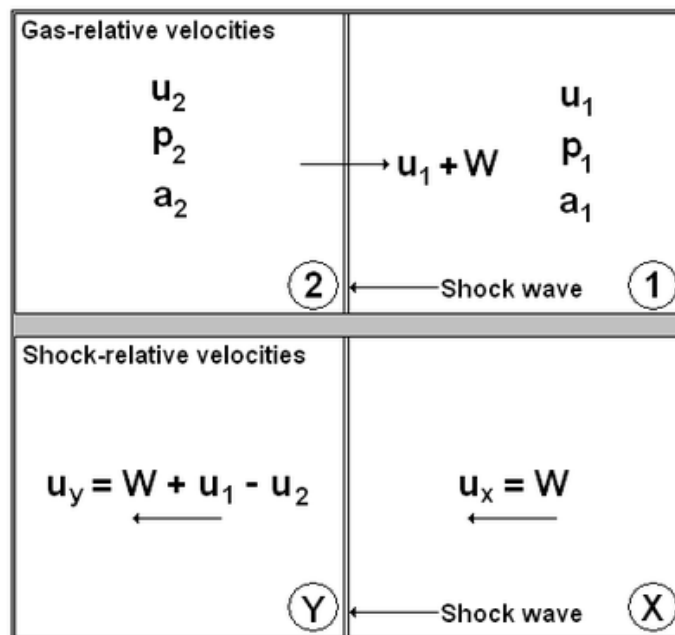
Figure 5.18: Moving shock representation[3]

The upper part of the figure shows the representation for the 'lab-frame' model, where the velocity of the shock wave relative to the velocity of the gas is denoted by W, as $U_1 = 0$. The velocity of interest is U_2, but there is a need to make a small conversion to get it.[3]

On the other hand, the picture below show the situation of the 'reference-frame' or 'shock-frame', the one that is used for the calculations of the system of equations. Following the subscripts, the velocity calculated by the program is U_y. Therefore, in

order to obtain the velocity in the 'lab-frame', the following equation is applied, as U_1 is 0 (initially no motion). The velocity of the shock-wave is denoted by W:[3]

$$U_2 = W - u_y \tag{5.2}$$

Once clarified this concept, figure 5.19 represents the variation of the velocity along the relaxation distance after the shock front. As Cantera does not provide a value for the final velocity of the gas, absolute values will be taken in this case for the initial conditions. A qualitative study will be provided.
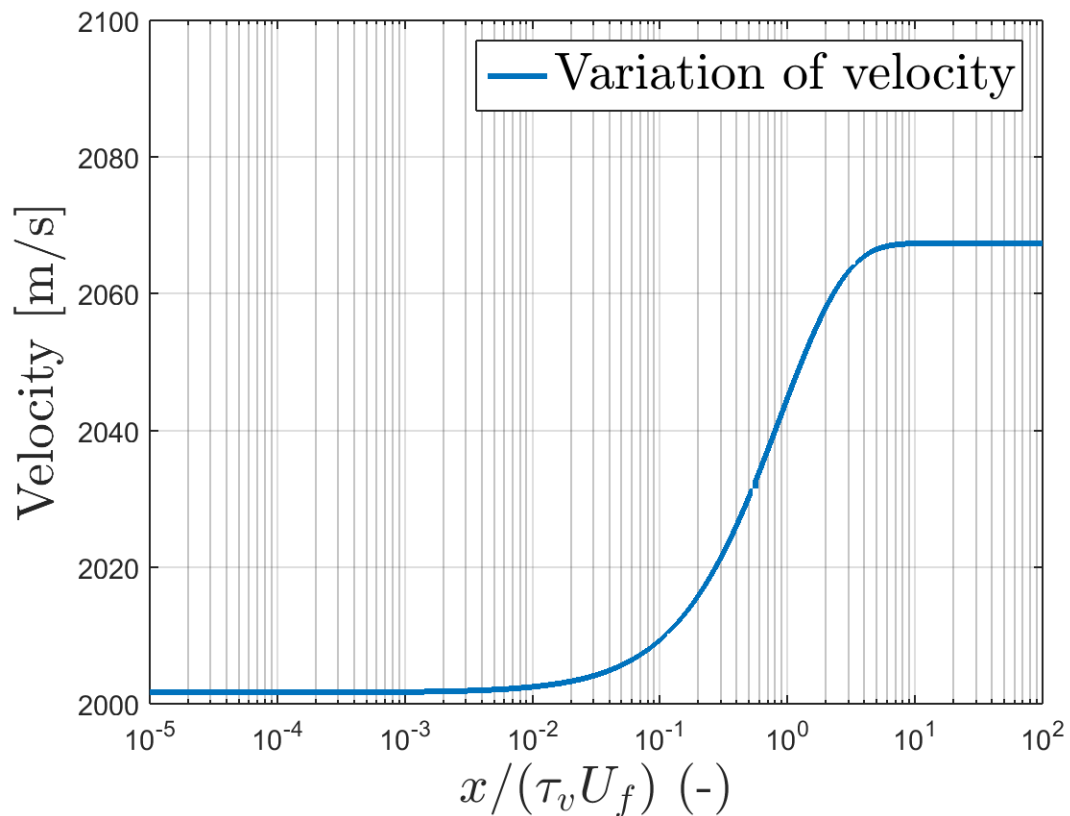
Figure 5.19: Velocity along relaxation distance

As it can be appreciated, when the vibrational energy goes up and due to the in-

crease in density (it will be seen afterward) velocity starts to increase. It increases approximately a 3.5% from its initial value. As explained, this graph represents the velocity in the 'lab-frame'.

5.3.4 Variation of pressure along relaxation distance

Another aspect of study is the variation of pressure. Although there is a small increase, it is considered to be constant though the whole process of non-equilibrium (only a 2% rate of change). The small differences can be due to the gradients in temperature and energy, which could cause small fluctuations in pressure. Figure 5.20 illustrates it:
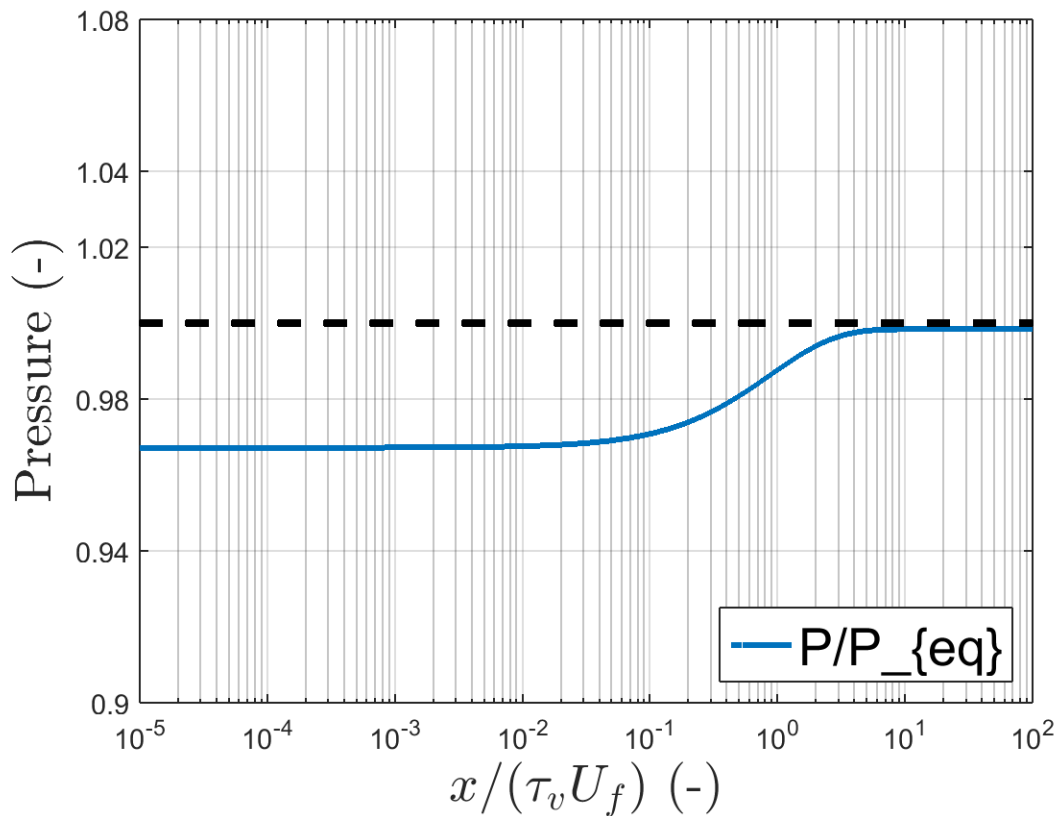
Figure 5.20: Pressure along relaxation distance

Comparing with Cantera results, it can be appreciated that values are really closed for equilibrium, where the dimensionless parameter for pressure reaches 1.

The fact that the pressure is constant during the process can lead to anticipated conclusions. One can note what could happen to density and velocity, applying the law of gases. It will be done in following sections.

5.3.5 Variation of density along relaxation distance

As said, another parameter of the study is density. By examining equation of ideal gases, the following relations can be appreciated between the parameters of interest.

$$p = \rho R T_{tr} \tag{5.3}$$

Where the temperature is referred to the translational/rotational temperature, as it is the one instant to equilibrium. Thus, considering the pressure constant through the process (isobaric), if translational/rotational temperature decreases as seen before due to the exchange with the vibrational temperature, the density must increase to maintain pressure constant.

These phenomena can be appreciated in figure 5.21.

In order to notice the change in density, graph should show at least differences about 10% between the initial value and the value reached in equilibrium.

The variation also depends on the variation the translational and rotational temperatures suffer. They must change at a similar rate in order to be compensated and maintain the process isobaric.
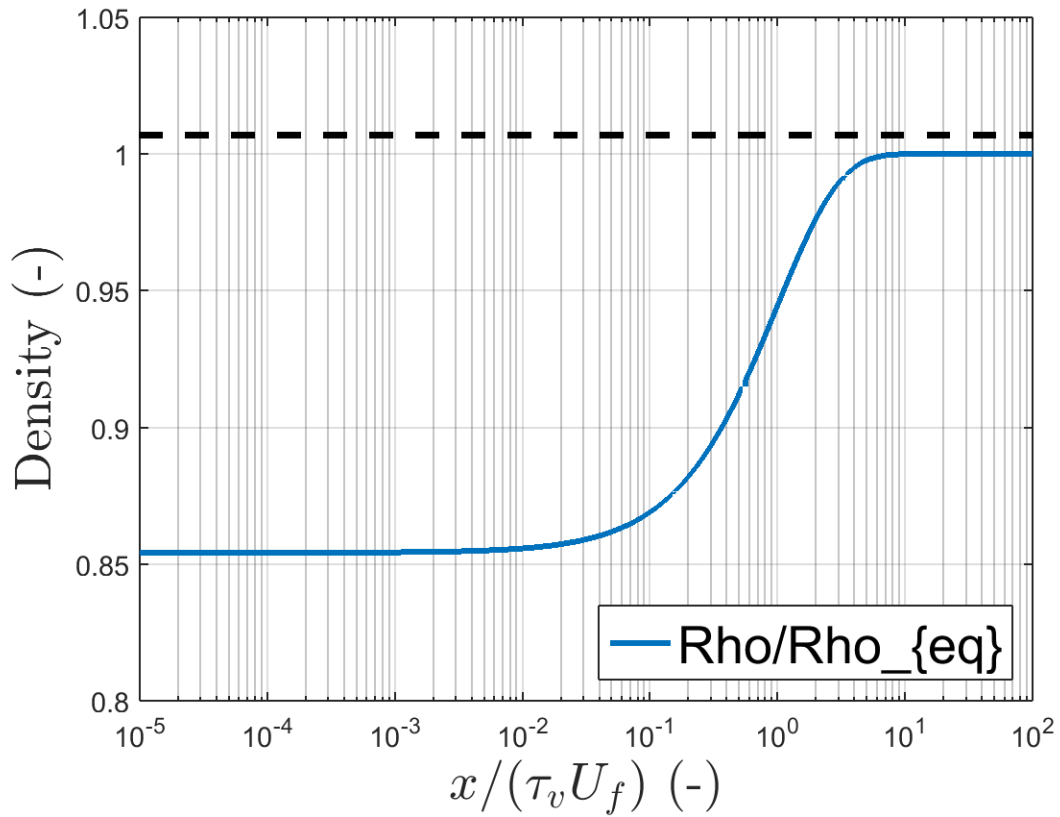
Figure 5.21: Density along relaxation distance

Exactly as predicted, the density increases in about 15%, which also the rate of change of translational/rotational temperature in figure 5.16. Besides, the results obtained by Cantera and quantum-mechanics show excellent agreement in the equilibrium value, reaching the same final steady state density.

5.3.6 Variation of enthalpy along relaxation distance

Finally, the variation of enthalpy is also plotted and examined. Attached in the graph is the total internal energy, as it is a component of the total enthalpy (see equation 4.6). By plotting the internal energy, one may note the fraction it takes from total enthalpy. It is sketched in figure 5.22.
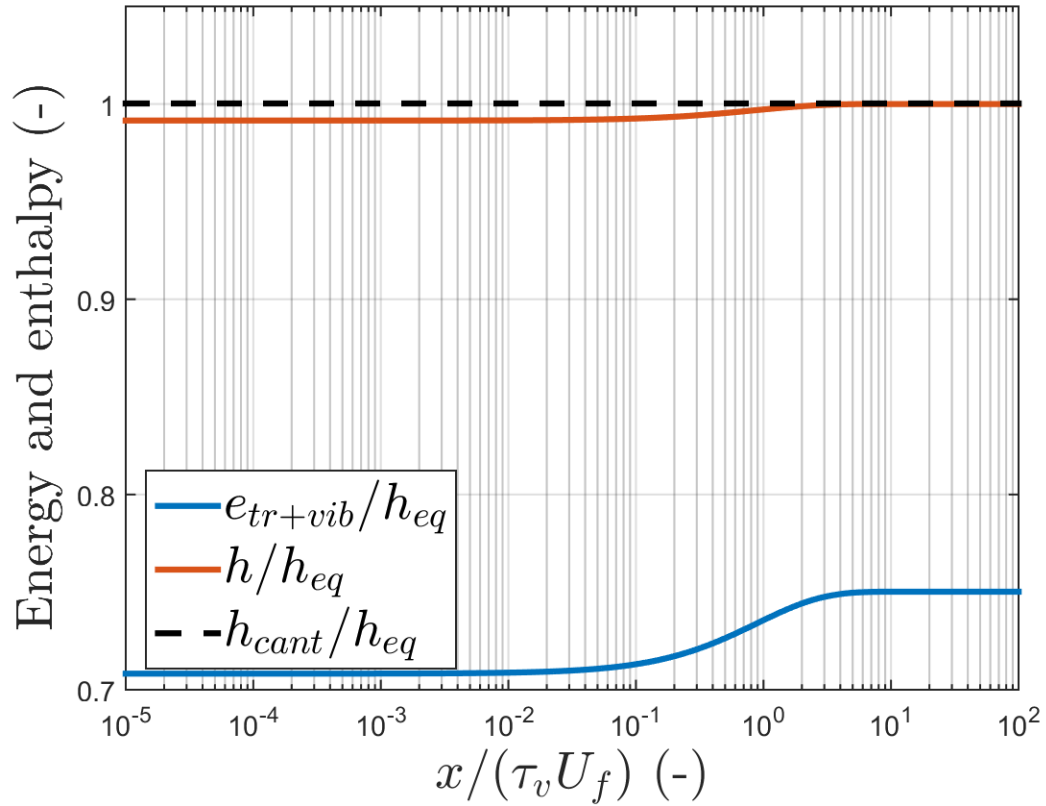
Figure 5.22: Enthalpy along relaxation distance

As it can be appreciated, the term of the internal energy contributes more than half to the total enthalpy (70% approximately) . The remaining quantity is stored in the term $\dfrac{P}{\rho}$, where pressure and density are computed locally for each step of iteration.

5.3.7 Variation of relaxation distance when varying the driven pressure

Finally, the last part of the project is studying how does the relaxation distance and Mach number vary when varying the driven pressure (p_1) for a fixed driver pressure (p_4). Results from this section can give an approach on future experiments for the better understanding of gas-dynamics inside the shock tube.

Driven pressure will be varied in small steps while of 5 torr, from 1-50 torr driver pressure will be set to a fixed value. Thus, the ratio (p_1/p_4) will be placed in the x-axis of the plots. In this first part, the study of the relaxation distance will be plotted as a function of the ratio between pressures.

Figure 5.23 shows this variation:
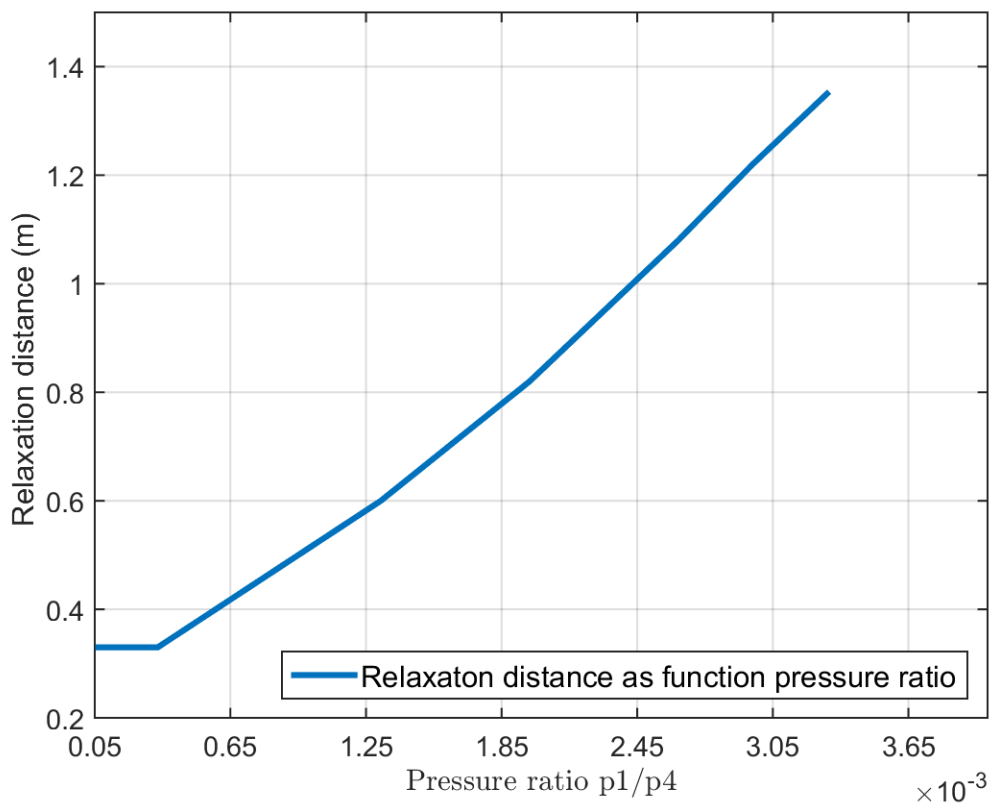
Figure 5.23: Relaxation distance as a function of pressure ratio

As figure 5.23 shows, the relaxation distance follows a linear relaxation with the pressure ratio. The greater the pressure ratio, the larger the relaxation distance. That can be explained by the fact that when the ratio increases, the differences between the translational/rotational and vibrational energies and temperature are higher, so it need more time to reach equilibrium. However, there is not a clear correlation since

it also depends in other initial parameters such as the initial temperatures of both chambers.

5.3.8 Variation of Mach number when varying the driven pressure

Last part of the results is studying how the Mach number varies when changing the pressure ratio. Unlike last study about the relaxation distance as a function of pressure ratio, Mach number is directly related with the pressure difference, as it is a measure of the strength of the system. Thus, applying the isentropic equations as well as the post-shock relations, the Mach number can be calculated. Figure 5.24 shows this effect:
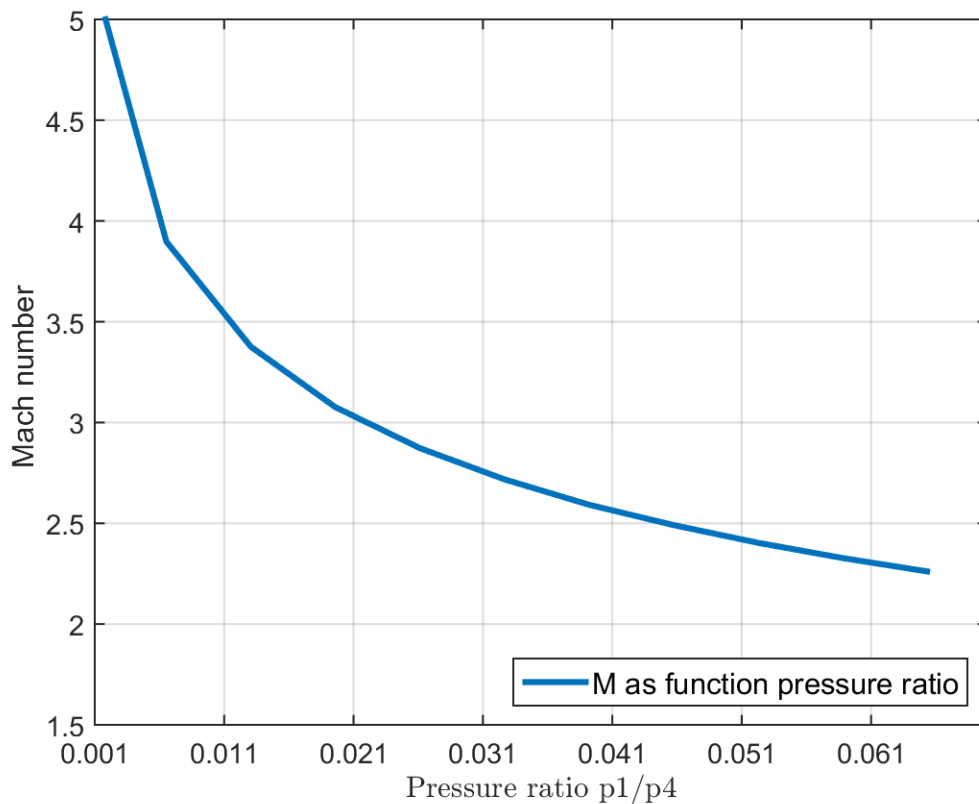
Figure 5.24: Mach number as a function of pressure ratio

As it can appreciated, the Mach number follows an exponential curve. For lower pressure ratios, that is, the bigger the difference between the chambers, the greater the Mach number (stronger force by high pressure ratio). When the pressure difference becomes smaller, the Mach number tends to decrease, as there is not a big force that could impulse the shock wave.

This graph can be useful when setting a desirable Mach number in the experiments. In order to achieve that, the correct pressure ratio must be established.

Chapter 6

Conclusions

6.1 Conclusions

The study was conducted on the different thermodynamic and chemical aspects of gas-dynamics. The effect of non-equilibrium in temperature, pressure, velocity, density and internal energy was monitored and prepared for future experimental data.

After a detailed explanation on the operating principle of a shock tube, as well as the different components that compose the facility, a series of simulations were performed in order to describe the changes on the driven gas when it was traversed by the shock wave.

The pressure-velocity diagram showed all different states withing the gases for specified given conditions. The velocity and pressure of the contact surface (region that separates both gases) were estimated, showing that their values fell in the expected range, between the driven-driver pressure and below the shock wave velocity.

The study continued testing and comparing different forms of computing the thermodynamic properties. It was shown how software Cantera and the quantum-mechanics equations (used for the computation of the project) matched with great accuracy (approximately 95%). The effect of disassociation and the presence of the vibrational energy was measured and monitored. For given initial conditions in the driven section (10 torr and room temperature), disassociation happened for Mach number of 8, which corresponds with a post-shock temperature of 4000K. This effect could also be appreciated in the C_v graph, where the comparisons between equations and Cantera

was no longer accurate for $T > 4500K$.

Last section of the project, in which converged all topics presented before, explained the non-equilibrium transient behavior after the shock wave. By monitoring translational/rotational and vibrational temperature, it could be appreciated how vibrational temperature started increasing and reaching the equilibrium value. The equilibrium distance can be easily displayed by running the corresponding script. Apart from that, the translational and rotational internal energy was seen to be more than 80% of total internal energy, where the rest corresponds to the vibrational energy.

Considering the process in non-equilibrium to be isobaric, it was seen how density and velocity of the gas increased due to the changes in temperature and internal energy. Internal energy was also monitored and compared to the total enthalpy, computing that it represents over 75% of its total quantity.

Last aspect of results showed the variation of relaxation distance and Mach number as a function of pressure ratio. While the variation of relaxation distance was found not to follow a specified patter (as relaxation distance also depends in other parameters, such as temperature of the different gases), Mach number showed a clear exponential behavior. That is, for larger differences in driven and driver pressure (smaller ratio), the Mach number was bigger. As it was explained in the body of the report, the Mach number within a shock tube represents the strength of the shock.

6.2 Further recommendations

Although this project aimed to give a theoretical predictions on the effect of non-equilibrium gas dynamics, further studies and experimental research must be conducted.

Once the shock tube is finished, comparison between theoretical and experimental results must be done. The accuracy of the predictions could be evaluated and better results could be achieved.

More research must also be completed when dealing with the vibrational relaxation constant τ. It is one of the crucial components when predicting the vibrational relaxation distance, so there is a huge necessity on deeply studying it. Also the experimental results will give an approach on how good this Millikan and White expression is.

Chapter 7

Appendix-Matlab scripts

7.1 Pressure-velocity diagram

Main Script

```
clc;
clear all;
Ru = 8.314472e3; %J/kmolK


%% the ics for the driven section for N2
T1          = 273.15+22; %Temperature (K)
p1          = 1* 133.322368; %Pressure (Pa)
R1          = Ru/(14*2); %J/KgK
g1          = 7/5; %Specific heat (Cp/Cv)
a1          = sqrt(g1*R1*T1); %Speed of sound
%% the ics for the driver section for He
p4          = 15/14.7/10*1e6;
g4          = 5/3;
T4          = 273.15+22;
R4          = Ru/4.00262;
a4          = sqrt(g4*R4*T4);


u=0:1:4000; %Velocity range


p2=p1.*(4.*(a1.^2)+g1.*(u.^2).*(g1+1)+((16.*(a1.^2).*(g1.^2).*(u.^2)...
+(g1.^2).*(u.^4).*((g1+1).^2)).^0.5))./(4.*(a1.^2));
```

```matlab
%Pressure 2 as a function of u2


p3=((p4.^((g4-1)./(2.*g4)))-((u.*(g4-1).*p4.^((g4-1)./(2.*g4)))./...
(2.*a4))).^((2.*g4)./(g4-1)); %Pressure 3 as a function of u3


s = p1.*(4.*(a1.^2)+g1.*(u.^2).*(g1+1)+((16.*(a1.^2).*(g1.^2).*(u.^2)...
+(g1.^2).*(u.^4).*((g1+1).^2)).^0.5))./(4.*(a1.^2))-((p4.^((g4-1)./...
(2.*g4)))-((u.*(g4-1).*p4.^((g4-1)./(2.*g4)))./(2.*a4))).^((2.*g4)...
./(g4-1));


grid on


%Pressure-velocity diagram
plot (u,p2,u,p3)


legend ('States from 1-2','States from 4-3','Difference between curves')


xlabel('Velocity [m/s]')
ylabel('Pressure[Pa]')


%Velocity after contact surface
VelocityContactSurface1=fzero(@ (u)  p1.*(4.*(a1.^2)+g1.*(u.^2).*...
(g1+1)+((16.*(a1.^2).*(g1.^2).*(u.^2)+(g1.^2).*(u.^4).*((g1+1).^2))...
.^0.5))./(4.*(a1.^2))-((p4.^((g4-1)./(2.*g4)))-((u.*(g4-1).*p4.^...
((g4-1)./(2.*g4)))./(2.*a4))).^((2.*g4)./(g4-1)), 1000)


%No decimals in velocity of the contact surface
VelocityContactSurface=fix(VelocityContactSurface1)


%Pressure contact surface
PressureContactSurface1=p2(VelocityContactSurface)
```

```matlab
%No decimals in pressure of the contact surface
PressureContactSurface=fix(PressureContactSurface1);


%Temperature behind expansion wave, freezing --> Isentropic Relation
T3=T4.*(PressureContactSurface./p4).^((g4-1)./g4)


%Rankine-Hugoniout relation for temperature after shock wave
%(hight tempeture)
T2=T1.*((1+((g1-1)./(g1+1)).*(PressureContactSurface./p1))./(1+((g1-1)...
./(g1+1)).*(p1./PressureContactSurface)))


%Maximum wave speed
MaximumWaveSpeed=VelocityContactSurface+sqrt(g1*R1*T2)


%Mach numer of shock wave, does not change
M1=sqrt(((g1-1)./(2.*g1))+(((g1+1)./(g1.*2)).*(PressureContactSurface...
./p1)))


%Initial shock wave speed
W=M1.*a1;
```

Function

```matlab
function [ s ] = Untitled( s )


funcion s = f(x) %Difference between the curves to find when it cuts...
%x-axis
s=p1.*(4.*(a1.^2)+g1.*(u.^2).*(g1+1)+((16.*(a1.^2).*(g1.^2).*(u.^2)...
+(g1.^2).*(u.^4).*((g1+1).^2)).^0.5))./(4.*(a1.^2))-((p4.^((g4-1)./...
```

```
(2.*g4)))-((u.*(g4-1).*p4.^((g4-1)./(2.*g4)))./(2.*a4))).^((2.*g4)...
./(g4-1))


end
```

7.2 Plots for post-shock state gas

Equilibrium state calculations

```
% Shock and Detonation Toolboox
%
% Different figures that illustrate how parameters of Nitrogen change
% as a function of
% shock speed in equilibrium state


clear;clc;close all
display('Frozen Post-Shock state with Nitrogen in driven section')


% set initial state of gas, avoid using precise stoichiometric ratios.
% Nitrogen in driven section
P1 = 10 * 133.322368; T1 = 273.15+22;
q = 'N2:1'; %Start as a molecule of N2 and in equilibrium disasociates
mech = 'gri30_highT.cti';
gas1 = importPhase(mech);
set(gas1,'Temperature',T1,'Pressure',P1,'MoleFractions',q);
display(['Computing postshock state for ',q,' using ',mech]);


% Evaluate the equilibrium  state of the gas behind a shock wave
% traveling at a
```

```matlab
% specified speed.

g1          = 7/5;
R1          = 296.95;
a1          = sqrt(g1*R1*T1)


i=1;


for speeds = (500:200:4699)
speed(i) = speeds;
[gas] = PostShock_eq(speed(i),P1, T1, q, mech);
P(i) = pressure(gas);
R(i) = density(gas);
T(i) = temperature(gas);
a(i) = soundspeed_fr(gas);
gamma(i) = a(i)*a(i)*R(i)/P(i);
w2(i) = density(gas1)*speed(i)/R(i);
u2(i) = speed(i) - w2(i);
x2 = moleFractions(gas);
MoleFractionN (i)= x2(31);
MoleFractionN2 (i)= x2(48);
Cp (i)= cp_mass(gas);
Cv (i)= cv_mass (gas);
gamma2 (i) = cp_mass(gas)/cv_mass(gas);
Enthalpy (i) = enthalpy_mass(gas);
M(i)=speed(i)/a1;
i=i+1;
end


%Plot gamma (Cp/Cv)
figure
```

```matlab
plot(T(:),gamma(:))
legend ('Values of gamma Cp/Cv for different temperatures')
xlabel('Temperature [K]')
ylabel('Gamma')


figure
plot(M(:),gamma(:))
legend ('Values of gamma Cp/Cv for different Mach numbers')
xlabel('Mach number')
ylabel('Gamma')


%Plot Specific heat Cp
figure
plot(T(:),Cp(:))
legend ('Values of heat capacity Cp for different temperatures  ')
xlabel('Temperature [K]')
ylabel('Heat capacity [J/KgK]')


%Plot Specific heat Cp
figure
plot(M(:),Cp(:))
legend ('Values of heat capacity Cp for different Mach number ')
xlabel('Mach number')
ylabel('Heat capacity [J/KgK]')


% %Plot enthalpy H
% figure
% plot(speed(:),Enthalpy(:))
% legend ('Values of Enthalpy for different shock speeds ')
% xlabel('Shock speed [m/s]')
% ylabel('Enthalpy [J/Kg]')
```

```
figure
plot(T(:),MoleFractionN2(:),T(:),MoleFractionN(:))
legend ('Mole Fraction of N2','Mole Fraction of N')
xlabel('T [K]')
ylabel('Mole fraction')


figure
plot(M(:),MoleFractionN2(:),M(:),MoleFractionN(:))
legend ('Mole Fraction of N2','Mole Fraction of N')
xlabel('Mach number')
ylabel('Mole fraction')
```

Frozen state calculations

```
% Shock and Detonation Toolboox
%
% Different figures that illustrate how parameters of Nitrogen change
% as a function of
% shock speed in frozen state


clear;clc;close all
display('Frozen Post-Shock state with Nitrogen in driven section')


% set initial state of gas, avoid using precise stoichiometric ratios.
% Nitrogen in driven section
P1 = 10 * 133.322368; T1 = 273.15+22;
q = 'N2:1'; %Start as a molecule of N2 and in equilibrium disasociates
mech = 'gri30_highT.cti';
```

```matlab
gas1 = importPhase(mech);
set(gas1,'Temperature',T1,'Pressure',P1,'MoleFractions',q);
display(['Computing postshock state for ',q,' using ',mech]);


% Evaluate the frozen  state of the gas behind a shock wave traveling at
% a specified speed.


g1          = 7/5;
R1          = 296.95;
a1          = sqrt(g1*R1*T1)


i=1


for speeds = (500:100:4000)
speed(i) = speeds;
[gas] = PostShock_fr(speed(i),P1, T1, q, mech);
P(i) = pressure(gas);
R(i) = density(gas);
T(i) = temperature(gas);
a(i) = soundspeed_fr(gas);
gamma(i) = a(i)*a(i)*R(i)/P(i);
w2(i) = density(gas1)*speed(i)/R(i);
u2(i) = speed(i) - w2(i);
x2 = moleFractions(gas);
MoleFractionN (i)= x2(31);
MoleFractionN2 (i)= x2(48);
Cp (i)= cp_mass(gas);
Enthalpy (i) = enthalpy_mass(gas);
M (i) = speed(i)/a1;
i=i+1;
end
```

```matlab
%Plot gamma (Cp/Cv)
figure
plot(M(:),gamma(:))
legend ('Values of gamma Cp/Cv for different Mach numbers ')
xlabel('Mach number')
ylabel('Gamma')


%Plot gamma (Cp/Cv)
figure
plot(T(:),gamma(:))
legend ('Values of gamma Cp/Cv for different temperatures ')
xlabel('Temperature [K]')
ylabel('Gamma')


%Plot Specific heat Cp
figure
plot(T(:),Cp(:))
legend ('Values of heat capacity Cp for different temperatures  ')
xlabel('Temperature [K]')
ylabel('Heat capacity [J/KgK]')


%Plot Specific heat Cp
figure
plot(M(:),Cp(:))
legend ('Values of heat capacity Cp for different Mach number ')
xlabel('Mach number')
ylabel('Heat capacity [J/KgK]')


%Plot enthalpy H
figure
```

```matlab
plot(speed(:),Enthalpy(:))

legend ('Values of Enthalpy for different shock speeds ')

xlabel('Shock speed [m/s]')

ylabel('Enthalpy [J/Kg]')


figure

plot(T(:),MoleFractionN2(:),T(:),MoleFractionN(:))

legend ('Mole Fraction of N2','Mole Fraction of N')

xlabel('T [K]')

ylabel('Mole fraction')
```

Comparison Cantera and Quantum-mechanics

```matlab
% Shock and Detonation Toolboox

%

% Different plot for translational, rotational and vibrational energy in

%  equilibrium for different temperatures

% Also plot of the Cv (heat capacity constant volume)


clear;clc;close all

display('Nitrogen in equilibrium')


% Set initial state of gas, avoid using precise stoichiometric ratios.

% Nitrogen in driven section

P1 = 500 * 133.322368; T1 = 273.15+22;

q = 'N2:1'; %Start as a molecule of N2 and in equilibrium disasociates


%Cantera implementation
```

```matlab
mech = 'gri30_highT.cti';
gas1 = importPhase(mech);
set(gas1,'Temperature',T1,'Pressure',P1,'MoleFractions',q);
display(['Computing postshock state for ',q,' using ',mech]);



% Evaluate the equilibrium  state of the gas behind a shock wave
% traveling at a
%specified speed.


Ru = 8.314472e3;
R1   = Ru/(14*2); %J/KgK
k = 1.38064852.*10.^-23; % Boltzman Constant m2 kg s-2 K-1
h = 6.62607004.*10.^-34; %Planck constant m2 kg / s
c = 2.99792458.*10.^10; %Speed of light cm s-1
VibFreqN2 = 2359; %cm-1
v = c.*VibFreqN2; %Vibrational frequency N2 in s-1
i=1;


D0=225.1.*4.184 %KJ
D02=0.5.*h.*v
De=-D0-0.5.*h.*v


%Loop for different shock speeds and compute postshock equilibrium state

for speeds = (0:200:5000)
speed(i) = speeds;
[gas] = PostShock_eq(speed(i),P1, T1, q, mech);
P(i) = pressure(gas);
R(i) = density(gas);
T(i) = temperature(gas);
```

```
a(i) = soundspeed_fr(gas);

gamma(i) = a(i)*a(i)*R(i)/P(i);

w2(i) = density(gas1)*speed(i)/R(i);

u2(i) = speed(i) - w2(i);

x2 = moleFractions(gas);

MoleFractionN (i)= x2(31);

MoleFractionN2 (i)= x2(48);

Cp (i)= cp_mass(gas);%cp cantera



Cv (i)= cv_mass(gas); %cv cantera

Cv_trans (i) = 1.5.*R1;

Cv_rot (i) = R1;

Cv_vib (i) =((((h.*v)./(k.*T(i))).^2).*exp((h.*v)./(k.*T(i))).*R1)./...

(exp((h.*v)./(k.*T(i)))-1).^2;

Cv_manual (i) = Cv_trans (i) + Cv_rot (i) + Cv_vib (i); %Cv

% quantomechanics



e (i)= intEnergy_mass(gas)+309781.81; %internal energy cantera with

% the offset

e_trans (i) = 1.5.*R1.*T(i);

e_rot (i) = R1.*T(i);

e_vib (i) =(((h.*v)./(k.*T(i))).*R1.*T(i))./(exp((h.*v)./(k.*T(i)))-1);

e_manual (i) = e_trans (i) + e_rot (i) + e_vib (i); %internal energy

% quantomechanics



Enthalpy(i)= enthalpy_mass(gas)+309781.81; %Enthalpy cantera with offset

ent (i) = e_manual (i) + (P(i)./R(i)); %Enthalpy thermodynamics

i=i+1;

end
```

```matlab
% Offset created because Cantera uses NASA 9 polinomios (with h=0 for
% T=298.15K) and quantomechanics set h=0 for T=0 (AREsultbsolute 0K)


% Plot Specific heat Cv as a function of T. The limit of the Temperature
% isset to 2000K
figure
plot(T(:),Cv(:),T(:),Cv_manual(:),T(:),Cv_trans(:),T(:),Cv_rot(:),...
T(:),Cv_vib(:))
AX=legend('Cv-T drawn by Cantera','Cv-T drawn manually',...
'Cv translational','Cv rotational','Cv vibrational','location',...
'Southeast')
set(AX,'FontSize',6)
xlabel('Temperature [K]')
ylabel('Heat capacity Cp [J/KgK]')


%Plot internal energy as a function of T. The limit of Temperature is
%set to 2000K
figure
plot(T(:),e(:),T(:),e_manual(:),T(:),e_trans(:),T(:),e_rot(:),T(:),...
e_vib(:))
legend ('e-T drawn by Cantera','e-T drawn manually','e translational',...
'e rotational','e vibrational')
xlabel('Temperature [K]')
ylabel('Internal energy [J/kg]')


figure
plot(T(:),Enthalpy(:),T(:),ent(:))
legend ('e-T drawn by Cantera','e-T drawn manually','e translational',...
'e rotational','e vibrational')
xlabel('Temperature [K]')
ylabel('Enthalpy [J/kg]')
```

```
%NASA 9 polynomiums
%http://www.cantera.org/docs/sphinx/html/cti/species.html
```

7.3 Vibrational rate equations

Main script

```
clc; clear all;


%Initial conditions


T1              = 300; %Vibrational temperature
T2              = 3000; %Translational/rotational temperature
P               = 1e2;
time            = 1e-0; %Final time


%Data for nitrogen


theta_v_n2      = 3390;
mW              = 14.0067 * 2;
R               = 8314/mW;


%Initial translational/rotational and vibrational energies


e_tr_2          = 5/2 * R * T2;
e_vb_2          = theta_v_n2/(exp(theta_v_n2/T1)-1) * R;


% break
```

```matlab
options         = 1;%odeset('Refine',1,'Stats','On','RelTol',1e-8,...
'MaxOrder',3);
[t,e]           = ode15s(@dedt,[0 time],[e_tr_2 e_vb_2],options,...
theta_v_n2,R,P);


Ttr             = 2 * e(:,1) / (5 * R);
Tvb             = theta_v_n2./(log(theta_v_n2 * R ./ e(:,2) +1));



figure(1);clf(1);
semilogx(t,Ttr,t,Tvb)
legend ('Translational/Rotational temperature','Vibrational temperature')
xlabel('Time[s]')
ylabel('Temperature [K]')
figure(2);clf(2);
plot(t,e(:,2))
legend ('Vibrational internal energy')
xlabel('Time[s]')
ylabel('Internal energy [J/kg]')
```

Function

```matlab
function df = dedt(t,e,theta_v,R,p)


%Computing vibrational relaxation tau


% tau        = 10e-6;
C1         = 7.12e-3;
```

```
C2          = 1.91e6;


Ttr         = 2 * e(1) / (5 * R)


tau         = (p/101325).^-1 * C1 * exp((C2/Ttr).^(1/3))*1e-6


e_vb_eq     = theta_v/(exp(theta_v/Ttr)-1) * R;


%Differential equations and system


de_vb_dt    = 1/tau * (e_vb_eq - e(2));
de_tr_dt    = -de_vb_dt;


df          = zeros(2,1);
df(1)       = de_tr_dt;
df(2)       = de_vb_dt;
```

7.4 Non-equilibrium flow

Main script

```
% Computes post-shock parameters in non-equilibrium. Key of the project.


clc; clear all;


%Initial conditions
Ru          = 8.314472e3; %J/kmolK
M           = 7;
```

```matlab
p1            = 5 * 133.322368; %Pressure (Pa)

T1            = 273.15+22; %Temperature (K)

R1            = Ru/(14*2); %J/KgK

g1            = 7/5; %Specific heat (Cp/Cv)

a1            = sqrt(g1*R1*T1); %Speed of sound

Dens1         = p1./(T1.*R1);


q = 'N2:1'; %Start as a molecule of N2 and in equilibrium disasociates

mech = 'gri30_highT.cti';

gas1 = importPhase(mech);

set(gas1,'Temperature',T1,'Pressure',p1,'MoleFractions',q);


%Compute Cantera post-shock gas in order to compare with system of
%equations


[gas] = PostShock_eq(M.*a1,p1, T1, q, mech);


T2_cant          = temperature(gas);

p2_cant          = pressure(gas);

rho2_cant        = density(gas);


x2                   = moleFractions(gas);

MoleFractionN        = x2(31);

MoleFractionN2       = x2(48);


%Shock wave relations. Subscript 1 driven gas, 2 for post-shock region

p2            = p1.*(2.*g1.*M.*M-(g1-1))./(g1+1);

T2            = T1.*((2.*g1.*M.*M-(g1-1)).*((g1-1).*M.*M+2))./((g1+1)...
.^2.*M.*M);

Dens2         = Dens1.*((g1+1).*M.*M)./((g1-1).*M.*M+2);

M2            = sqrt(((g1-1).*M.*M+2)./(2.*g1.*M.*M-(g1-1)));
```

```matlab
a2          = sqrt(g1*R1*T2);
u2          = M2.*a2;


distance    = logspace(-8,3,1e4);
% distance  = linspace(1e-6,1e-3,1e3);
theta_v_n2  = 3390;


e_tr_2      = 5/2 * R1 * T2; %iplnitial translational/rotational energy
e_vb_2      = theta_v_n2/(exp(theta_v_n2/T1)-1) * R1; %Initial vib


e2          = e_tr_2 + e_vb_2; %Initial internal energy;


y0          = [u2 p2 Dens2 e_tr_2 e_vb_2]; %initial conditions
yp0         = [0 0 0 0 0]; %Initial derivative values


options     =odeset('Stats','On','RelTol',1e-3,'AbsTol',100,'refine',3);
[y0m,yp0m]  =decic(@mysysfun4,0,y0,[1 1 1 1 1],yp0,[0 0 0 0 0],options);
[X,Y]       =ode15i(@mysysfun4,[0 distance],y0m,yp0m,options);


Ttr         = 2 * Y(:,4) / (5 * R1);
Tvb         = theta_v_n2./(log(theta_v_n2 * R1 ./ Y(:,5) +1));


U           = Y(:,1);
P           = Y(:,2);
rho         = Y(:,3);
etr         = Y(:,4);
ev          = Y(:,5);
e           = Y(:,4) +Y(:,5);
h           = Y(:,4) +Y(:,5) + (Y(:,2)./Y(:,3));


h0          = etr + ev + P./rho + U.^2./2;
```

```matlab
dUdx          = diff(Y(:,1))./diff(X);

dPdx          = diff(Y(:,2))./diff(X);

drhodx        = diff(Y(:,3))./diff(X);

detrdx        = diff(Y(:,4))./diff(X);

devdx         = diff(Y(:,5))./diff(X);


%% non-dimensionalize numbers


%Compute relaxation time scale

mu            = 14; %N2 weighted average amu

Asr           = (1.16e-3).*(mu.^0.5).*(theta_v_n2.^(4./3)); %Factor in tau

tau           = 1./(P(1)./101325).*exp(Asr.*(Ttr(1).^(-1./3)-0.015.*mu...

.^(0.25))-18.42); %Milikan and White expression

% e_vb_eq     = theta_v_n2/(exp(theta_v_n2/Ttr()-1) * R;

e_cant        = intEnergy_mass(gas)+309781.81; %Internal energy with

%offset because of 9-Nasa polinomia.

rho_cant      = density (gas);

h_cant        = enthalpy_mass(gas)+309781.81 %With offset


%Variation of velocity


figure(1);clf(1); fs = 26;

hold on

semilogx(X./(tau.*U(1)),M*a1-Y(:,1),'linewidth',3)

hold off

set(gca,'FontSize',14,'LineWidth',1,'GridLineStyle','-',...

'MinorGridLineStyle','-','xscale','log','xtick',...

[1e-5 1e-4 1e-3 1e-2 1e-1 1e0 1e1 1e2],'ytick',...

[2000 2020 2040 2060 2080 2100])
```

```matlab
xlim([1e-5 1e2])
ylim([2000 2100])
xlabel('$x/(\tau_v U_f)$ (-)','FontSize',fs,'interpreter','latex')
ylabel('Velocity [m/s]','FontSize',fs,'interpreter','latex')
grid on; box on;
leg = legend('Variation of velocity');
set(leg,'Interpreter','Latex','fontsize',fs*1);


%Variation of pressure


figure(2);clf(2); fs = 26;
hold on
semilogx(X./(tau.*U(1)),Y(:,2)/p2_cant,'linewidth',3)
semilogx([X(2) X(end)]./(tau.*U(1)),[p2_cant p2_cant]/p2_cant,'k--',...
'linewidth',3)
hold off
set(gca,'FontSize',14,'LineWidth',1,'GridLineStyle','-',...
'MinorGridLineStyle','-','xscale','log','xtick',...
[1e-5 1e-4 1e-3 1e-2 1e-1 1e0 1e1 1e2],'ytick',...
[0.9 0.94 0.98 1.02 1.04 1.08])
xlim([1e-5 1e2])
ylim([0.9 1.08])
xlabel('$x/(\tau_v U_f)$ (-)','FontSize',fs,'interpreter','latex')
ylabel('Pressure (-) ','FontSize',fs,'interpreter','latex')
grid on; box on;
leg = legend('P/P_{eq}','location','southeast');


%Variation of density


figure(3);clf(3); fs = 26;
hold on
```

```matlab
semilogx(X./(tau.*U(1)),Y(:,3)/rho(end),'linewidth',3)
semilogx([X(2) X(end)]./(tau.*U(1)),[rho_cant rho_cant]/rho(end),...
'k--','linewidth',3)
hold off
set(gca,'FontSize',14,'LineWidth',1,'GridLineStyle','-',...
'MinorGridLineStyle','-','xscale','log','xtick',...
[1e-5 1e-4 1e-3 1e-2 1e-1 1e0 1e1 1e2],'ytick',...
[0.8 0.85 0.9 0.95 1 1.05])
xlim([1e-5 1e2])
ylim([0.8 1.05])
xlabel('$x/(\tau_v U_f)$ (-)','FontSize',fs,'interpreter','latex')
ylabel('Density (-) ','FontSize',fs,'interpreter','latex')
grid on; box on;
leg = legend('Rho/Rho_{eq}','location','southeast');
set(leg,'Interpreter','Latex','fontsize',fs*1);


%Variation of modes of energy


figure(4);clf(4); fs = 26;
hold on
semilogx(X./(tau.*U(1)),Y(:,4)/e_cant,X./(tau.*U(1)),...
Y(:,5)/e_cant,'linewidth',3)
semilogx([X(2) X(end)]./(tau.*U(1)),[e_cant e_cant]/e_cant,...
'k--','linewidth',3)
hold off
set(gca,'FontSize',14,'LineWidth',1,'GridLineStyle','-',...
'MinorGridLineStyle','-','xscale','log','xtick',...
[1e-5 1e-4 1e-3 1e-2 1e-1 1e0 1e1 1e2],'ytick',[0:0.1:1.2])
xlim([1e-5 1e2])
ylim([0 1.2])
xlabel('$x/(\tau_v U_f)$ (-)','FontSize',fs,'interpreter','latex')
```

```matlab
ylabel('Energy (-) ','FontSize',fs,'interpreter','latex')
grid on; box on;
leg = legend('$e_{tr}/e_{eq}$','$e_{v}/e_{eq}$','$e_{cant}/e_{eq}$',...
'location','southwest');
set(leg,'Interpreter','Latex','fontsize',fs*1);


%Variation of the different temperatures


figure(6);clf(6); fs = 26;
hold on
semilogx(X./(tau.*U(1)),Ttr/Ttr(end),X./(tau.*U(1)),Tvb/Ttr(end),...
'linewidth',3)
semilogx([X(2) X(end)]./(tau.*U(1)),[T2_cant T2_cant]/Ttr(end),...
'k--','linewidth',3)
hold off
set(gca,'FontSize',14,'LineWidth',1,'GridLineStyle','-',...
'MinorGridLineStyle','-','xscale','log','xtick',...
[1e-5 1e-4 1e-3 1e-2 1e-1 1e0 1e1 1e2],'ytick',[0:0.1:1.2])
xlim([1e-5 1e2])
ylim([0 1.2])
xlabel('$x/(\tau_v U_f)$ (-)','FontSize',fs,'interpreter','latex')
ylabel('Temperature (-) ','FontSize',fs,'interpreter','latex')
grid on; box on;
leg = legend('$T_{tr}/T_{eq}$','$T_{v}/T_{eq}$','$T_{cant}/T_{eq}$',...
'location','southeast');
set(leg,'Interpreter','Latex','fontsize',fs*1);


%Variation of internal energy and enthalpy


figure(7);clf(7); fs = 26;
hold on
```

```matlab
semilogx(X./(tau.*U(1)),e/((etr(end)+ev(end))+(P(end)/rho(end))),...
X./(tau.*U(1)),h./((etr(end)+ev(end))+(P(end)/rho(end))),'linewidth',3)
semilogx([X(2) X(end)]./(tau.*U(1)),[h_cant h_cant]/((etr(end)+...
ev(end))+(P(end)/rho(end))),'k--','linewidth',3)
hold off
set(gca,'FontSize',14,'LineWidth',1,'GridLineStyle','-',...
'MinorGridLineStyle','-','xscale','log','xtick',...
[1e-5 1e-4 1e-3 1e-2 1e-1 1e0 1e1 1e2],'ytick',[0.7:0.1:1.05])
xlim([1e-5 1e2])
ylim([0.7 1.05])
xlabel('$x/(\tau_v U_f)$ (-)','FontSize',fs,'interpreter','latex')
ylabel('Energy and enthalpy (-) ','FontSize',fs,'interpreter','latex')
grid on; box on;
leg = legend('$e_{tr+vib}/h_{eq}$','$h/h_{eq}$','$h_{cant}/h_{eq}$',...
'location','southwest');
set(leg,'Interpreter','Latex','fontsize',fs*1);


%Data for Mach number is taken from P-v diagram script simulations


pp1=133.322368*[1 5 10 15 20 25 30 35 40 45 50];
Mach=[5.124 3.8980 3.3759 3.0760 2.8728 2.7180 2.5920 2.4911...
    2.4031 2.3275 2.2613];


p4          = 15/14.7/10*1e6; %Fixed driver pressure


%Plot Mach number as a function of pressure ratio


figure (9);clf(9); fs = 15;
plot(pp1/p4,Mach,'linewidth',3)
set(gca,'FontSize',14,'LineWidth',1,'GridLineStyle','-',...
'MinorGridLineStyle','-','xtick',[0.001:0.01:0.07],'ytick',[1.5:0.5:5])
```

```
xlim([0.001 0.07])

ylim([1.5 5])

xlabel('Pressure ratio p1/p4','FontSize',fs,'interpreter','latex')

ylabel('Mach number ','FontSize',15)

grid on; box on;

leg = legend('M as function pressure ratio','location','southeast');

set(leg,'fontsize',15);


%Data for Relaxation distance


tauVresult= 1./(P(1)./101325).*exp(Asr.*(Ttr(1).^(-1./3)-...

0.015.*mu.^(0.25))-18.42)*U(1)


pp4=101325*20; %Driver pressure


tauV=[0.33 0.33 0.42 0.51 0.60 0.71 0.82 0.95 1.08 1.22 1.35];


%Plot relaxation distance as a function of pressure ratio


figure (10);clf(10); fs = 15;

plot(pp1/pp4,tauV,'linewidth',3)

set(gca,'FontSize',14,'LineWidth',1,'GridLineStyle','-',...

'MinorGridLineStyle','-','xtick',[5e-5:6e-4:4e-3],'ytick',[0.2:0.2:1.5])

xlim([0.00005 0.004])

ylim([0.2 1.5])

xlabel('Pressure ratio p1/p4','FontSize',fs,'interpreter','latex')

ylabel('Relaxation distance (m) ','FontSize',15)

grid on; box on;

leg = legend('Relaxaton distance as function pressure ratio',...

'location','southeast');

set(leg,'fontsize',15);
```

Function

```
function f = mysysfun4(x,y,dy)



%Data for nitrogen



Ru          = 8.314472e3; %J/kmolK

R           = Ru/(14*2); %J/KgK

theta_v     = 3390;

mu          = 14; %N2 weighted average amu



%Compute vibrational relaxation tau



Asr         = (1.16e-3).*(mu.^0.5).*(theta_v.^(4./3)); %Factor in tau



%Compute translational/rotational and vibrational temperature in

%each stel of iteration



Ttr         = 2 * (y(4)) / (5 * R);

Tvb         = theta_v./(log(theta_v * R ./ y(5) +1));



%Compute tau



tau         = 1./(y(2)./101325).*exp(Asr.*(Ttr.^(-1./3)-0.015.*mu...
.^(0.25))-18.42); %Milikan and White expression

e_vb_eq     = theta_v/(exp(theta_v/Ttr)-1) * R;
```

```matlab
%Sytem of differential equations as explained in chapter Model in report


%Subscripts corrspond to the paramter below each number
% y 1 2 3 4  5
%   u p r tr v


%Implicit solver, ode15i
f            = [
y(1).*dy(3) + y(3).*dy(1)                                  % mass
dy(2) + y(1).*y(3).*dy(1)                                  % momentum
dy(4) + dy(5) + dy(2)./y(3) - dy(3).*y(2)./y(3).^2 + y(1).*dy(1)% energy
-dy(4) + 5/2*R*Ttr*(dy(2)./y(2)-dy(3)./y(3))              % detr
-y(1).*dy(5) + 1./(tau) .* (e_vb_eq - y(5)) ];            % dev


end
```

Bibliography

[1] Y. B. Zel'dovich and Y. P. Raizer. *Physics of Shock Waves and High-Temperature Hydrodynamic Phenomena.* Dover, 2002.

[2] J.D. Anderson. *Hypersonic and high-temperature gas dynamics.* AIAA Education Series, 2010.

[3] H. Shapiro, Ascher. *Dyanmics and Thermodynamics of Compressible Fluid Flow.* Krieger, 1983.

[4] N.A. Fomin. Years of experiments on shock tubes. *Journal of Engineering Physcis and Thermophysics*, 83:1118–1134, 2010.

[5] B.C. Henshall. Reports and memoranda. *On some aspects of the use of shock tubes in aerodynamic research*, 1:1–10, 1957.

[6] W.A. Crede. The design and construction of a shock tube. Master's thesis, Missouri University, 1965.

[7] T.A. Erikson. Shock tube testing. Master's thesis, Illinois Institute of Technology, 1998.

[8] C.R. Mulvihill. Shock tube time history measurements. Master's thesis, Texas University, 2015.

[9] Curchack H.D. Davis, H.J. Gas dynamics. *Shock tube Techniches and instrumentation*, 10:1–40, 1969.

[10] Davidson D.F. Hanson, R.K. Recent advances in laser absorption and shock tube methods for studies of combustion chemistry. *Progress in Energy and Combustion Science*, 44:103–114, 2014.

[11] Davidson D.F. Hanson, R.K. Advances in shock tube techniques for fundamental studies of combustion kinetics. *Progress in Energy and Combustion Science*, 1:1–5, 2015.

[12] S. Chen. Numerical study of shock/boundary layer interaction of chemically reacting flow in shock tube. *Procedia engineering*, 126:617–621, 2015.

[13] R. Andreotti. Performance of a shock tube facility for impact response of structures. *International Journal of Non-Linear Mechanics*, 72:53–66, 2015.

[14] A.J. Fletcher. *The Riemann Problem and Discontinuous solutions: application to the shock tube problem.* Pearson, 1991.

[15] Wisconsin. WiSTL Wisconsin Shock Tune Laboratory, 2015.

[16] Manuel Martinez. Reacting nozzle flow, 2015.

[17] Caltech. Spectroscopy, 2015.

[18] N.M. Laurendeau. *Statistical thermodynamics.* Cambridge, 2010.

[19] D Arovas. *Notes on thermodynamics and statistical mechanics.* University of San Diego, 2013.

[20] J. Fedor. *Statistical Thermodynamics.* University of Fribourg, 2013.

[21] R.C. Tolman. *The Principles of Statistical Mechanics.* Dover.

[22] F. Reif. *Fundamentals of Statistical and Thermal Physics.* McGraw-Hill, 1965.

[23] White D.R. Millikan, C.R. Systematics of vibrational relaxation. *Journal of chemical physics*, 39:1–10, 1963.

[24] P.D. Edmonds. Process of physics. *Journal of chemical physics*, 72:100–150, 1958.

[25] Blackman V. Fluid mechanics. *Journal of fluid mechanics*, 61:1–10, 1956.

[26] R. Holmes. Physics procedures. *Journal of chemical physics*, 81:311, 1963.

[27] P.G. Dickens. Translational faradag. *Journal of chemical physics*, 57:735, 1961.

[28] Varghese P.L. Gonzales, D.A. A simple model for state-specific diatomic dissociaiton. *Physical chemistry*, 97:7612–7622, 1993.

[29] D. Bernstein R.B. Levine, R. Thermodynamic approach to collision processes. *Dynamics of Molecular Collisions*, B:323–364, 1976.

[30] Escobar J. Hillers L. Hillers L. Mustafa M. Oswin E. Chu, R. Engineering design shock tube. Master's thesis, Stevens Institute of Technology, 2016.

[31] T. Bui. Explicit and implicit methods in solving differential equations. *Digital Commons*, 1:1–48, 2010.

[32] B.J.P. Kaus. Numerische methoden 1, 2015.

[33] J.T. Foster. Brief explanation of integration schemes, 2015.

[34] Inc MathWorks. Solver for fully implicit odes, 2005.

[35] B. Gear. Backward differentiation formulas, 214.

[36] Inc MathWorks. Ode15i, 2010.

[37] Cantera. Chemical kinetics, thermodynamics and ransport processesi, 2016.